Green Energy and Technology

Nadarajah Mithulananthan
Duong Quoc Hung
Kwang Y. Lee

# Intelligent Network Integration of Distributed Renewable Generation

Springer

# Green Energy and Technology

More information about this series at http://www.springer.com/series/8059

Nadarajah Mithulananthan
Duong Quoc Hung · Kwang Y. Lee

# Intelligent Network Integration of Distributed Renewable Generation

Springer

Nadarajah Mithulananthan
School of Information Technology
and Electrical Engineering
The University of Queensland
Brisbane
Australia

Kwang Y. Lee
Department of Electrical and Computer
Engineering
Baylor University
Waco, TX
USA

Duong Quoc Hung
School of Engineering
Deakin University
Geelong, VIC
Australia

ISSN 1865-3529 ISSN 1865-3537 (electronic)
Green Energy and Technology
ISBN 978-3-319-49270-4 ISBN 978-3-319-49271-1 (eBook)
DOI 10.1007/978-3-319-49271-1

Library of Congress Control Number: 2016958981



Printed on acid-free paper

This Springer imprint is published by Springer Nature
The registered company is Springer International Publishing AG
The registered company address is: Gewerbestrasse 11, 6330 Cham, Switzerland

# Preface

Renewable energy resources such as wind, solar and biomass are well on the way to dominate the supply-side of power systems as their penetration is increasing at a staggering rate all over the world. In this early stage of the renewable energy era, most of these integrations are happening at the distribution system level, close to customers. Increases in renewable energy penetration in distribution systems are expected to revolutionize power systems in many ways.

The number of sub-systems such as airports, businesses and cities fully powered by renewable sources is steadily increasing every year. Large-scale or utility-scale renewable plants will follow in the near future to fill the gap in achieving a so-called "100%" target. However, one of the key concerns about renewable energy including wind and solar, regardless of whether a utility-scale or small-scale Distributed Generation (DG) source is considered, is its intermittency that can bring uncertainty to the supply-side of power systems. This supply-side uncertainty combined with existing demand-side variations has been creating a number of challenges in operation and control of power systems. In order to deal with the issue of intermittency, innovative demand-side programs have been developed and successfully deployed via smart grid solutions. Nevertheless, a higher penetration level of unplanned renewable energy sources in distribution systems could lead to greater technical challenges such as voltage rises, voltage instability, reverse power flows and excessive power and energy losses, to name a few. It is possible to remove some of these challenges with strategic planning and operations, which are called as *intelligent network integration* in this book. There is no doubt that the integration of renewable sources is primarily driven by the availability of resources. However, as the resources are available, DG sizes cannot be arbitrarily chosen; consequently, the technically unsuitable locations should be avoided and the plants should be operated in a smart way to help in alleviating technical challenges and keeping the integrity of the grid.

The main idea behind the intelligent integration is strategically locating, sizing and operating renewable-based DG units coordinated with Battery Energy Storage (BES) units and Electric Vehicle (EV) charging stations in power distribution networks by considering various technical, economic and environmental issues.

Hence, the aim of this book is to develop methodologies for strategic planning and operations of highly penetrated renewable DG units along with an efficient usage of BES units in distribution systems. Biomass and PV power plants integrations are considered comprehensively, along with a combination of PV and BES units and a coordination of PV units and EV charging stations. The time-varying natures of loads and PV outputs are also considered throughout the chapters with step-by-step calculations and in an easy to understand manner. These sections will be useful sources of references to better understand and further conduct research on planning of renewable energy integration with outputs represented as a probability density function.

It can be seen from a number of examples found in this book that a huge quantity of technical, economic and environmental benefits from intelligent integration approaches are highlighted and quantified on different test distribution systems. As the book follows a strong mathematical foundation for various algorithms and methodologies developed, it looks simple and easy to follow. The book is targeted for distribution system planners, operation engineers, and undergraduate and postgraduate students. A wide variety of test distribution systems used in this book for showcasing various methodologies could be useful for further research in this domain.

Brisbane, Australia — Nadarajah Mithulananthan
Geelong, Australia — Duong Quoc Hung
Waco, USA — Kwang Y. Lee

# Contents

# About the Authors

**Nadarajah Mithulananthan** received the Ph.D. degree in Electrical and Computer Engineering from the University of Waterloo, Ontario, Canada, in 2002, the B.Sc. (Eng.) degree from the University of Peradeniya, Sri Lanka, in May 1993, and the M. Eng. degree from the Asian Institute of Technology (AIT), Bangkok, Thailand, in August 1997. He was a planning engineer at the Generation Planning Branch of the Ceylon Electricity Board, and a project leader at Chulalongkorn University, Bangkok, Thailand. He is currently Associate Professor with the University of Queensland (UQ), Brisbane, Australia. Prior to joining UQ, he was with the AIT, Bangkok, Thailand. At AIT he held several academic and administrative positions, including Coordinator of Energy Field of Study and Director of Regional Energy Resource Information Centre (RERIC). His research interests include the integration of renewable energy, electric vehicle, energy storage and power system stability and dynamics. Dr. Mithulan is a senior member of IEEE.

**Duong Quoc Hung** received the M. Eng. degree in Electric Power System Management with an excellent thesis from the Asian Institute of Technology, Bangkok. He was then awarded an International Postgraduate Research Scholarship and a University of Queensland Cent Scholarship, and completed his Ph.D. degree in Electrical Engineering at the University of Queensland, Brisbane, in October 2014. Following his 9-month stay at the University of Sydney and the University of Queensland as postdoctoral research associates, Dr. Hung took up a prestigious Alfred Deakin Postdoctoral Research Fellowship at Deakin University, Geelong, Australia, in February 2016, where he is an early career researcher, working on an emerging area, namely future microgrids powered by renewable sources and electric vehicles. Prior to spending his life in academia, he had 10 years of industry experience as a power systems engineer, serving in a wide variety of roles covering planning, design and operations of power distribution networks including SCADA systems, commissioning, project management, etc. Dr. Hung has a constant passion for research that provides fascinating insights into future real-world power distribution networks. Over the years, he has carried out extensive research into developing various theories and frameworks to facilitate planning and operations of

emerging technologies, namely distributed generation, renewable energy, energy storage and electric vehicles in active distribution systems towards the Smart Grid era.

**Kwang Y. Lee** received the B.S. degree in Electrical Engineering in 1964 from Seoul National University, M.S. degree in Electrical Engineering in 1968 from North Dakota State University, and Ph.D. degree in Systems Science in 1971 from Michigan State University. He was elected as a Fellow of IEEE in January 2001 for his contributions to the development and implementation of intelligent system techniques for power plants and power systems control. He has been working in the area of power systems control for over 30 years at Michigan State, Oregon State, U. of Houston, Penn State, and Baylor University, where he is currently Professor and Chair of the Electrical and Computer Engineering Department. Dr. Lee has served as Editor of IEEE Transactions on Energy Conversion, Associate Editor of IEEE Transactions on Neural Networks, and Associate Editor of IFAC Journal on Control Engineering Practice. He is currently serving as the Chair of the IFAC Power & Energy Technical Committee and IEEE PES Working Group on Modern Heuristic Optimization Techniques. His research interests include control, operation, and planning of power and energy systems intelligent control and their applications to power and energy systems and modeling, simulation and control of microgrids with renewable and distributed energy sources.

# Acronyms and Symbols

## Abbreviations

| | |
|---|---|
| A1, A2, A3 | Analytical approach 1, 2 and 3, respectively |
| ABC | Artificial Bee Colony algorithm |
| BES | Battery Energy Storage |
| $CO_2$ | Carbon dioxide |
| CP | Critical Point |
| CPF | Continuation Power Flow |
| DFIG | Doubly Fed Induction Generator |
| DG | Distributed Generation |
| EPF | Exhaustive Power Flow |
| GA | Genetic Algorithm |
| GSA | Gravitational Search Algorithm |
| HSA | Harmony Search Algorithm |
| IGA | Immune-Genetic Algorithm |
| MTLBO | Modified Teaching-Learning Based Optimization |
| $NO_x$ | Nitrogen oxide |
| OPF | Optimal Power Flow |
| PDF | Probability Density Function |
| PSO | Particle Swarm Optimization |
| PV-BES | PV and BES system |
| PV | Photovoltaic |
| SA | Simulated Annealing |
| SCA | Self-correction Algorithm |
| $SO_2$ | Sulphur dioxide |
| VSM | Voltage Stability Margin |

## Nomenclature

| | |
|---|---|
| $AE_y$ | Actual annual emission of the system with DG units ($TonCO_2$) |
| $ALoss_y$ | Actual annual energy loss of the system with DG units (MWh) |

| | |
|---|---|
| $AIMO$ | Average multi-objective index |
| $AVSM$ | Average voltage stability margin of the system |
| $B$ | Present value benefit over a planning horizon ($) |
| $BCR$ | Benefit and cost ratio |
| $C$ | Present value cost over a planning horizon ($) |
| $C_{DG}$ | Capital cost of DG ($/kW) |
| $CE_y$ | Cost of each ton of generated $CO_2$ ($/Ton$CO_2$) |
| $CF$ | Capacity factor |
| $CLoss_y$ | Loss value ($/MWh) |
| $d$ | Discount rate |
| $E_{BESk}$ | Total energy stored in the BES unit at bus $k$ |
| $E_{PV}^{unit}$ | Amount of PV module generated energy |
| $EI_y$ | Emission incentive ($/year) |
| $E_{loss}$ | Total annual system energy loss, MWh |
| $E_{PV_k}^{GRID}$ | Amount of PV energy delivering to the grid at bus $k$ |
| $E_{(PV+BES)}$ | Energy amount of a combination of PV and BES units |
| $ILP$, $ILQ$ | Active and reactive power loss indices, respectively |
| $IMO$ | Multi-objective index |
| $I_{ai}$ | Active current of branch $i$ |
| $I_{ak}$ | Active current of DG unit at bus $k$ |
| $I_i$ | Current magnitude of branch $i$, $I_i = \sqrt{I_{ai}^2 + I_{ri}^2}$ |
| $I_{ri}$ | Reactive current of branch $i$ |
| $I_{rk}$ | Reactive current of DG unit at bus $k$ |
| $IRR$ | Internal rate of return |
| $IVD$ | Voltage deviation index |
| $LF$ | Load factor |
| $LI_y$ | Loss incentive ($/year) |
| $n$ | Number of branches |
| $N$ | Number of buses |
| $ND$ | Network deferral benefit ($/kW) |
| $NPV$ | Net present value |
| $N_y$ | Planning horizon (years) |
| $OM_y$ | Annual operation, maintenance and fuel costs ($/year) |
| $opf_{DGi}$ | Optimal power factor of DG unit at bus $i$ |
| $pf_{DGi}$ | Power factor of DG unit at bus $i$ |
| $P_{BESk}^{CH}$ and $P_{BESk}^{DISCH}$ | Charge and discharge power of the BES unit at bus $k$, respectively |
| $P_{bi}$, $Q_{bi}$ | Active and reactive power flow through branch $i$ respectively |
| $P_{DGi}$, $Q_{DGi}$, $S_{DGi}$ | Active, reactive and apparent power sizes of DG unit, respectively at bus $i$ |
| $P_{Di}$, $Q_{Di}$ | Active and reactive power of load, respectively at bus $i$ |
| $P_i$, $Q_i$ | Net active and reactive power injections, respectively at bus $i$ |
| $P_k$, $Q_k$ | Active and reactive power of the combination of PV and BES units at bus $k$ |

| | |
|---|---|
| $P_L$, $Q_L$ | Total system active and reactive power losses without DG unit (MW), respectively |
| $P_{LDG}$, $Q_{LDG}$ | Total system active and reactive power losses with DG unit (MW), respectively |
| $P_{PV}^{unit}$ | Maximum output of a PV module unit |
| *p.u. demand(t)* | Demand in p.u. at period $t$ |
| *p.u. DG ouput(t)* | DG output in p.u. at period $t$ |
| $R_i$, $X_i$ | Resistance and reactance of branch $i$ |
| $R_y$ | Annual energy sales ($/year) |
| $TE_y$ | Annual emission target level of the system without DG ($TonCO_2$) |
| $TLoss_y$ | Annual energy loss target level of the system without DG (MWh) |
| $VD$ | Voltage deviation |
| $V_i$, $\delta_i$ | Voltage and angle, respectively at bus $i$ |
| $Z_{ij}$ | $ij_{th}$ element of impedance matrix ($Z_{ij} = r_{ij} + jx_{ij}$) |
| $\alpha_{ij}$, $\beta_{ij}$ | Loss coefficients |
| $\delta$ | Growth rate of demand a year |
| $\Delta AVSM$ | An increase in the average voltage stability margin |
| $\Delta E$ | Energy loss reduction |
| $\Delta P_{loss}$ | System loss reduction due to DG injection, kW |
| $\Delta t$ | Time duration, h |
| $\lambda_{max}$ | Maximum loading |
| $\rho$ | Probability of the solar irradiance |
| $\eta_{BES}$ | Round trip efficiency ($\eta_{BES} = \eta_c \times \eta_d$) |
| $\eta_c$, $\eta_d$ | Charge and discharge efficiencies of the BES unit |

# Chapter 1
# Introduction

## 1.1 DG History

Distributed Generation (DG) based on renewable resources such as solar, wind, ocean, hydro, biomass and geothermal heat are considered as green power because of the negligible impact on greenhouse gas emissions. Such sources have emerged as an alternative energy solution to mitigating the dependence on fossil fuels since the mid-1970s after the first oil crisis [1]. However, during this period, due to its high energy production costs along with a lack of incentives from power utilities and governments, renewable DG remained relatively dormant until the mid-2000s [2].

There has been a renewed interest in the deployment of renewable DG since the mid-2000s when the issue of global warming came to the forefront of concerns by many parts of the world [2]. In addition, the technical and economic benefits, government incentives, and advancements in the technologies have lead to a significantly increased interest in the usage of renewable DG worldwide. For example, as of 2014, renewable energy supplied an approximately 22.8% of the global energy consumption [3]. Among all renewable technologies, solar photovoltaic (PV) grew the fastest with a yearly increase of 58% worldwide during the period of late 2006–2011 and achieved just over 178 GW of the global installed capacity in 2014 [4]. It is expected that this figure will increase to more than 540 GW by 2019. This resource is popularly used in Germany and Italy. Wind energy is growing globally at a yearly rate of 44%, and was just more than 370 GW of the global capacity at the end of 2014 [3]. Such a resource is popularly used in Europe, Asia, and the United States.

From the utilities' perspective, intermittent renewable DG units (e.g., wind and solar) located close to loads in distribution systems can create several economic, technical and environmental benefits. However, the high penetration of such resources, together with demand variations has introduced many challenges to distribution networks such as power fluctuations, high losses, voltage rises and low voltage stability [5]. Consequently, in the last decade, the grid codes in many



N. Mithulananthan et al., *Intelligent Network Integration of Distributed Renewable Generation*, Green Energy and Technology,
DOI 10.1007/978-3-319-49271-1_1

countries such as the United State, Germany, the United Kingdom, Denmark, Australia and Spain have been modified to accommodate such resources [6]. This modification has also aimed at modernizing the electric power grid to satisfy the demand for higher energy efficiency, reliability and security of the system. Meanwhile, the concept of the smart grid has been introduced as an important part of this modification to facilitate high penetration of renewable DG [7]. The smart grid is a complicated infrastructure as a combination of power systems, telecommunication and information technology. As an integral part of the smart grid, an intelligent integration approach is presented in this book. The main idea behind the intelligent integration is to accommodate and operate renewable DG coordinated with Battery Energy Storage (BES) units and Electric Vehicles (EVs) in distribution networks strategically by considering various technical, economic and environmental issues.

## 1.2 DG Definitions

Distributed Generation (DG) can be defined as "small-scale generating units located close to the loads that are being served" [8]. It is possible to classify DG technologies into two broad categories: non-renewable and renewable energy sources [9]. The former comprises reciprocating engines, combustion gas turbines, micro-turbines, fuel cells, and micro Combined Heat and Power (CHP) plants. The latter includes biomass, wind, solar PV, geothermal and tide power plants.

## 1.3 DG Technologies

### *1.3.1 Solar Photovoltaic*

Solar PV technologies use some of the properties of semiconductors to directly convert sunlight into electricity [1]. The advantages are that these technologies are characterized by zero emissions, silent operation, and a long life service. They also require low maintenance and no fuel costs. In addition, solar energy is redundant and inexhaustible. However, it is weather-dependent, intermittent and unavailable at nighttime. Given a high PV penetration level together with demand variations, power distribution systems would experience power fluctuations along with unexpected voltage rises, high losses and low voltage stability. Another drawback is that PV technologies require a high-capital investment cost.

### 1.3.2 Wind Turbines

Wind turbines are devices that convert kinetic energy from the wind into electricity. They can be classified into two types: vertical axis wind turbines and horizontal axis wind turbines [1]. Like solar PV, wind turbines are emissions free and require no fuel costs. Wind energy is also redundant and inexhaustible. However, the main challenges are that wind turbines have an unpredictable and intermittent output, and a high-capital investment cost. In addition, the simultaneous occurrence of excessive wind generation and low demand could lead to the possibility of encountering voltage rises, high losses and low voltage stability in power distribution systems.

### 1.3.3 Biomass Gas Turbines

Biomass power plants can generate electricity using a steam cycle where biomass raw materials such as waste are converted into steam in a boiler [1]. The resulting steam is then used to spin a turbine which is connected to a generator. Alternatively, biomass materials can be converted to biogas. This biogas can be cleaned and upgraded to natural gas standards when it becomes bio methane. The biogas can be used in gas turbines, piston-driven engines or fuel cells to generate electricity. The advantage is that as a renewable energy source, biomass-based power plants produce low emission.

As reported in [10], gas turbines have smaller sizes than any other source of rotating power and provide higher reliability than reciprocating engines. They also have superior response to load variations and excellent steady state frequency regulation when compared to steam turbines or reciprocating engines. In addition, gas turbines require lower maintenance and produce lower emissions than reciprocating engines.

### 1.3.4 Battery Energy Storage

In addition to the wind, solar PV and biomass presented above, energy storage is also considered in this book. This source is becoming a crucial component in the distribution system, especially in the smart grid, to enhance the reliability, efficiency and sustainability. More importantly, energy storage can support to accommodate a higher penetration level of intermittent renewable DG.

Energy storage is being developed in a variety of solutions such as batteries, flywheels, ultracapacitors and superconducting energy storage systems. Among them, Battery Energy Storage (BES) has recently emerged as one of the most promising near-term storage technologies for power applications [11]. There are a number of leading battery technologies such as lead-acid, nickel cadmium, nickel-metal hydride and lithium iron. Among them, the lead-acid battery is the

oldest, most mature technology, and low investment costs [12]. Another advantage is that it can be designed for bulk energy storage or for rapid charge and discharge; however, it is limited in terms of low energy efficiency and a short life cycle [11]. The rest of the battery technologies also present promise for energy storage applications. These technologies have higher energy density capabilities than lead-acid batteries, but they are currently not cost-effective for higher power applications [11].

## 1.4 Renewable DG Integration

From the perspective of utilities, DG units can bring multiple technical benefits to distribution networks such as loss reduction, voltage profile improvement, voltage stability, network upgrade deferral and reliability while supplying energy sales as a primary task. These can be classified into three major categories: economic, technical and environmental benefits, as illustrated in Fig. 1.1. In addition, DG units can participate into the competitive market to provide ancillary services such as spinning reserve, voltage regulation, reactive power support and frequency control [13–15]. However, the inappropriate planning and operations of these resources may lead to high losses, voltage rises and low system stability as a result of reverse power flows [5, 16]. Consequently, it is necessary to develop proper methodologies to accommodate renewable DG resources.

DG planning considering various technical, economic and environmental issues has been discussed considerably over the last fifty-years [17]. The aim of researches is to bring a wide variety of benefits shown in Fig. 1.1 to distribution systems while satisfying technical constraints such as penetration levels, bus voltages and feeder thermal capacity. Some of the relevant methodologies found in the literature are reported below.

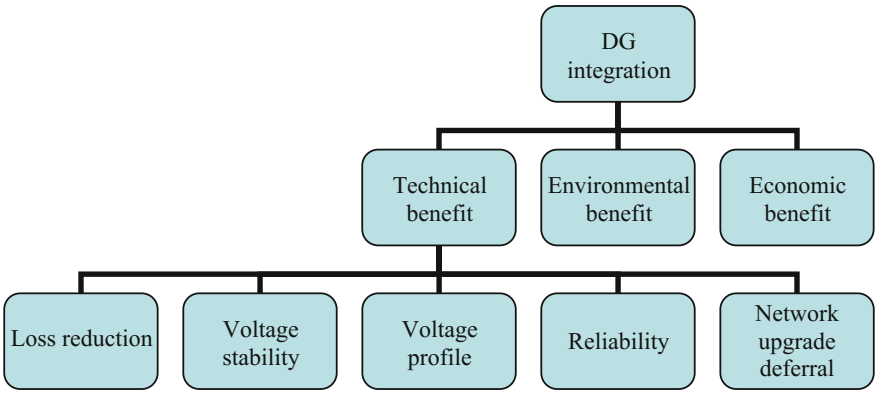


**Fig. 1.1** Overall DG benefits

## *1.4.1 Technical Benefits*

### 1.4.1.1 Energy Losses

The distribution system is well-known for its high *R*/*X* ratio and significant voltage drops that could cause substantial power losses along the feeders. It is added that the distribution system incurs a power loss which is normally higher than the transmission system. For instance, a study in [18] has showed that an American Electric Power's distribution system incurred a loss in the range of 6–8% when compared to the transmission loss of 2.5–7.5%. This figure would be much higher in radial distribution systems with a high *R*/*X* ratio. Consequently, distribution loss reduction has been one of the greatest challenges to power distribution utilities worldwide, both in matured and growing power systems. Power losses leading to energy losses could be significant if a long term and life span of plants and systems are considered. It is necessary to study the loss reduction at the distribution system level.

Loss reduction at the distribution system level is one of the major benefits due to its impact on the utilities' revenue. In addition, as a key consideration for DG planning, the loss reduction can lead to positive impacts on system capacity release, voltage profiles and voltage stability [19]. DG planning methods for minimising losses can be classified into two groups, namely *power* and *energy losses*.

The optimal DG placement and sizing issues for minimising *power losses* in distribution networks have attracted great attention in recent years. Most traditional methods have assumed that DG units are dispatchable and placed at the peak load [20]. Typical examples for such researches are analytical methods [21–25], numerical approaches [19, 26, 27] and a wide range of heuristic algorithms such as Simulated Annealing (SA) [28], Genetic Algorithm (GA) [29], Particle Swarm Optimization (PSO) [30, 31], Artificial Bee Colony (ABC) algorithm [32], Modified Teaching-Learning Based Optimization (MTLBO) [33], and Harmony Search Algorithm (HSA) [34]. However, such traditional methods may not address a practical case of the time-varying characteristics of demand and renewable generation (e.g., nondispatchable wind output) as the optimum DG size at the peak demand may not remain at other loading levels. Hence, the energy loss minimization may not be optimal.

Recently, there are two major approaches based on *time-series* and *probabilistic* models found in the literature to estimate *energy losses* in the presence of DG, especially intermittent renewable resources. For the first model, few studies have presented renewable DG integration for minimising energy losses that considers the time-varying characteristics of demand and generation. For example, wind DG units were sized using a GA-based approach [35] and an Optimal Power Flow (OPF)-based method [26], but the locations were not considered in these works. For the second model, a probabilistic planning method was introduced to accommodate renewable resources mix (i.e. biomass, wind and solar) while considering the time-varying demand and probabilistic generation [27]. The loads were assumed to follow the hourly load profile of IEEE-RTS system [36]. The probabilistic nature of

wind speed and solar irradiance was respectively described using the Weibull and Beta Probability Density Function (PDF) models [37, 38]. Biomass DG units were assumed to have constant rated outputs without associated uncertainties. A combined generation-load model was proposed to incorporate the DG output powers as multistate variables in the problem planning. In addition, a planning method that considers the probability of both demand and generation for locating and sizing wind and PV-based DG units were also reported in [19, 39]. In general, the *time-series* or *probabilistic* planning method can provide a more accurate result than the traditional planning approach presented earlier. In addition, the relevant literature review shows that most of the existing studies have assumed that DG units operate at pre-specified power factor, normally unity power factor according to the standard IEEE 1547. In such researches, only the location and size have been considered, while the optimal power factor for each DG unit that would be a crucial part for minimising energy losses has been neglected. Depending on the characteristics of loads served, each DG unit that can deliver both active and reactive power at optimal power factor may have positive impacts on energy loss reduction.

#### 1.4.1.2 Voltage Stability

The voltage stability at the transmission system level has been studied considerably over the last thirty-years [40]. Voltage instability normally occurs under heavily loaded system conditions together with a deficiency of reactive power support and this may lead to voltage collapse. At the distribution system level, the voltage instability has been identified during the last decade. For instance, a voltage instability problem in a power distribution network, which was widespread to a corresponding power transmission network, caused a major blackout in the S/SE Brazilian system in 1997 [41]. Another study has reported that under critical loading conditions in a certain industrial area, the distribution network experienced voltage collapse [42]. In recent years, due to high intermittent renewable energy penetration, sharply increased loads and the demand for higher system security, it is necessary to study the voltage stability at the distribution system level.

The placement and sizing of DG units for enhancing voltage stability in the distribution system are a new concept, but this topic has attracted the interest of some recent research efforts. Like the DG allocation as previously reported for minimising power losses, most traditional methods for enhancing voltage stability have assumed that DG units are dispatchable and placed at the peak load. Typical examples of such studies are iterative techniques based on Continuation Power Flow (CPF) [43, 44], a hybrid of model analysis and CPF [45], a power stability index-based method [46], a numerical approach [47] and heuristic algorithms such as SA [28] and PSO [48–50]. Although well-suited to accommodate dispatchable DG units such as gas turbines, the approaches presented above may not solve a practical scenario that considers the time-characteristics of the varying demand and nondispatchable renewable DG output.

Recently, a *probabilistic* planning approach was successfully developed for renewable DG allocation (i.e., biomass, wind and solar) that considers the varying-time demand and probabilistic generation [51]. This model was presented in the previous study in [27] to accommodate renewable DG units for minimising energy losses. In [51], a sensitivity technique was used for searching the candidate buses to effectively reduce the search space. However, studies [22, 47, 52] indicated that sensitivity techniques may not be effective to capture the candidate buses for DG installation on radial distribution feeders with goals of minimising losses and enhancing voltage stability. Using these techniques would also potentially limit DG penetration levels in the feeders since the most sensitive buses are normally found at the end of feeders as reported in [25, 34, 43–45, 51, 52]. Another limitation of the study in [51] as well as [28, 43–50] is that the optimal power factor for each DG unit was not considered. Depending on the nature of loads served, DG operation at optimal power factor may have positive impacts on the voltage stability.

#### 1.4.1.3 Voltage Profiles

The voltage profile issue of distribution systems, which is relevant to power quality, is normally less important than the energy loss from the viewpoint of utilities. However, in recent years, it appears that due to high intermittent renewable DG penetration, there has been an increasing interest in the voltage profile issue at the distribution system level [53].

The voltage profile is normally considered together with other technical network constraints, which can be formulated as a multiobjective optimization problem, for determining the location and size of DG units. For example, exhaustive load flow analyses were adopted to address multiobjective index [54, 55]. This index is defined as a combination of impact indices by assigning a weight for each one. These impact indices are related to active and reactive power losses, voltage drops, conductor capacity and short-circuit currents. Similarly, a study in [56] proposed a hybrid of PSO and Gravitational Search Algorithm (PSO-GSA). The aim is to minimize the multiobjective index, which is a combination of different indices related to power losses, voltage profiles, MVA capacity, emissions, and the number of DG units. Overall, a constant load model was assumed in the works presented above. However, the voltage-dependent load models also need to be examined to make a realistic case and improve the accuracy of the results.

Recently, few studies [29, 57, 58] indicated that the voltage-dependent load models (i.e., industrial, residential and commercial) considerably affect the DG penetration when compared to the constant power load model. The research in [29] presented a multiobjective optimization planning using GA to allocate a DG unit in distribution networks with different load models. The multiobjective index is a combination of various impact indices related to active and reactive power losses, system MVA capacity and voltage profiles. It was shown that DG allocation with different types of load models can produce dissimilar outcomes in terms of locations and sizes. Similarly, a multiobjective planning approach was developed using PSO

for multiple DG allocation in distribution networks with different load models [58]. The multiobjective index is a combination of different indices related to active and reactive power losses, voltage profiles, MVA capacity and short circuit levels. However, the above works assumed that DG units are dispatchable and allocated at the peak load demand. Although a research in [59] indicated the effect of time-varying load models on energy loss assessment in a distribution system with wind DG units, the optimal location and size were not addressed. Another study in [60] reported that time-varying voltage-dependent load models have a critical impact on the location and size of DG. The benefit is the energy sales from DG, while the costs are related to DG investment, operation and imported energy. However, nondispatchable renewable DG that considers time-varying load models and probabilistic generation was not reported in this work.

#### 1.4.1.4 Network Upgrade Deferral

The network upgrade deferral is the ability to defer the required investment on reinforcing feeders and transformers due to DG integration. In the last decade, it has been reported that the network upgrade deferral is an attractive option for DG planning to meet load growth [61–63]. The study in [61] showed that depending on technologies adopted, DG units have diverse impacts on the network deferral. For example, due to their intermittency, wind units have the ability to release the overloads of power networks less than CHP units. In addition, the report in [62] indicated that DG operation at lagging power factor, which delivers both active and reactive power, obtains a higher benefit than DG generation at unity and leading power factor. However, the importance of the location and size of DG units needs to be considered in DG integration.

The issues of locating and sizing DG units for deferring the distribution network investment are normally evaluated with other associated aspects such as technical and economic benefits and system constraints. For example, DG placement for maximizing the benefits of network upgrade deferral and loss reduction were reported using different approaches: hybrid GA-OPF [64], ordinal optimization [65] and Immune-Genetic Algorithm (IGA) [66]. Moreover, an OPF-based method was proposed for distribution system planning in presence of DG over a given planning horizon [67]. The objective is to minimize the costs related to feeder reinforcement, operation and energy losses. Similarly, a multiyear multiperiod OPF-based method was successfully developed for DG planning considering the network investment deferral [68, 69]. Another study in [70] developed a GA-based multiobjective framework to locate and size DG units to find the best compromise between the network upgrade deferral and the costs related to energy losses, unserved energy, and imported energy. In addition, a recent study in [71] proposed a GA-based approach to place and size renewable DG units (i.e., biomass, wind and solar) for maximizing the benefits from deferring network investments and reducing energy losses and interruption costs. The probability of renewable energy and the variability of demand were also incorporated in this approach.

In addition to the benefits presented above, reliability is another technical benefit that DG can bring to distribution systems. However, it was not considered in this book.

### *1.4.2 Environmental Benefits*

The global climate change agreements such as Kyoto Protocol aim at reducing greenhouse gas emissions. Three main components to emissions from electricity production are carbon dioxide ($CO_2$), nitrogen oxide ($NO_X$) and sulphur dioxide ($SO_2$). These components are emitted from the centralized power plants due to burning fossil fuels. Emissions can be lowered by increasing the amount of clean and renewable energy DG resources in power systems, thereby reducing the usage of electricity generated from centralized power plants [72]. For example, a British study estimated that CHP-based power plants reduced an estimated 41% of $CO_2$ emission in 1999 [17]. Similarly, a report on the Danish power system showed that the usage of DG contributed an emission reduction of 30% during the period of 1998–2001. However, DG technologies adopted may have a significant impact on the amount of emission reduction. For example, renewable DG technologies such as biomass, wind and solar PV produce low or zero emissions when compared to non-renewable DG technologies, which consume fossil fuels, such as fuel cells, natural gas turbine engines and micro-turbines. It is clear that increasing DG penetration in distribution systems can reduce emissions. However, the emission reduction could be limited by technical and economic restrictions and system constraints.

The literature shows that different approaches have been developed for locating and sizing DG units for maximizing emission reduction associated with technical and economic benefits while satisfying system constraints. For example, a Honey Bee mating optimization approach was proposed to reduce the emission while minimising the DG installation and operation costs, voltage deviation and energy losses [73]. Similarly, a multiobjective planning model based on an IGA approach was presented to reduce the emission while minimising the costs related to DG installation and operation, network reinforcement and imported electricity [74]. In a similar study [75], a multiobjective planning model was developed to make a trade-off between emission and cost reductions. The cost is related to DG investment and operation, energy losses and imported energy. However, the limitation of studies [73–75] is that DG units were assumed to operate as a dispatchable source without associated uncertainties. In contrast to these works, a GA-based multiobjective model was developed for wind DG planning that considers the uncertainty of generation [76]. The objective is to improve the reliability while minimising the costs related to DG investment and operation, and emission penalty.

### 1.4.3 Economic Benefits

In addition to the technical and environmental benefits from DG units thoroughly discussed above, it is necessary to consider a comprehensive work through their cost and benefit analysis including the energy sales. The monetary values converted from the technical and environmental benefits from DG units are also included in the analysis.

The literature review presented in the previous subsections shows that considerable works have been done with respect to DG planning. However, most of them have considered the cost analysis only. In addition, a study in [77] presented an approach to determine the location and number of DG units. The objective is to minimize the fuel cost and power losses. A planning framework was also developed for PV integration by reducing the investment, operation and imported energy costs [78]. Moreover, heuristic approaches were proposed to locate and size DG units with an objective of minimising the costs of investment, operation, imported energy and energy losses [79, 80]. With the same objective, a research in [81] presented a DG planning approach using PSO. However, the importance of the benefit of DG units also needs to be considered in the analysis.

A study in [82] presented a dynamic programming algorithm to place and size DG units through the cost and benefit analysis. The total cost is a sum of DG investment, operation and maintenance costs, while the total benefit is a sum of the benefits arising from reducing the power loss, imported energy and unserved energy. However, it seems that inclusion of the DG energy sales in the analysis may provide a more precise result.

Few studies have reported comprehensive frameworks for DG investment planning on the basis of the cost and benefit analysis including the energy sales from DG. For instance, a study in [8] presented a heuristic approach to locate and size DG units by maximizing the utility's profit as a function of the benefit and cost. The benefit is the energy sales, whereas the costs are related to DG investment, operation, imported energy, unserved energy, and energy losses. A research in [83] developed a GA-based cost and benefit method to accommodate DG units. The benefit is the energy sales, while the cost includes DG investment and energy loss costs. In addition, a heuristic approach was introduced to locate and size DG units through the cost and benefit analysis [84]. The benefit is the energy sales, while the costs are related to DG investment and operation, substation and feeder investments, imported energy and unserved energy.

In conclusion, the above review shows that numerous methodologies have been developed for DG integration in distribution systems, considering different aspects: technical, economic and environmental benefits. However, most of them have assumed that DG units operate at a pre-defined power factor. Depending on the nature of loads served, DG operation at optimum power factor may have positive impacts on system losses, voltage stability, and system capacity release. Moreover, a comprehensive benefit-cost study on multiple DG allocation with optimal power

factor that considers the issues of energy losses and voltage stability has not been reported in the literature. In addition, the importance of time-varying voltage-dependent load models also needs to be considered in the analysis to obtain a more realistic result.

## 1.5 Renewable DG Integration with BES

Unlike conventional technologies-based DG units such as reciprocating engines and gas turbines, PV sources are time and weather-dependent, intermittent and nondispatchable. Advances in dispatchable BES technologies provide an opportunity to make these nondispatchable PV sources dispatchable like conventional generators [85, 86]. Over the last fifteen-years, a hybrid PV and BES system has been designed for stand-alone applications [87–89]. In recent years, the hybrid of BES and PV system has been utilized as one of the most viable solutions in grid-connected applications to mitigate the impacts of PV intermittency, increase PV penetration and provide multiple benefits for utilities, customers and PV owners. This topic has attracted the interest of numbers of recent research efforts [85, 90–98]. A hybrid PV-BES system was developed for demand-side applications to enhance the system electrical efficiency [92, 93]. An optimal charging and discharging schedule of BES units utilized in a grid-connected PV system was presented for peak load shaving [94]. A study in [95] proposed a methodology to determine the size of BES units for power arbitrage and peak shaving used in a grid-connected PV system. Authors in [96] presented a methodology to size BES units for increasing PV penetration in a residential system with the objectives of voltage regulation and reductions in peak power and annual costs. A strategy for charging and discharging BES units was proposed for mitigating sudden changes in PV outputs and supporting evening peak load in residential systems [97]. A concept to regulate voltages in distribution systems with high PV penetration by controlling the output of customer-side BES units was reported in [90]. In this concept, a distribution utility is permitted to control the output of BES units during a specific time period in exchange for subsidizing a part of BES investment costs. BES units are sized and controlled to eliminate the power fluctuation of PV outputs [85, 98]. Finally, an optimal charging and discharging schedule of BES units on an hourly basis was developed to mitigate the intermittency of PV-based DG outputs by minimising energy losses [91]. Overall, the above review shows that considerable works have discussed the charging and discharging schedules and size of BES units utilized in grid-connected PV systems. However, most of the studies presented have assumed that the size of PV units utilized in hybrid PV-BES systems is pre-defined and the optimal power factor dispatch for each hybrid PV-BES unit over all periods is neglected as well. Depending on the characteristics of loads served, each PV-BES hybrid unit that can deliver active and reactive power at optimal power factor may have positive impacts on minimising energy losses and stabilizing the bus voltages of distribution systems.

## 1.6 Grid Codes for DG Integration

Under the recommendation of the current standard IEEE 1547, most of the DG units are normally designed to operate at unity power factor [99]. Consequently, an inadequacy of reactive power support for voltage regulation may exist in distribution networks, given a high DG penetration level. Conventional devices such as switchable capacitors, voltage regulators and tap changers are practically employed for automatic voltage regulation, but they are not fast enough to compensate for transient events [100, 101]. It is likely that the shortage of reactive power support may be an immediate concern at the distribution system level in the future. On the other hand, depending on time and weather variability, the simultaneous occurrence of excess intermittent renewable generation (i.e., wind and solar PV) and low demand would lead to loss of voltage regulation along with unexpected voltage-rises on the feeders due to reverse power flows [102]. As a fast response device, the inverter-based PV unit is allowed to inject or absorb reactive power to stabilize load voltages as per the new German grid code [103] while supplying energy as a primary task [101, 104]. Other technologies such as synchronous machines used in biomass power plants, and Doubly-Fed Induction Generators (DFIGs) or full converter synchronous machines employed in wind farms are also capable of controlling reactive power while supplying active power [105].

## 1.7 Outline of the Book

This book is organised as follows:

Chapter 1 provides background knowledge about DG and BES technologies, which are needed to comprehend this book. This chapter also includes an overall literature review on current approaches for DG and BES integration in distribution systems.

Chapter 2 describes the modelling of loads and renewable generation, which is used in the next chapters, including time-varying voltage dependent load models and the probability of intermittent renewable energy, namely solar and wind. The test systems used throughout this research is also briefly described in this chapter.

Chapter 3 introduces the concept of optimal DG power factor operation and its impact on power losses. This introduction provides a foundation for developing methodologies with different applications presented in the next chapters. Analytical expressions are then presented in this chapter to identify the location, size and power factor of a single DG unit with a goal of minimising power losses. These expressions are easily adapted to accommodate different types of dispatchable renewable DG units for minimizing energy losses while considering the time-varying characteristics of demand and generation. The study reveals that the

time-varying demand and generation models play a significant role in renewable DG planning. It is shown that optimal power factor operation could be one of the aspects to be considered in the strategy of smart renewable DG integration.

Chapter 4 studies the determination of nondispatchable photovoltaic (PV) penetration into distribution systems while considering time-varying voltage-dependent load models and probabilistic generation. The system loads are classified as an industrial, commercial or residential type or a mix of them with different normalised daily patterns. The Beta probability density function model is used to describe the probabilistic nature of solar irradiance. An analytical expression is proposed to size a PV unit. This expression is based on the derivation of a multiobjective index (*IMO*) that is formulated as a combination of three indices, namely active power loss, reactive power loss and voltage deviation. The *IMO* is minimised in determining the optimal size and power factor of a PV unit.

Chapter 5 discusses the integration of PV and BES units considering optimal power dispatch. In this work, each nondispatchable PV unit is converted into a dispatchable source by adding a BES unit with sufficient capacity. An analytical expression is proposed to determine the optimal size and power factor of PV and BES units for reducing energy losses and enhancing voltage stability. A self-correction algorithm is then developed for sizing multiple PV and BES units. The study indicates that a significant energy loss reduction and voltage stability enhancement can be achieved for all the proposed scenarios with DG operation at optimal power factor when compared to DG generation at unity power factor which follows the current standard IEEE 1547.

Chapter 6 presents an analytical approach to adopt plug-in hybrid EV charging stations that can support reactive power for a commercial distribution network in the presence of photovoltaic (PV) units. Such stations are employed to charge aggregated EVs parked in a public area while considering the time-varying voltage-dependent load models and the probability of PV generation and EV charging.

Chapter 7 reports a comprehensive framework for DG planning. In this framework, analytical expressions are proposed to efficiently capture the optimal power factor of each DG unit with a standard size for minimising energy losses and enhancing voltage stability. The decision for the optimal location, size and number of DG units is obtained through a benefit-cost analysis over a given planning horizon. Here, the total benefit includes energy sales, loss reduction, network investment deferral and emission reduction, while the total cost is a sum of capital, operation and maintenance expenses. It is shown that inclusion of energy loss reduction together with other benefits such as network investment deferral and emission reduction in the analysis would recover DG investments faster.

## References


1. Rahman S (2003) Green power: what is it and where can we find it? IEEE Power Energ Mag 1(1):30–37. doi:10.1109/mpae.2003.1180358
2. Mozina CJ (2010) Impact of green power distributed generation. IEEE Ind Appl Mag 16(4):55–62. doi:10.1109/mias.2010.936970
3. Renewables 2015 global status report. http://www.ren21.net/wp-content/uploads/2015/07/REN12-GSR2015_Onlinebook_low1.pdf. Assessed 19 May 2015
4. Global market outlook for solar power/2015–2019. European Photovoltaic Industry Association. http://helapco.gr/pdf/Global_Market_Outlook_2015_-2019_lr_v23.pdf. Assessed 19 May 2015
5. Katiraei F, Aguero JR (2011) Solar PV integration challenges. IEEE Power Energ Mag 9(3):62–71. doi:10.1109/mpe.2011.940579
6. Call for papers for the IEEE Transactions on Sustainable Energy special issue on large scale grid integration and regulatory issues of variable power generation. http://www.ieee-pes.org/images/large-scale-grid-integration-and-regulatory-issues-of-variable-power-generation-cfp.pdf
7. Simoes MG, Roche R, Kyriakides E, Suryanarayanan S, Blunier B, McBee KD, Nguyen PH, Ribeiro PF, Miraoui A (2012) A comparison of smart grid technologies and progresses in Europe and the U.S. IEEE Trans Ind Appl 48(4):1154–1162. doi:10.1109/tia.2012.2199730
8. El-Khattam W, Bhattacharya K, Hegazy Y, Salama MMA (2004) Optimal investment planning for distributed generation in a competitive electricity market. IEEE Trans Power Syst 19(3):1674–1684. doi:10.1109/tpwrs.2004.831699
9. Puttgen HB, MacGregor PR, Lambert FC (2003) Distributed generation: Semantic hype or the dawn of a new era? IEEE Power Energ Mag 1(1):22–29. doi:10.1109/mpae.2003.1180357
10. Willis HL, Scott WG (eds) (2000) Distributed power generation: Planning and evaluation. Marcel Dekker Inc, New York
11. Ribeiro PF, Johnson BK, Crow ML, Arsoy A, Liu Y (2001) Energy storage systems for advanced power applications. Proc IEEE 89(12):1744–1756. doi:10.1109/5.975900
12. Nair N-KC, Garimella N (2010) Battery energy storage systems: assessment for small-scale renewable energy integration. Energy Build 42(11):2124–2130. doi:10.1016/j.enbuild.2010.07.002
13. Mashhour E, Moghaddas-Tafreshi SM (2011) Bidding strategy of virtual power plant for participating in energy and spinning reserve market—Part I: problem formulation. IEEE Trans Power Syst 26(2):949–956. doi:10.1109/tpwrs.2010.2070884
14. Rueda-Medina AC, Padilha-Feltrin A (2013) Distributed generators as providers of reactive power support—a market approach. IEEE Trans Power Syst 28(1):490–502. doi:10.1109/tpwrs.2012.2202926
15. Yuen C, Oudalov A, Timbus A (2011) The provision of frequency control reserves from multiple microgrids. IEEE Trans Ind Electron 58(1):173–183. doi:10.1109/tie.2010.2041139
16. Eftekharnejad S, Vittal V, Heydt GT, Keel B, Loehr J (2013) Impact of increased penetration of photovoltaic generation on power systems. IEEE Trans Power Syst 28(2):893–901. doi:10.1109/tpwrs.2012.2216294
17. Viral R, Khatod DK (2012) Optimal planning of distributed generation systems in distribution system: A review. Renew Sustain Energy Rev 16(7):5146–5165. doi:10.1016/j.rser.2012.05.020
18. Nourai A, Kogan VI, Schafer CM (2008) Load leveling reduces T&D line losses. IEEE Trans Power Deliv 23(4):2168–2173. doi:10.1109/tpwrd.2008.921128
19. Atwa YM, El-Saadany EF (2011) Probabilistic approach for optimal allocation of wind-based distributed generation in distribution systems. IET Renew Power Gen 5(1):79–88. doi:10.1049/iet-rpg.2009.0011

20. Georgilakis PS, Hatziargyriou ND (2013) Optimal distributed generation placement in power distribution networks: Models, methods, and future research. IEEE Trans Power Syst 28(3):3420–3428. doi:10.1109/tpwrs.2012.2237043
21. Caisheng W, Nehrir MH (2004) Analytical approaches for optimal placement of distributed generation sources in power systems. IEEE Trans Power Syst 19(4):2068–2076. doi:10.1109/tpwrs.2004.836189
22. Acharya N, Mahat P, Mithulananthan N (2006) An analytical approach for DG allocation in primary distribution network. Int J Electr Power Energy Syst 28(10):669–678. doi:10.1016/j.ijepes.2006.02.013
23. Gözel T, Hocaoglu MH (2009) An analytical method for the sizing and siting of distributed generators in radial systems. Electr Power Syst Res 79(6):912–918. doi:10.1016/j.epsr.2008.12.007
24. Hung DQ, Mithulananthan N, Bansal RC (2010) Analytical expressions for DG allocation in primary distribution networks. IEEE Trans Energy Convers 25(3):814–820. doi:10.1109/TEC.2010.2044414
25. Hung DQ, Mithulananthan N (2013) Multiple distributed generator placement in primary distribution networks for loss reduction. IEEE Trans Ind Electron 60(4):1700–1708. doi:10.1109/TIE.2011.2112316
26. Ochoa LF, Harrison GP (2011) Minimizing energy losses: optimal accommodation and smart operation of renewable distributed generation. IEEE Trans Power Syst 26(1):198–205. doi:10.1109/TPWRS.2010.2049036
27. Atwa YM, El-Saadany EF, Salama MMA, Seethapathy R (2010) Optimal renewable resources mix for distribution system energy loss minimization. IEEE Trans Power Syst 25(1):360–370. doi:10.1109/TPWRS.2009.2030276
28. Injeti SK, Prema Kumar N (2013) A novel approach to identify optimal access point and capacity of multiple DGs in a small, medium and large scale radial distribution systems. Int J Electr Power Energy Syst 45(1):142–151. doi:10.1016/j.ijepes.2012.08.043
29. Singh D, Verma KS (2009) Multiobjective optimization for DG planning with load models. IEEE Trans Power Syst 24(1):427–436. doi:10.1109/TPWRS.2008.2009483
30. AlRashidi MR, AlHajri MF (2011) Optimal planning of multiple distributed generation sources in distribution networks: a new approach. Energy Convers Manage 52(11):3301–3308. doi:10.1016/j.enconman.2011.06.001
31. Kansal S, Kumar V, Tyagi B (2013) Optimal placement of different type of DG sources in distribution networks. Int J Electr Power Energy Syst 53:752–760. doi:10.1016/j.ijepes.2013.05.040
32. Abu-Mouti FS, El-Hawary ME (2011) Optimal distributed generation allocation and sizing in distribution systems via artificial bee colony algorithm. IEEE Trans Power Deliv 26(4):2090–2101. doi:10.1109/TPWRD.2011.2158246
33. Martín García JA, Gil Mena AJ (2013) Optimal distributed generation location and size using a modified teaching–learning based optimization algorithm. Int J Electr Power Energy Syst 50:65–75. doi:10.1016/j.ijepes.2013.02.023
34. Rao RS, Ravindra K, Satish K, Narasimham SVL (2013) Power loss minimization in distribution system using network reconfiguration in the presence of distributed generation. IEEE Trans Power Syst 28(1):317–325. doi:10.1109/tpwrs.2012.2197227
35. Ugranlı F, Karatepe E (2013) Optimal wind turbine sizing to minimize energy loss. Int J Electr Power Energy Syst 53:656–663. doi:10.1016/j.ijepes.2013.05.035
36. Pinheiro JMS, Dornellas CRR, Schilling MT, Melo ACG, Mello JCO (1998) Probing the new IEEE reliability test system (RTS-96): HL-II assessment. IEEE Trans Power Syst 13(1):171–176. doi:10.1109/59.651632
37. Salameh ZM, Borowy BS, Amin ARA (1995) Photovoltaic module-site matching based on the capacity factors. IEEE Trans Energy Convers 10(2):326–332. doi:10.1109/60.391899
38. Boyle G (ed) (2004) Renewable energy. Oxford University Press, Oxford, UK

39. Khatod DK, Pant V, Sharma J (2013) Evolutionary programming based optimal placement of renewable distributed generators. IEEE Trans Power Syst 28(2):683–695. doi:10.1109/tpwrs.2012.2211044
40. Ajjarapu V, Lee B (1998) Bibliography on voltage stability. IEEE Trans Power Syst 13 (1):115–125. doi:10.1109/59.651622
41. Prada RB, Souza LJ (1998) Voltage stability and thermal limit: constraints on the maximum loading of electrical energy distribution feeders. IEE Proc Gen, Transm Distrib 145(5):573–577. doi:10.1049/ip-gtd:19982186
42. Chakravorty M, Das D (2001) Voltage stability analysis of radial distribution networks. Int J Electr Power Energy Syst 23(2):129–135. doi:10.1016/S0142-0615(00)00040-5
43. Hedayati H, Nabaviniaki SA, Akbarimajd A (2008) A method for placement of DG units in distribution networks. IEEE Trans Power Deliv 23(3):1620–1628. doi:10.1109/tpwrd.2007.916106
44. Hemdan NGA, Kurrat M (2009) Allocation of decentralized generators in distribution networks for enhancing normal operation loadability. In: IEEE Bucharest PowerTech, 28 June 2009–2 July 2009, pp 1–7. doi:10.1109/ptc.2009.5281890
45. Ettehadi M, Ghasemi H, Vaez-Zadeh S (2013) Voltage stability-based DG placement in distribution networks. IEEE Trans Power Deliv 28(1):171–178. doi:10.1109/tpwrd.2012.2214241
46. Aman MM, Jasmon GB, Mokhlis H, Bakar AHA (2012) Optimal placement and sizing of a DG based on a new power stability index and line losses. Int J Electr Power Energy Syst 43 (1):1296–1304. doi:10.1016/j.ijepes.2012.05.053
47. Esmaili M (2013) Placement of minimum distributed generation units observing power losses and voltage stability with network constraints. IET Gen, Transm Distrib 7(8). doi:10.1049/iet-gtd.2013.0140
48. Aman MM, Jasmon GB, Bakar AHA, Mokhlis H (2013) A new approach for optimum DG placement and sizing based on voltage stability maximization and minimization of power losses. Energy Convers Manage 70:202–210. doi:10.1016/j.enconman.2013.02.015
49. Kayal P, Chanda CK (2013) Placement of wind and solar based DGs in distribution system for power loss minimization and voltage stability improvement. Int J Electr Power Energy Syst 53:795–809. doi:10.1016/j.ijepes.2013.05.047
50. Hien NC, Mithulananthan N, Bansal RC (2013) Location and sizing of distributed generation units for loadabilty enhancement in primary feeder. IEEE Syst J 7(4):797–806. doi:10.1109/jsyst.2012.2234396
51. Al Abri RS, El-Saadany EF, Atwa YM (2013) Optimal placement and sizing method to improve the voltage stability margin in a distribution system using distributed generation. IEEE Trans Power Syst 28(1):326–334. doi:10.1109/tpwrs.2012.2200049
52. Kollu R, Rayapudi SR, Sadhu VLN (2014) A novel method for optimal placement of distributed generation in distribution systems using HSDO. Int Trans Electr Energy Syst 24 (4):547–561. doi:10.1002/etep.1710
53. Tan W-S, Hassan MY, Majid MS, Abdul Rahman H (2013) Optimal distributed renewable generation planning: a review of different approaches. Renew Sustain Energy Rev 18:626–645. doi:10.1016/j.rser.2012.10.039
54. Ochoa LF, Padilha-Feltrin A, Harrison GP (2006) Evaluating distributed generation impacts with a multiobjective index. IEEE Trans Power Deliv 21(3):1452–1458. doi:10.1109/TPWRD.2005.860262
55. Ochoa LF, Padilha-Feltrin A, Harrison GP (2008) Evaluating distributed time-varying generation through a multiobjective index. IEEE Trans Power Deliv 23(2):1132–1138. doi:10.1109/TPWRD.2008.915791
56. Wen Shan T, Hassan MY, Rahman HA, Abdullah MP, Hussin F (2013) Multi-distributed generation planning using hybrid particle swarm optimisation-gravitational search algorithm including voltage rise issue. IET Gen Transm Distrib 7(9):929–942. doi:10.1049/iet-gtd.2013.0050

57. Singh D, Misra RK (2007) Effect of load models in distributed generation planning. IEEE Trans Power Syst 22(4):2204–2212. doi:10.1109/TPWRS.2007.907582
58. El-Zonkoly AM (2011) Optimal placement of multi-distributed generation units including different load models using particle swarm optimisation. IET Gen Transm Distrib 5(7):760–771. doi:10.1049/iet-gtd.2010.0676
59. Qian K, Zhou C, Allan M, Yuan Y (2011) Effect of load models on assessment of energy losses in distributed generation planning. Int J Electr Power Energy Syst 33(6):1243–1250. doi:10.1016/j.ijepes.2011.04.003
60. Ebrahimi R, Ehsan M, Nouri H (2013) A profit-centric strategy for distributed generation planning considering time varying voltage dependent load demand. Int J Electr Power Energy Syst 44(1):168–178. doi:10.1016/j.ijepes.2012.07.039
61. Méndez VH, Rivier J, Fuente JIDL, Gómez T, Arceluz J, Marín J, Madurga A (2006) Impact of distributed generation on distribution investment deferral. Int J Electr Power Energy Syst 28(4):244–252. doi:10.1016/j.ijepes.2005.11.016
62. Gil HA, Joos G (2006) On the quantification of the network capacity deferral value of distributed generation. IEEE Trans Power Syst 21(4):1592–1599. doi:10.1109/tpwrs.2006.881158
63. Favuzza S, Graditi G, Ippolito MG, Sanseverino ER (2007) Optimal electrical distribution systems reinforcement planning using gas micro turbines by dynamic ant colony search algorithm. IEEE Trans Power Syst 22(2):580–587. doi:10.1109/tpwrs.2007.894861
64. Harrison GP, Piccolo A, Siano P, Wallace AR (2008) Hybrid GA and OPF evaluation of network capacity for distributed generation connections. Electr Power Syst Res 78(3):392–398. doi:10.1016/j.epsr.2007.03.008
65. Jabr RA, Pal BC (2009) Ordinal optimisation approach for locating and sizing of distributed generation. IET Gen Transm Distrib 3(8):713–723. doi:10.1049/iet-gtd.2009.0019
66. Soroudi A, Ehsan M (2011) Efficient immune-GA method for DNOs in sizing and placement of distributed generation units. Eur Trans Electr Power 21(3):1361–1375. doi:10.1002/etep.501
67. Naderi E, Seifi H, Sepasian MS (2012) A dynamic approach for distribution system planning considering distributed generation. IEEE Trans Power Deliv 27(3):1313–1322. doi:10.1109/tpwrd.2012.2194744
68. Siano P, Ochoa LF, Harrison GP, Piccolo A (2009) Assessing the strategic benefits of distributed generation ownership for DNOs. IET Gen Transm Distrib 3(3):225–236. doi:10.1049/iet-gtd:20080235
69. Piccolo A, Siano P (2009) Evaluating the impact of network investment deferral on distributed generation expansion. IEEE Trans Power Syst 24(3):1559–1567. doi:10.1109/tpwrs.2009.2022973
70. Celli G, Ghiani E, Mocci S, Pilo F (2005) A multiobjective evolutionary algorithm for the sizing and siting of distributed generation. IEEE Trans Power Syst 20(2):750–757. doi:10.1109/tpwrs.2005.846219
71. Shaaban MF, Atwa YM, El-Saadany EF (2013) DG allocation for benefit maximization in distribution networks. IEEE Trans Power Syst 28(2):639–649. doi:10.1109/tpwrs.2012.2213309
72. Tsikalakis AG, Hatziargyriou ND (2007) Environmental benefits of distributed generation with and without emissions trading. Energy Policy 35(6):3395–3409. doi:10.1016/j.enpol.2006.11.022
73. Niknam T, Taheri SI, Aghaei J, Tabatabaei S, Nayeripour M (2011) A modified honey bee mating optimization algorithm for multiobjective placement of renewable energy resources. Appl Energy 88(12):4817–4830. doi:10.1016/j.apenergy.2011.06.023
74. Soroudi A, Ehsan M, Zareipour H (2011) A practical eco-environmental distribution network planning model including fuel cells and non-renewable distributed energy resources. Renew Energy 36(1):179–188. doi:10.1016/j.renene.2010.06.019

75. Vahidinasab V (2014) Optimal distributed energy resources planning in a competitive electricity market: multiobjective optimization and probabilistic design. Renew Energy 66:354–363. doi:10.1016/j.renene.2013.12.042
76. Tongdan J, Yu T, Cai Wen Z, Coit DW (2013) Multicriteria planning for distributed wind generation under strategic maintenance. IEEE Trans Power Deliv 28(1):357–367. doi:10.1109/tpwrd.2012.2222936
77. Kumar A, Gao W (2010) Optimal distributed generation location using mixed integer non-linear programming in hybrid electricity markets. IET Gen Transm Distrib 4(2):281–298. doi:10.1049/iet-gtd.2009.0026
78. Kucuksari S, Khaleghi AM, Hamidi M, Zhang Y, Szidarovszky F, Bayraksan G, Son Y-J (2014) An Integrated GIS, optimization and simulation framework for optimal PV size and location in campus area environments. Appl Energy 113:1601–1613. doi:10.1016/j.apenergy.2013.09.002
79. El-Khattam W, Hegazy YG, Salama MMA (2005) An integrated distributed generation optimization model for distribution system planning. IEEE Trans Power Syst 20(2):1158–1165. doi:10.1109/PES.2005.1489232
80. Porkar S, Poure P, Abbaspour-Tehrani-fard A, Saadate S (2010) A novel optimal distribution system planning framework implementing distributed generation in a deregulated electricity market. Electr Power Syst Res 80(7):828–837. doi:10.1016/j.epsr.2009.12.008
81. Mistry KD, Roy R (2014) Enhancement of loading capacity of distribution system through distributed generator placement considering techno-economic benefits with load growth. Int J Electr Power Energy Syst 54:505–515. doi:10.1016/j.ijepes.2013.07.032
82. Khalesi N, Rezaei N, Haghifam MR (2011) DG allocation with application of dynamic programming for loss reduction and reliability improvement. Int J Electr Power Energy Syst 33(2):288–295. doi:10.1016/j.ijepes.2010.08.024
83. Akorede MF, Hizam H, Aris I, Ab Kadir MZA (2011) Effective method for optimal allocation of distributed generation units in meshed electric power systems. IET Gen Transm Distrib 5(2):276–287. doi:10.1049/iet-gtd.2010.0199
84. Bin Humayd AS, Bhattacharya K (2013) Comprehensive multi-year distribution system planning using back-propagation approach. IET Gen Transm Distrib 7(12):1415–1425. doi:10.1049/iet-gtd.2012.0706
85. Teleke S, Baran ME, Bhattacharya S, Huang AQ (2010) Rule-based control of battery energy storage for dispatching intermittent renewable sources. IEEE Trans Sustain Energy 1(3):117–124. doi:10.1109/tste.2010.2061880
86. Hill CA, Such MC, Dongmei C, Gonzalez J, Grady WM (2012) Battery energy storage for enabling integration of distributed solar power generation. IEEE Trans Smart Grid 3(2):850–857. doi:10.1109/tsg.2012.2190113
87. Borowy BS, Salameh ZM (1996) Methodology for optimally sizing the combination of a battery bank and PV array in a wind/PV hybrid system. IEEE Trans Energy Convers 11(2):367–375. doi:10.1109/60.507648
88. Ekren O, Ekren BY (2008) Size optimization of a PV/wind hybrid energy conversion system with battery storage using response surface methodology. Appl Energy 85(11):1086–1101. doi:10.1016/j.apenergy.2008.02.016
89. Avril S, Arnaud G, Florentin A, Vinard M (2010) Multi-objective optimization of batteries and hydrogen storage technologies for remote photovoltaic systems. Energy 35(12):5300–5308. doi:10.1016/j.energy.2010.07.033
90. Sugihara H, Yokoyama K, Saeki O, Tsuji K, Funaki T (2013) Economic and efficient voltage management using customer-owned energy storage systems in a distribution network with high penetration of photovoltaic systems. IEEE Trans Power Syst 28(1):102–111. doi:10.1109/tpwrs.2012.2196529
91. Teng JH, Luan SW, Lee DJ, Huang YQ (2013) Optimal charging/discharging scheduling of battery storage systems for distribution systems interconnected with sizeable PV generation systems. IEEE Trans Power Syst 28(2):1425–1433. doi:10.1109/tpwrs.2012.2230276

92. Castillo-Cagigal M, Gutiérrez A, Monasterio-Huelin F, Caamaño-Martín E, Masa D, Jiménez-Leube J (2011) A semi-distributed electric demand-side management system with PV generation for self-consumption enhancement. Energy Convers Manage 52(7):2659–2666. doi:10.1016/j.enconman.2011.01.017
93. Wei-Fu S, Shyh-Jier H, Chin EL (2001) Economic analysis for demand-side hybrid photovoltaic and battery energy storage system. IEEE Trans Ind Appl 37(1):171–177. doi:10.1109/28.903143
94. Nottrott A, Kleissl J, Washom B (2013) Energy dispatch schedule optimization and cost benefit analysis for grid-connected, photovoltaic-battery storage systems. Renew Energy 55:230–240. doi:10.1016/j.renene.2012.12.036
95. Yu R, Kleissl J, Martinez S (2013) Storage size determination for grid-connected photovoltaic systems. IEEE Trans Sustain Energy 4(1):68–81. doi:10.1109/tste.2012.2199339
96. Tant J, Geth F, Six D, Tant P, Driesen J (2013) Multiobjective battery storage to improve PV integration in residential distribution grids. IEEE Trans Sustain Energy 4(1):182–191. doi:10.1109/tste.2012.2211387
97. Alam MJE, Muttaqi KM, Sutanto D (2013) Mitigation of rooftop solar PV impacts and evening peak support by managing available capacity of distributed energy storage systems. IEEE Trans Power Syst 28(4):3874–3884. doi:10.1109/tpwrs.2013.2259269
98. Daud MZ, Mohamed A, Hannan MA (2013) An improved control method of battery energy storage system for hourly dispatch of photovoltaic power sources. Energy Convers Manage 73:256–270. doi:10.1016/j.enconman.2013.04.013
99. IEEE 1547 Standard for interconnecting distributed resources with electric power systems (2003). doi:10.1109/ieeestd.2003.94285
100. Yeh HG, Gayme DF, Low SH (2012) Adaptive VAr control for distribution circuits with photovoltaic generators. IEEE Trans Power Syst 27(3):1656–1663. doi:10.1109/tpwrs.2012.2183151
101. Turitsyn K, Sulc P, Backhaus S, Chertkov M (2011) Options for control of reactive power by distributed photovoltaic generators. Proc IEEE 99(6):1063–1073. doi:10.1109/JPROC.2011.2116750
102. Thomson M, Infield DG (2007) Network power-flow analysis for a high penetration of distributed generation. IEEE Trans Power Syst 22(3):1157–1162. doi:10.1109/tpwrs.2007.901290
103. Samadi A, Ghandhari M, Söder L (2012) Reactive power dynamic assessment of a PV system in a distribution grid. Energy Proc 20:98–107. doi:10.1016/j.egypro.2012.03.012
104. Albuquerque FL, Moraes AJ, Guimarães GC, Sanhueza SMR, Vaz AR (2010) Photovoltaic solar system connected to the electric power grid operating as active power generator and reactive power compensator. Sol Energy 84(7):1310–1317. doi:10.1016/j.solener.2010.04.011
105. Blaabjerg F, Teodorescu R, Liserre M, Timbus AV (2006) Overview of control and grid synchronization for distributed power generation systems. IEEE Trans Ind Electron 53(5):1398–1409. doi:10.1109/TIE.2006.881997

# Chapter 2
# Distribution System Modelling

## 2.1 Introduction

As discussed in this chapter, an accurate modelling of the time-varying load models can help in determining the penetration of renewable DG in a distribution system precisely. In addition, the generation characteristics of intermittent renewable resources: wind and solar, which depend on meteorological conditions (e.g., weather and temperature), should be captured correctly in DG planning.

In this chapter, different time-varying voltage dependent load models are first defined. The generation characteristics of renewable DG (i.e., solar PV, wind and biomass) and BES are next presented. Finally, three different distribution test systems used throughout in this study are also described.

## 2.2 Load Modelling

The time-varying voltage-dependent load model or the time-varying load model is defined as a load model, which is dependent on the time and voltage. Accordingly, the voltage dependent load model in [1] which incorporates time-varying loads at period $t$ can be expressed as follows:

$$P_k(t) = P_{ok}(t) \times V_k^{n_p}(t); \quad Q_k(t) = Q_{ok}(t) \times V_k^{n_q}(t) \tag{2.1}$$

where $P_k$ and $Q_k$ are respectively the active and reactive power injections at bus $k$, $P_{ok}$ and $Q_{ok}$ are respectively the active and reactive load at bus $k$ at nominal voltage; $V_k$ is the voltage at bus $k$; $n_p$ and $n_q$ are, respectively, the active and reactive load voltage exponents as given in Table 2.1 [1].



N. Mithulananthan et al., *Intelligent Network Integration of Distributed Renewable Generation*, Green Energy and Technology,
DOI 10.1007/978-3-319-49271-1_2

**Table 2.1** Load types and exponents for voltage-dependent loads

| Load types | $n_p$ | $n_q$ |
|---|---|---|
| Constant | 0 | 0 |
| Industrial | 0.18 | 6.00 |
| Residential | 0.92 | 4.04 |
| Commercial | 1.51 | 3.40 |

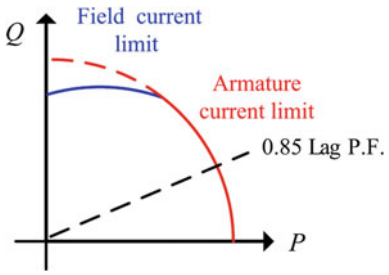


**Fig. 2.1** Synchronous machine-based DG capability curve [2]

## 2.3 Generation Modelling

Renewable resources (i.e., solar, wind and biomass) and BES are considered in this book. They can be classified into two major categories: dispatchable and nondispatchable generation as far as their capability of energy delivery is concerned. DG units are considered as a dispatchable source, if its output power can be controlled at a fixed output automatically, typically by varying the rate of fuel consumption. This includes generation technologies such as biomass-based gas turbines and small hydro power plants. In contrast, DG units are considered as a nondispatchable source, if its output power cannot be automatically controlled and totally depends on weather conditions (e.g., wind speed and solar irradiance). Solar PV and wind turbines are examples of such generation technologies.

### *2.3.1 Biomass*

Biogas produced from biomass raw materials or steam produced from the heat by burning biomass can be used to run steam or gas turbines, which are connected to synchronous machines. These machines can be dispatched according to the load demand curve. The reactive generation by the synchronous machines is limited by armature and field currents as illustrated in Fig. 2.1 [2].

### 2.3.2 Solar Irradiance

The probabilistic nature of solar irradiance can be described using the Beta Probability Density Function (PDF) [3]. This model has been employed in many PV studies such as [4–7]. Over each period (e.g., 1 h), the PDF for solar irradiance $s$ can be expressed as follows:

$$f_b(s) = \begin{cases} \frac{\Gamma(\alpha+\beta)}{\Gamma(\alpha)\Gamma(\beta)} s^{(\alpha-1)}(1-s)^{(\beta-1)} & 0 \le s \le 1,\ \alpha,\ \beta \ge 0 \\ 0 & otherwise \end{cases} \tag{2.2}$$

where $f_b(s)$ is the Beta distribution function of $s$, $s$ is the random variable of solar irradiance (kW/m$^2$); $\alpha$ and $\beta$ are parameters of $f_b(s)$, which are calculated using the mean ($\mu$) and standard deviation ($\sigma$) of $s$ as follows:

$$\beta = (1-\mu)\left(\frac{\mu(1+\mu)}{\sigma^2} - 1\right);\ \alpha = \frac{\mu \times \beta}{1-\mu}.$$

The output power from the PV module at solar irradiance $s$, $P_{PV_o}(s)$ can be expressed as follows [4–6]:

$$P_{PV_o}(s) = N \times FF \times V_y \times I_y \tag{2.3}$$

where

$$FF = \frac{V_{MPP} \times I_{MPP}}{V_{oc} \times I_{sc}};\ V_y = V_{oc} - K_v \times T_{cy}$$
$$I_y = s\left[I_{sc} + K_i \times \left(T_{cy} - 25\right)\right];\ T_{cy} = T_A + s\left(\frac{N_{OT} - 20}{0.8}\right).$$

Here, $N$ are the number of modules; $T_{cy}$ and $T_A$ are respectively cell and ambient temperatures (°C); $K_i$ and $K_v$ are respectively current and voltage temperature coefficients (A/°C and V/°C); $N_{OT}$ is the nominal operating temperature of cell in °C; $FF$ is fill factor; $V_{oc}$ and $I_{sc}$ are respectively the open circuit voltage (V) and short circuit current (A); $V_{MPP}$ and $I_{MPP}$ are respectively the voltage and current at maximum power point.

### 2.3.3 Wind Speed

The probabilistic nature of the wind speed can be described using the Weibull PDF [5, 8]. Over each period (e.g., 1 h), the PDF for wind speed $v$ can be expressed as follows:

$$f_w(v) = \frac{k}{c}\left(\frac{v}{c}\right)^{k-1} \exp\left[-\left(\frac{v}{c}\right)^{k}\right] \tag{2.4}$$

where $f_w(v)$ is the Weibull distribution function of $v$, $v$ is the random variable of wind speed (m/s); $k = 2$ is the shape index, $c \approx 1.128 v_m$ is the Rayleigh scale index; $v_m$ is the mean value of wind speed that is calculated using the historical data for each time period. The output power at wind speed $v$ ($P_{wo}$) can be expressed as follows [9]:

$$P_{w_o}(v) = \begin{cases} 0 & 0 \le v \le v_{ci} \\ a_0 + a_1 v + a_2 v^2 + a_3 v^3 & v_{ci} \le v \le v_r \\ P_{rated} & v_r \le v \le v_{co} \\ 0 & v_{co} \le v \end{cases} \tag{2.5}$$

where $v_{ci}$, $v_r$, and $v_{co}$ are cut in, rated and cut out speed of the wind turbine, respectively; $P_{rated}$ is the rating of wind turbine; $a_0$, $a_1$, $a_2$ and $a_3$ are the coefficients calculated using any standard curve fitting technique such as 'polyfit' routine in Matlab [9].

### 2.3.4 Battery Energy Storage

The BES unit is assumed to be connected to an AC system via bidirectional DC/AC converters that can be dispatched in all four quadrants. It can operate at any desired power factor (lagging/leading) to charge or discharge active power. In other words, the BES unit can operate as a load during charging periods and a generator during discharging periods. It can inject or absorb reactive power as well.

### 2.3.5 DG Penetration Level

The DG penetration level in percent is defined as the ratio of the total energy generated by a DG unit divided by the total energy consumed by a network.

### 2.3.6 Generation Criteria

As reported in Sect. 2.5, most of the DG units are normally designed to operate at unity power factor under the recommendation of the standard IEEE 1547, [10]. This study assumes that inverter-based PV units are allowed to inject or absorb reactive power in compliance with the new German grid code [11]. Biomass gas turbines are

modelled as synchronous machines. Wind farms are modelled as Doubly-Fed Induction Generators (DFIGs) or full converter synchronous machines. Such machines are also capable of controlling reactive power while delivering active power [12]. The relationship between the active and reactive power of a DG unit ($P_{DG}$ and $Q_{DG}$) can be expressed as [13]:

$$Q_{DG} = aP_{DG} \tag{2.6}$$

where, $a = \pm \tan(\cos^{-1}(pf_{DG}))$; $a$ is positive for the DG unit supplying reactive power and negative for the DG unit consuming reactive power; and $pf_{DG}$ is the operating power factor of the DG unit.

## 2.4 Test System Modelling

Three test distribution systems with varying sizes and complexities have been used in this book for showcasing the benefits of intelligent or smart integration of renewable energy sources. These test systems are widely used in the literature of distribution system planning and operation. Single line diagrams of the test systems along with pertinent basic information for DG planning are presented below.

### *2.4.1 33-Bus Test System*

Figure 2.2 shows a single line diagram of the 12.66 kV, 33-bus test radial distribution system. It has one feeder with four different laterals, 32 branches and a total peak load of 3715 kW and 2300 kVAr. The total loss of the base case system is

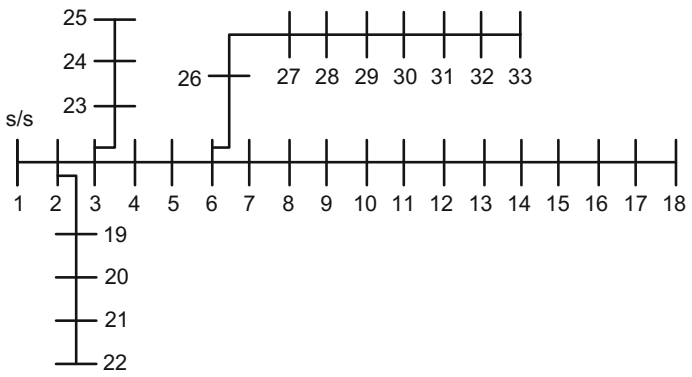


**Fig. 2.2** The 33-bus test distribution system

211.20 kW. The complete load data are given in Table A.1 (Appendix A) [14]. This system has been used in Chaps. 3, 4, 5 and 6.

### 2.4.2 69-Bus One Feeder Test System

A single line diagram of the 12.66 kV, 69-bus test radial distribution system is shown in Fig. 2.3. It has one feeder with eight laterals, 68 branches, a total peak load of 3800 kW and 2690 kVAr and its corresponding loss of 224.93 kW. Its complete load data are provided in Table A.2 (Appendix A) [15]. This system has been used in Chap. 3.

### 2.4.3 69-Bus Four Feeder Test System

Figure 2.4 shows a single line diagram of the 11 kV, 69-bus test radial distribution system, which is fed by a 6 MVA 33/11 kV transformer [16]. This system consists of four feeders with 68 branches, a total peak load of 4.47 MW and 3.06 MVAr and its corresponding loss of 227.53 kW. The complete load data of this system are provided in Table A.3 (Appendix A) [16]. This system has been used in Chap. 7.

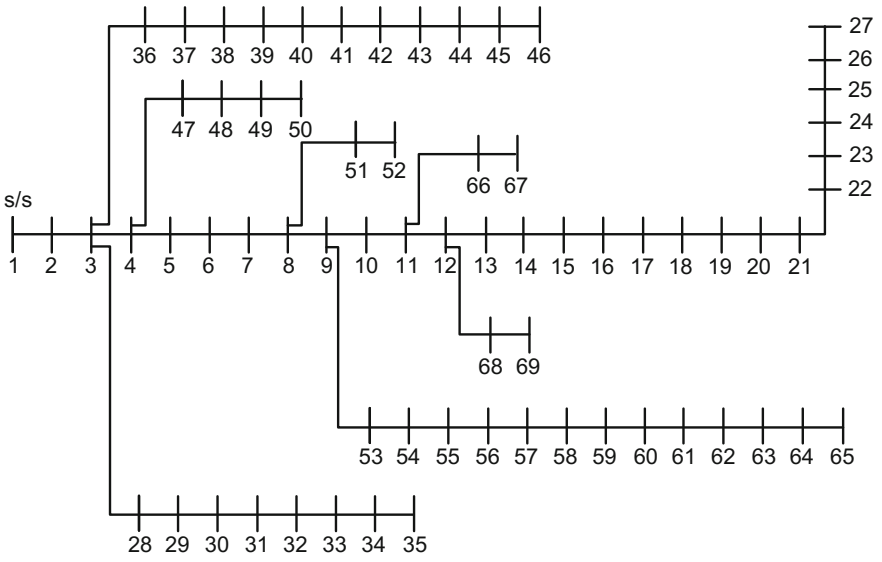


**Fig. 2.3** The 69-bus one feeder test distribution system

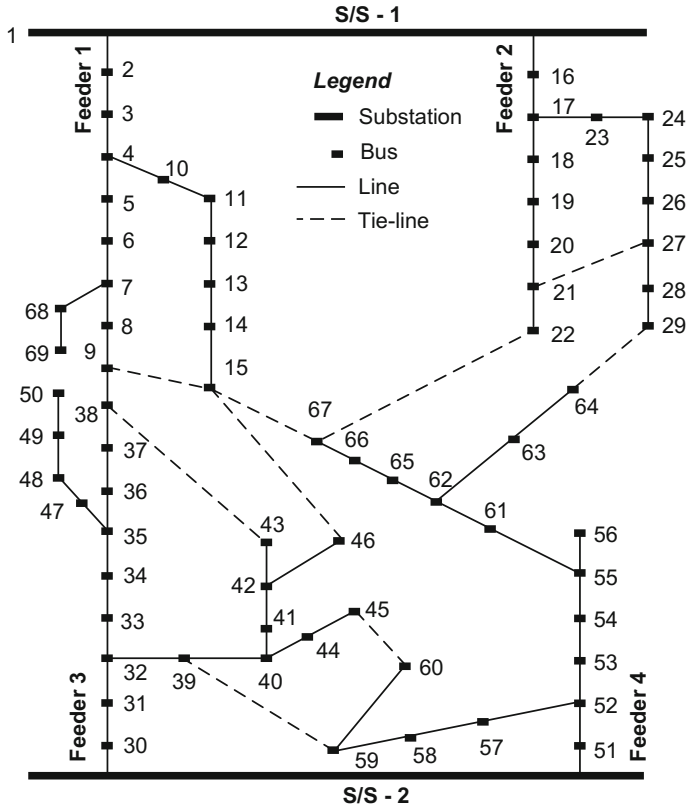


**Fig. 2.4** The 69-bus four feeders test distribution system [16]

## 2.5 Conclusions

This chapter provided a definition of time-varying voltage-dependent load models and modelling of renewable energy resources. Three test distribution systems used in the book were also explained in this chapter.

## References

1. Casper SG, Nwankpa CO, Bradish RW, Chiang H-D, Concordia C, Staron JV, Taylor CW, Vaahedi E, Wu G (1995) Bibliography on load models for power flow and dynamic performance simulation. IEEE Trans Power Syst 10(1):523–538. doi:10.1109/59.373979
2. Kundur P, Balu NJ, Lauby MG (1994) Power system stability and control. New York: McGraw-Hill

3. Salameh ZM, Borowy BS, Amin ARA (1995) Photovoltaic module-site matching based on the capacity factors. IEEE Trans Energy Convers 10(2):326–332. doi:10.1109/60.391899
4. Khatod DK, Pant V, Sharma J (2013) Evolutionary programming based optimal placement of renewable distributed generators. IEEE Trans Power Syst 28(2):683–695. doi:10.1109/tpwrs.2012.2211044
5. Atwa YM, El-Saadany EF, Salama MMA, Seethapathy R (2010) Optimal renewable resources mix for distribution system energy loss minimization. IEEE Trans Power Syst 25 (1):360–370. doi:10.1109/TPWRS.2009.2030276
6. Teng JH, Luan SW, Lee DJ, Huang YQ (2013) Optimal charging/discharging scheduling of battery storage systems for distribution systems interconnected with sizeable PV generation systems. IEEE Trans Power Syst 28(2):1425–1433. doi:10.1109/tpwrs.2012.2230276
7. Soroudi A, Aien M, Ehsan M (2012) A probabilistic modeling of photo voltaic modules and wind power generation impact on distribution networks. IEEE Syst J 6(2):254–259. doi:10.1109/jsyst.2011.2162994
8. Hemdan NGA, Kurrat M (2009) Allocation of decentralized generators in distribution networks for enhancing normal operation loadability. In: IEEE Bucharest Power Tech, June 28 2009–July 2 2009, pp 1–7. doi:10.1109/ptc.2009.5281890
9. Alternative sectoral load shapes for NEMS (2001) http://www.onlocationinc.com/LoadShapesAlternative2001.pdf
10. IEEE 1547 Standard for interconnecting distributed resources with electric power systems (2003). doi:10.1109/ieeestd.2003.94285
11. Samadi A, Ghandhari M, Söder L (2012) Reactive power dynamic assessment of a PV system in a distribution grid. Energy Procedia 20:98–107. doi:10.1016/j.egypro.2012.03.012
12. Blaabjerg F, Teodorescu R, Liserre M, Timbus AV (2006) Overview of control and grid synchronization for distributed power generation systems. IEEE Trans Industr Electron 53 (5):1398–1409. doi:10.1109/TIE.2006.881997
13. Hung DQ, Mithulananthan N, Bansal RC (2010) Analytical expressions for DG allocation in primary distribution networks. IEEE Trans Energy Convers 25(3):814–820. doi:10.1109/TEC.2010.2044414
14. Baran ME, Wu FF (1989) Network reconfiguration in distribution systems for loss reduction and load balancing. IEEE Trans Power Delivery 4(2):1401–1407. doi:10.1109/61.25627
15. Baran ME, Wu FF (1989) Optimal capacitor placement on radial distribution systems. IEEE Trans Power Delivery 4(1):725–734. doi:10.1109/61.19265
16. Das D (2006) A fuzzy multiobjective approach for network reconfiguration of distribution systems. IEEE Trans Power Delivery 21(1):202–209. doi:10.1109/tpwrd.2005.852335

# Chapter 3
# Biomass DG Integration

## 3.1 Introduction

Energy loss is one of the major concerns at the distribution system level due to its immediate impact on utilities' revenue. In addition, loss reduction can reduce power flows on distribution feeders, thus resulting in positive impacts on system capacity release, voltage profiles and voltage stability [1]. From the utilities' perspective, DG units located close to loads can significantly lower energy losses in distribution systems. However, a high penetration level of DG units can introduce many challenges to distribution systems such as power fluctuations, voltage rises, high losses and low voltage stability as a result of reverse power flows [2].

Under the current standard IEEE 1547, DG units are not allowed to supply reactive power [3]. Consequently, it is likely that the shortage of reactive power support may be an immediate concern at the distribution system level in the future with a high penetration level of DG units. Given the fact that not only does the active power, but also the reactive power injected by DG units play a significant role in enhancing system performances such as energy savings, voltage profiles, system capacity release and loadability. Depending on the nature of distribution systems, the former or the latter may be dominant. It could be highlighted that a lack of attention to reactive power support at the DG planning stage would potentially result in an increase in investment costs used to add reactive power resources and other devices at the operation stage. However, the redundancy of reactive power can lead to reverse power flows, thereby leading to high losses, voltage rises, low system stability, etc. To address those challenges, it becomes necessary to study the optimal power factor of DG units, to which the active and reactive power injections are optimized simultaneously.

This chapter investigates the impact of DG power factor operation on distribution system losses. It then presents an analytical approach to determine the optimum size and operating strategy of a dispatchable DG unit such as a synchronous machine-based biomass gas turbine to reduce power losses and a methodology to



N. Mithulananthan et al., *Intelligent Network Integration of Distributed Renewable Generation*, Green Energy and Technology,
DOI 10.1007/978-3-319-49271-1_3

identify the best location. The approach is easily adapted to accommodate DG units under different operating conditions for minimising energy losses while considering the time-varying load demand for planning purposes.

## 3.2 Load and Biomass DG Modelling

The distribution systems under the study are assumed to follow the nominalised 24-h load profile of the IEEE-RTS system as shown in Fig. 3.1 [4]. The time-varying constant P and Q load model defined in Eq. (3.1) is incorporated in the load characteristics. In this study, a biomass-based DG unit, which is modelled as a synchronous machine is considered. The output of the DG unit can be dispatched according to the nominalised load curve illustrated in Fig. 3.1, where the peak demand of 1 p.u. occurred at hour 12.

## 3.3 Power and Energy Losses

The total active and reactive power losses (i.e., $P_L$ and $Q_L$) in a distribution system with $N$ buses can be calculated by the "exact loss formula" as follows [5]:

$$P_L = \sum_{i=1}^{N} \sum_{j=1}^{N} \left[ \alpha_{ij} \left( P_i P_j + Q_i Q_j \right) + \beta_{ij} \left( Q_i P_j - P_i Q_j \right) \right] \tag{3.1}$$

$$Q_L = \sum_{i=1}^{N} \sum_{j=1}^{N} \left[ \gamma_{ij} \left( P_i P_j + Q_i Q_j \right) + \xi_{ij} \left( Q_i P_j - P_i Q_j \right) \right] \tag{3.2}$$

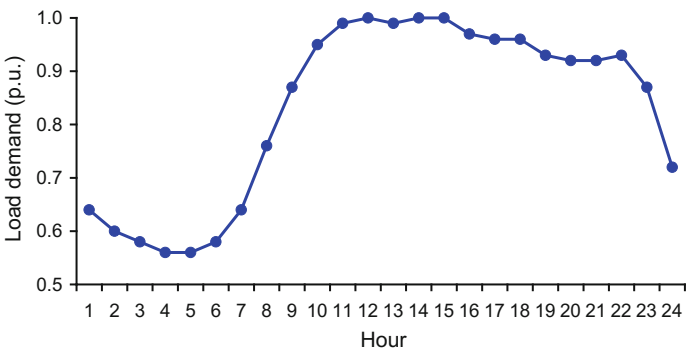


**Fig. 3.1** Normalized daily load demand curve

where

$$\alpha_{ij} = \frac{r_{ij}}{V_i V_j}\cos(\delta_i - \delta_j);\ \beta_{ij} = \frac{r_{ij}}{V_i V_j}\sin(\delta_i - \delta_j);$$
$$\gamma_{ij} = \frac{x_{ij}}{V_i V_j}\cos(\delta_i - \delta_j);\ \xi_{ij} = \frac{x_{ij}}{V_i V_j}\sin(\delta_i - \delta_j);$$

| | |
|---|---|
| $V_i\angle\delta_i$ | the complex voltage at the bus $i$th |
| $r_{ij} + jx_{ij} = Z_{ij}$ | the $ij$th element of $[Zbus]$ impedance matrix |
| $P_i$, $P_j$ | the active power injections at the $i$th and $j$th buses, respectively |
| $Q_i$, $Q_j$ | the reactive power injections at the $i$th and $j$th buses, respectively |
| $N$ | the number of buses. |

The relationship between the active and reactive power of a DG unit connected at bus $i$ in a distribution network can be expressed as follows:

$$Q_{DGi} = a_i P_{DGi} \tag{3.3}$$

where

$$a_i = (sign)\ \tan(\cos^{-1}(pf_{DGi}))$$

| | |
|---|---|
| $sign = +1$ | the DG unit injecting reactive power, |
| $sign = -1$ | the DG unit consuming reactive power, |
| $pf_{DGi}$ | the operating power factor of the DG unit at bus $i$ |
| $P_{DGi}$, $Q_{DGi}$ | the active and reactive power injections from the DG unit at bus $i$, respectively. |

The total active and reactive power injections at bus $i$ where a DG unit is installed can be written respectively as follows:

$$P_i = P_{DGi} - P_{Di} \tag{3.4}$$

$$Q_i = Q_{DGi} - Q_{Di} = a_i P_{DGi} - Q_{Di} \tag{3.5}$$

where, $P_{DGi}$ and $Q_{DGi}$ are respectively the active and reactive power injections from the DG unit at bus $i$.

Substituting Eqs. (3.4) and (3.5) into Eq. (3.1), we obtain the total active power loss with a DG unit (i.e., $P_{LDG}$) described as follows:

$$P_{LDG} = \sum_{i=1}^{N}\sum_{j=1}^{N}\left[\begin{array}{l}\alpha_{ij}\big((P_{DGi} - P_{Di})P_j + (a_i P_{DGi} - Q_{Di})Q_j\big) \\ +\beta_{ij}\big((a_i P_{DGi} - Q_{Di})P_j - (P_{DGi} - P_{Di})Q_j\big)\end{array}\right] \tag{3.6}$$

The power loss at each period $t$, $P_{loss}(t)$ can be derived from Eqs. (3.1) to (3.6) with and without DG, respectively. Hence, the total annual energy loss ($E_{loss}$) over

the total period ($T$ = 24 h) in a distribution system with a time period duration ($\Delta t$) of 1 − h can be expressed as follows:

$$E_{loss} = 365 \int_0^T P_{loss}(t)dt = 365 \sum_{t=1}^{24} P_{loss}(t)\Delta t \tag{3.7}$$

## 3.4 Sizing at Various Locations [6]

The total active power loss in a distribution system is minimized if the partial derivative of Eq. (3.6) with respect to the active power injection from the DG unit at bus $i$ becomes zero. This can be described as follows:

$$\frac{\partial P_{LDG}}{\partial P_{DGi}} = 2 \sum_{j=1}^{N} \left[\alpha_{ij}\left(P_j + a_i Q_j\right) + \beta_{ij}(a_i Pj - Qj)\right] = 0 \tag{3.8}$$

Equation (3.8) can be rearranged as follows:

$$\alpha_{ii}(P_i + a_i Q_i) + X_i + a_i Y_i = 0 \tag{3.9}$$

where

$$X_i = \sum_{\substack{j=1 \\ j \neq i}}^{N} \left(\alpha_{ij} P_j - \beta_{ij} Q_j\right); \quad Y_i = \sum_{\substack{j=1 \\ j \neq i}}^{N} \left(\alpha_{ij} Q_j + \beta_{ij} P_j\right)$$

Substituting Eqs. (3.4) and (3.5) into Eq. (3.9), we obtain the size of the DG unit at bus $i$ for minimizing the power loss as follows:

$$P_{DGi} = \frac{\alpha_{ii}(P_{Di} + a_i Q_{Di}) - X_i - a_i Y_i}{\alpha_{ii}(a_i^2 + 1)} \tag{3.10}$$

Equation (3.10) gives the optimum size of a DG unit for each bus $i$, for the loss to be minimum. Any size of DG other than $P_{DGi}$ placed at bus $i$, will lead to a higher loss. Such a loss, however, is a function of loss coefficients $\alpha$ and $\beta$. When a DG unit is installed in a distribution system, the values of the loss coefficients will change as they depend on the voltages and phase angles. Updating such values again requires another load flow calculation. However, numerical results showed that the accuracy gained in the size of the DG unit by updating the loss coefficients is small and negligible [6, 7]. With this assumption, the optimum size of DG for each bus, given by Eq. (3.10) can be calculated from the base-case power flow (i.e. without DG). This methodology requires power flow to be performed only twice,

one for the base-case and another at the end with DG included to obtain the final solution. Hence, the approach demands less computational effort.

DG units can be classified into four major types based on their terminal characteristics in terms of delivery of active and reactive power to the grid. As a synchronous machine, a biomass DG unit can operate in different manners as described below.

DG Type 1 ($pf_{DGi} = 1$, $a_i = 0$): is capable of injecting active power only. The optimal DG size for minimizing the power loss at bus $i$ can be derived from Eq. (3.10) as follows:

$$P_{DGi} = P_{Di} - \frac{1}{\alpha_{ii}} \sum_{\substack{j=1 \\ j \neq i}}^{N} \left(\alpha_{ij} P_j - \beta_{ij} Q_j\right) \tag{3.11}$$

DG Type 2 ($pf_{DGi} = 0$, $a_i = \infty$): is capable of injecting reactive power only. The optimal DG size for minimizing the power loss at bus $i$ can be derived from Eq. (3.10) as follows:

$$Q_{DGi} = Q_{Di} - \frac{1}{\alpha_{ii}} \sum_{\substack{j=1 \\ j \neq i}}^{N} \left(\alpha_{ij} Q_j + \beta_{ij} P_j\right) \tag{3.12}$$

DG Type 3 ($0 < pf_{DGi} < 1$ and $sign = +1$, i.e., lagging power factor): is capable of injecting both active and reactive power. Given a $pf_{DGi}$, the size of a DG unit can be obtained from Eq. (3.10).

DG Type 4 ($0 < pf_{DGi} < 1$ and $sign = -1$, i.e., leading power factor): is capable of injecting active power and absorbing reactive power. Given a $pf_{DGi}$, the size of a DG unit can be obtained from Eq. (3.10).

## 3.5 Estimating Power Factors at Various Locations

Given the optimal active and reactive power dispatch needed from a DG unit, which is obtained from Eqs. (3.11) to (3.12) respectively, the optimal power factor can be expressed as follows [8]:

$$pf_{DGi} = \frac{P_{DGi}}{\sqrt{P_{DGi}^2 + Q_{DGi}^2}} \tag{3.13}$$

## 3.6 Computational Procedure [8]

This section presents a computational procedure to accommodate dispatchable biomass DG units for minimizing the energy loss using the expressions developed earlier. As DG units were assumed to be dispatchable, their size, location and power factor are estimated for minimizing the power loss at the peak load [8]. The DG output is then dispatched following the load demand curve. Finally, the energy loss is calculated based on the DG output pattern.

*Step 1*: Run base-case power flow at the peak load level and calculate the total power loss using Eq. (3.1).
*Step 2*: Identify the optimal location, size and power factor of a DG unit at the peak load level only.

(a) Calculate the size of the DG unit or its maximum output for each bus ($S_{DGi}^{\max}$) as below, where $P_{DGi}$ and $Q_{DGi}$ are respectively calculated using Eqs. (3.11) and (3.12), and find the power factor for each bus using Eq. (3.13).

$$S_{DGi}^{\max} = \sqrt{P_{DGi}^2 + Q_{DGi}^2} \tag{3.14}$$

(b) Place the DG unit obtained earlier at each bus, one at a time and calculate the approximate power loss for each case using Eq. (3.6).
(c) Locate the optimal bus at which the power loss is minimum with the corresponding optimal size of the DG unit at that bus.

*Step 3*: Find the optimal output of the DG unit at the optimal location only for period $t$ as below, where $p.u.\,demand(t)$ is the load demand in p.u. at period $t$ (see Fig. 3.1).

$$S_{DGi}(t) = p.u.\,demand(t) \times S_{DGi}^{\max} \tag{3.15}$$

*Step 4*: Run power flow with each DG output obtained in *Step 3* for each period and calculate the total annual energy loss using Eq. (3.7).

The above procedure is developed to accommodate a DG unit with optimal power factor. Such a procedure can be modified to adopt a DG unit with a pre-specified power factor. When the power factor is pre-specified, the procedure is similar to the above with exception that in *Step 2.a*, the size is calculated using Eqs. (3.11) and (3.3).

## 3.7 Example 1: DG Impacts on Power Losses [9, 10]

The case study considered in this example is the 33-bus distribution network found in Fig. 2.2. In this system, the individual load power factors at buses are substantially different, ranging from 0.31 to 0.99 (lagging). The load power factor of the system is 0.82 (lagging), which is calculated as the total active power load of the system divided by its total apparent power load.

To evaluate the impact of the DG power factor on power losses, the Exhaustive Power flow solution (EPF) [11] is adopted in this study. In this solution, a DG unit is first placed at each bus. Its size or penetration as defined in Sect. 2.3.3. is changed from 0 to 100% of the total system load in a step of 0.25%. For each case, the power factor of the DG unit is also varied from 0 to unity (leading/lagging) in a step of 0.001. The total system power loss with the DG unit using Eq. (3.6) is calculated for each case by power flow analyses. The optimal location, size and power factor

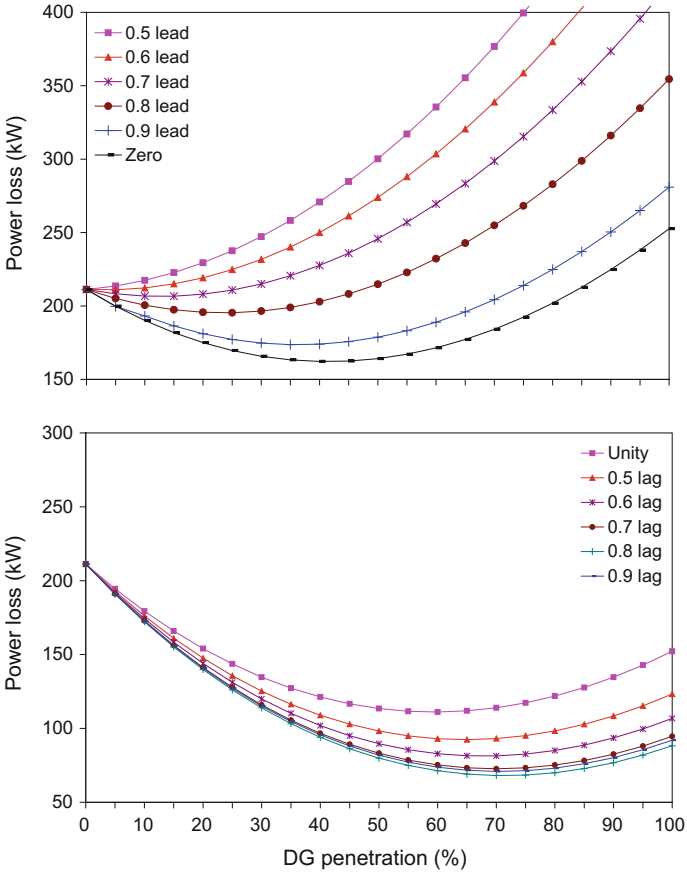


**Fig. 3.2** Power factor impact with respect to penetration on power losses

are then obtained for the case where the total power loss in the system is lowest without any voltage violations.

Figure 3.2 shows the DG power factor impact with various penetrations on the distribution system power loss at bus 6. The power factors are pre-specified at 0.5, 0.6, 0.7, 0.8 and 0.9 (lagging/leading), zero and unity. This study is implemented to highlight the importance of power factor operation with respect to DG penetration for minimizing power losses. It can be observed that for each power factor concerned (e.g., 0.9 lagging power factor), the power loss variation as a function of the DG penetration level shows a U-shape curve. Losses commence to reduce when small sizes of DG unit are connected until they reach their minimum value. Once the minimum losses are obtained, if DG penetration still increases, losses start to increase significantly, even higher than the case without any DG unit connected to the system. At the minimum loss value, DG units with leading power factors have the optimal size with the lowest penetration. In contrast, DG units with lagging power factors have the optimal size with the highest penetration. The power factor plays a significant role in power loss minimization. At the same penetration, a DG unit operating at a lagging power factor that is capable of delivering both active and reactive power can produce the lowest loss. Conversely, a DG unit with a leading power factor that can inject active power and consume reactive power can yield the highest loss. Similar performances have been observed for all the power factors in the range from 0 to 1 (leading/lagging). The above observation raises the question that the power factor of a DG unit should be appropriately selected to minimize the total power and energy losses.

Figure 3.3 illustrates the plot of the optimal DG size for each power factor with respect to the minimum power loss at bus 6. This study is carried out using the EPF

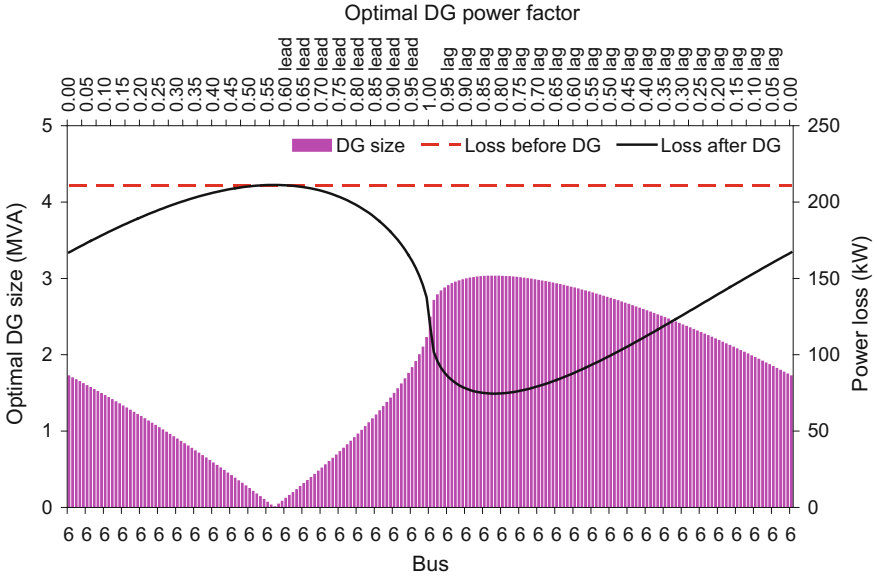


**Fig. 3.3** Optimal DG size for each power factor with respect to power loss

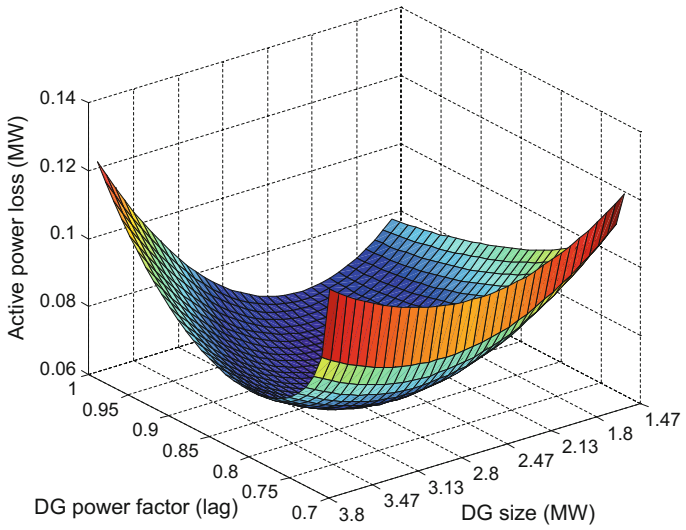


**Fig. 3.4** Impacts of the size and power factor of a DG unit on the power loss at bus 6

solution described earlier to determine the optimal power factor for each location to which the system power loss is minimum. The power factor is varied from 0 to 1 (leading/lagging) in a step of 0.01. A DG unit is optimally sized at each power factor at which the system loss is lowest. Overall, the power loss variation as a function of the power factor and size of the DG unit shows a two opposite U-shape curve. The lagging power factor has more positive impact on power losses than the leading power factor. The optimal power factor is found to be 0.82 lagging at which the system loss is lowest at 67.90 kW with a maximum penetration level of 3.097 MVA. A similar trend has been found for the rest of locations (buses) in the distribution system.

Figure 3.4 plots a valley-shaped curve of the power loss versus the size and power factor at bus 6. This work has been carried out using the EPF to show the impact of the power factor on the power loss. It can be found from the figure that the optimal power factor is 0.82 (lagging). An attempt to change the power factor around their optimal values leads to a significant increase in the power loss as illustrated in Fig. 3.4.

## 3.8 Example 2: Optimal DG Placement [8]

The case study considered in this example is the 33-bus distribution system found in Fig. 2.2 and 69-bus *one feeder* distribution system in Fig. 2.3. The load power factor of the system or the load power factor at each bus is assumed to remain unchanged for each load level (period). The loading at each bus is assumed to

follow the 24-h load profile depicted in Fig. 3.1. The load power factor of the 33 and 69-bus systems is 0.82 (lagging). It is assumed that biomass DG units can be allocated at all buses in the system as the required raw material can be transported.

### 3.8.1 DG Location and Size Selection

As previously mentioned, to select the best location, a base-case load flow analysis is implemented at the peak load level. A DG unit is then sized at various buses using Eq. (3.14) and the corresponding power loss for each bus is also calculated. The best location (at which the loss is lowest) is subsequently determined. Figure 3.5a, b shows the total approximate power losses at various locations with respect to the optimum sizes and power factors after "one load flow run" in the 33 and 69-bus systems, respectively. The figure also provides the exact power losses, which are determined by running load flow again for the system with the DG unit, one at a time at each bus. As can be revealed from Fig. 3.5a, b, the pattern of the approximate power losses at various locations totally follows the exact power loss pattern. Such a trend would be sufficient to identify the best location where the power loss is at minimum. As shown in the figure, the sizes are significantly different in the range of 0.77–4.61 MVA for the 33-bus system and between 0.03 and 4.90 MVA for the 69-bus system. It is observed from both systems that the largest size is found closest to the bus substation where the loss is highest when compared to the other locations.

Figure 3.5a, b also shows the optimal power factor of the DG unit for each location. In the 33-bus system, the individual power factors at various buses are in a broad range from 0.77 to 0.89 (lagging) as the individual load power factors of this system are substantially different in a large range of 0.31–0.99 (lagging). However, this is not the case for the 69-bus system where the power factors are insignificantly different, in a narrow range from 0.81 to 0.83 (lagging) as the individual load power factors are in a narrow range of 0.76–0.86 (lagging). Furthermore, as far as one bus in each system is concerned, the respective figure would provide the optimum size and corresponding optimal power factor to which the power loss is the lowest. From operation and planning perspectives, the figure can be used as a useful lookup table for restricting the size and power factor of a DG unit to retain the system loss at minimum.

In addition to the optimal size and power factor, the optimal location for each system can be identified from Fig. 3.5a, b. In the 33-bus system, the optimum location is found to be at bus 6 where the size of the DG unit is 3.03 MVA and the total approximate power loss is 74.58 kW. However, by running load flow again with the above DG unit at the best location (bus 6) only, the total accurate loss is found to 67.98 kW with a difference of nearly 8.85%. This difference has no impact

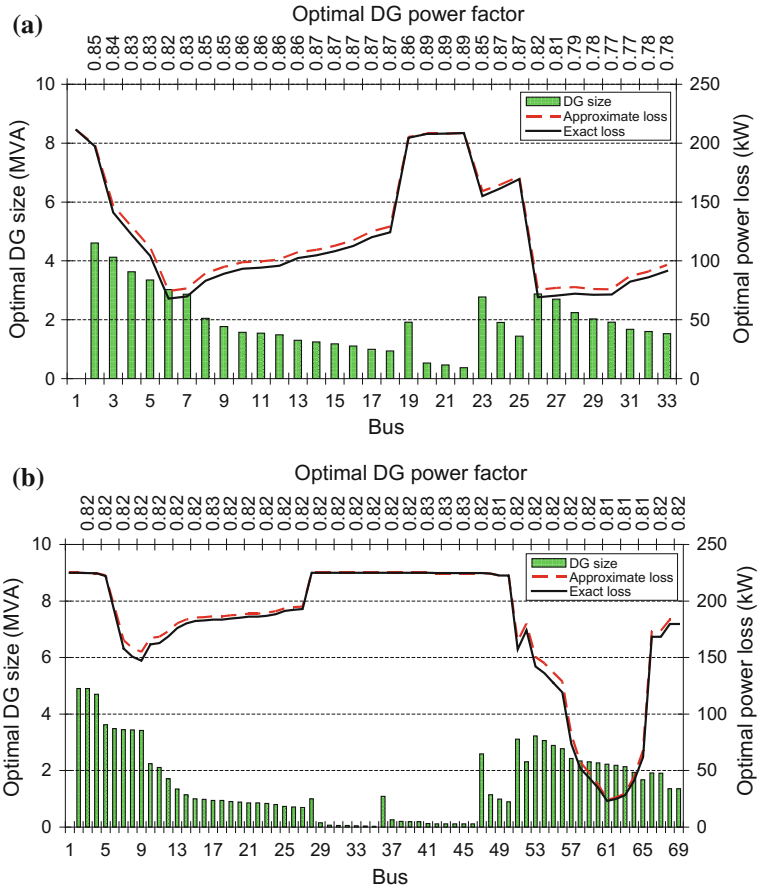


**Fig. 3.5** Optimal sizes and power factors at various locations with respect to minimum power losses for **a** 33-bus system and **b** 69-bus system

on the final outcomes of the optimum location, size and power factor of DG. Similarly, in the 69-bus system, the best location is bus 61 where the size of the DG unit is 2.22 MVA and the total approximate and accurate power losses are determined to be 24.17 and 23.15 kW respectively at a difference of 3.80%. It is noted that given a fixed location due to resource availability and geographic limitations, the optimal size and power factor to which the power loss is lowest can be identified from the respective figures.

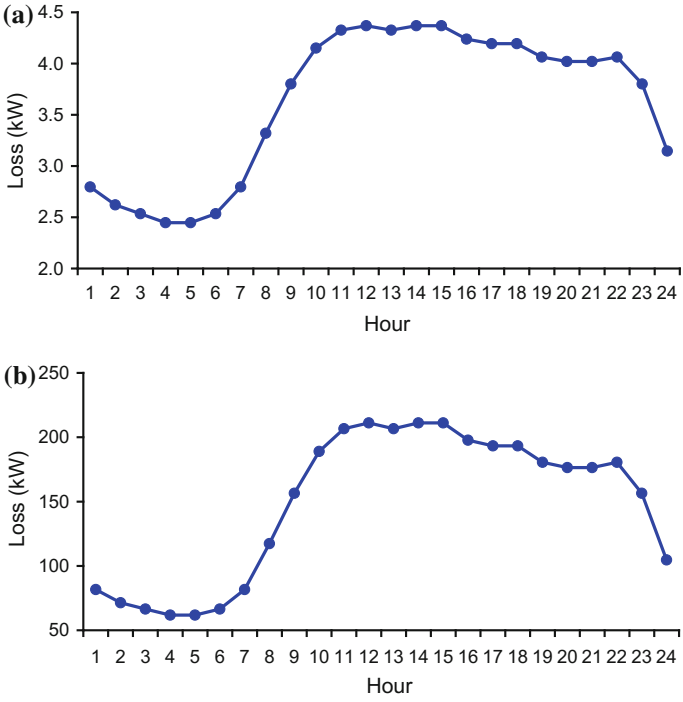


**Fig. 3.6** The 33-bus base case system without DG units: **a** hourly load demand and **b** hourly energy loss

### *3.8.2 Sizing DG with Respect to Hourly Energy Loss*

Figure 3.6a shows hourly load demand over a day for the 33-bus base case system (i.e., without DG units). This pattern exactly follows the nominalised load profile (see Fig. 3.1). Figure 3.6b presents hourly energy loss over the day, which is obtained by running load flow for each load level in the base case system. In this case, the annual energy loss is 1299.59 MWh, which is estimated as tracing the area under Fig. 3.6b times 365 days as defined in Eq. (3.7). Similarly, Fig. 3.7a, b shows hourly load demand and energy loss over a day in the 69-bus distribution system. The annual energy loss in the system is estimated at 1381.53 MWh.

Figure 3.8a shows the hourly dispatchable outputs of the DG unit at the optimal location (bus 6) over a 24-h day in the 33-bus system, which were obtained earlier.

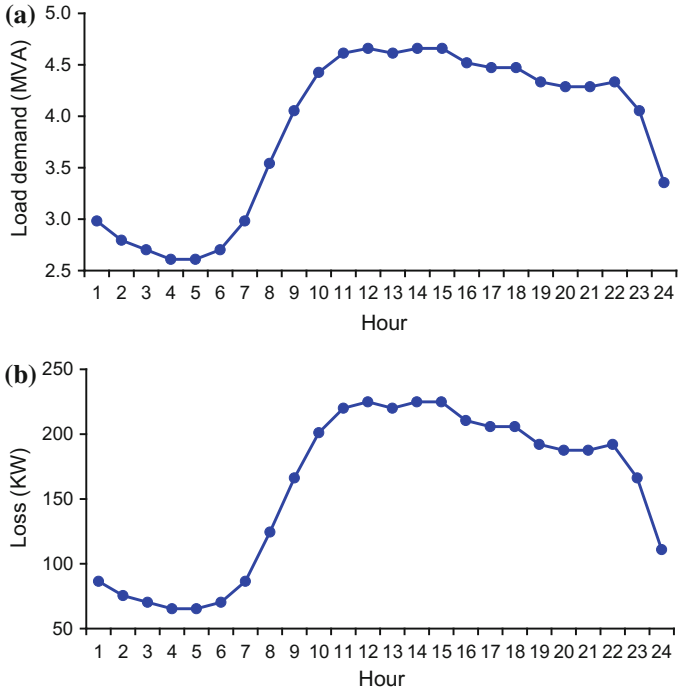


**Fig. 3.7** The 69-bus base case system without DG units: **a** hourly load demand and **b** hourly energy loss

The output pattern exactly follows the normalized load demand curve depicted in Fig. 3.1. The maximum output of the DG unit which is identified at hour 12 (the peak load), shows its optimum size as found in the previous section. Figure 3.8b presents the hourly power losses which corresponds to the DG output generation for each hour. At each hour period of the day, the loss in the system with the DG unit is substantially lower than that without the DG unit. This indicates that the DG installation positively affects the loss. It is observed that the hourly DG output shown in Fig. 3.8a follows the load pattern illustrated in Fig. 3.6a. Similarly, the hourly loss in the 33-bus system with the DG unit in Fig. 3.8b also follows the energy loss pattern in the system without the DG unit found in Fig. 3.6b. Similar results have been found for the 69-bus system, as presented in Fig. 3.9a, b.

Table 3.1 summarises the results of the DG allocation in the 33 and 69-bus distribution systems, respectively. These results include the location, size and power factor. The annual energy losses in the systems without and with the DG unit are also included in the table. The energy losses without and with the DG unit in the

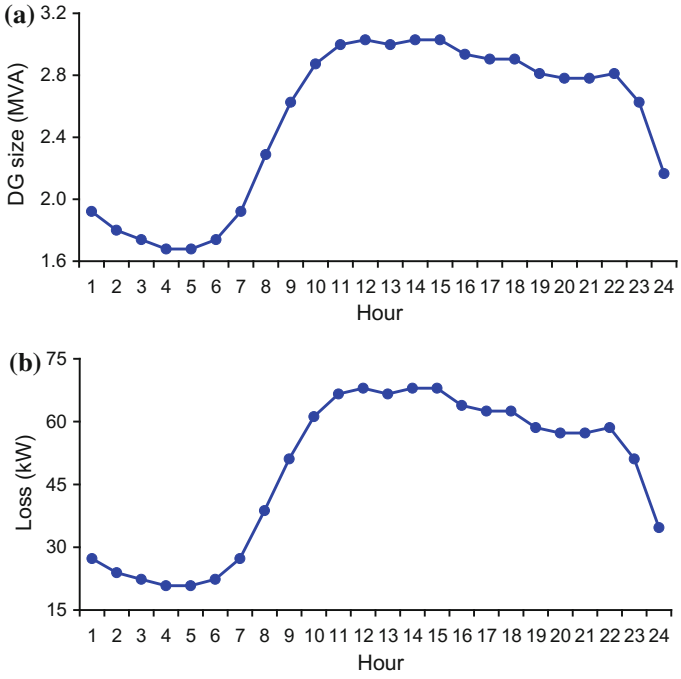


**Fig. 3.8** The 33-bus base case system with DG units: **a** hourly load demand and **b** hourly energy loss

33-bus system are calculated using Eq. (3.7), where the power loss for each hour is obtained from Figs. 3.6b and 3.8b, respectively. Similarly, the energy losses before and after the introduction of the DG unit in the 69-bus system are estimated based on Figs. 3.7b and 3.9b. It is observed from Table 3.1 that in the presence of the DG units, significant reductions in the energy losses in the 33 and 69-bus systems are found to be 67.44 and 89.55% respectively.

### *3.8.3 DG Power Factor Operation*

Figure 3.10a, b shows the results of DG allocation at buses 6 and 61 in the 33 and 69-bus systems, respectively. The results include the optimal DG size and its corresponding energy loss reduction with respect to the power factor as well as type of DG adopted. It is observed from the figure that the power factor of DG units adopted plays a significant role in minimising energy losses. As shown in Fig. 3.10a, the loss reduction commences to increase when the power factor is varied in order of leading, unity and lagging values and until it reaches the maximum value when the DG unit operates at 0.82 optimal lagging power factor. It is

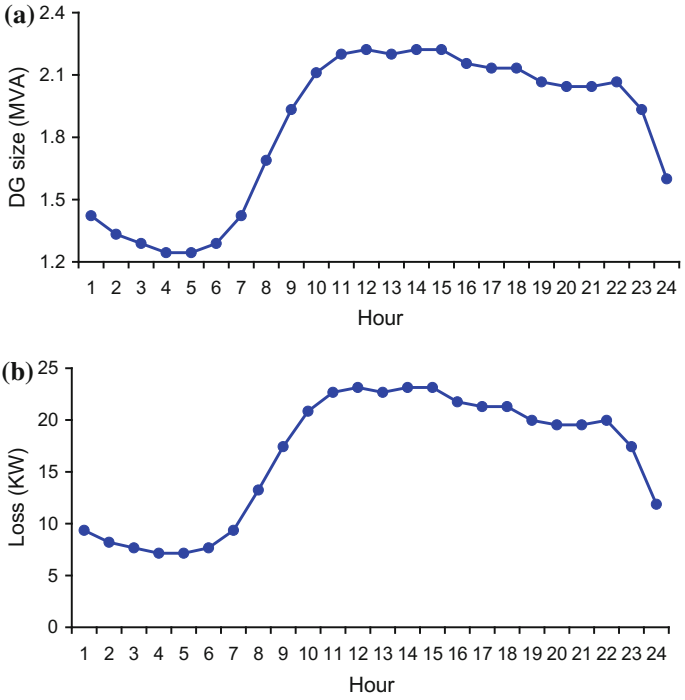


**Fig. 3.9** The 69-bus base case system with DG units: **a** hourly load demand and **b** hourly energy loss

**Table 3.1** Results of DG placement

| System | 33-Bus | 69-Bus |
|---|---|---|
| Location (bus) | 6 | 61 |
| Size (MVA) | 3.025 | 2.222 |
| Optimal power factor | 0.82 (lagging) | 0.82 (lagging) |
| DG penetration (%) | 69.31 | 47.73 |
| Annual energy loss before DG (MWh) | 1299.59 | 1381.53 |
| Annual energy loss after DG (MWh) | 423.13 | 144.35 |
| Annual energy loss reduction (%) | 67.44 | 89.55 |

observed from the figure that in both systems, DG operation at lagging power factors has the most positive impact on loss reduction while the lowest impact is determined in DG generation at leading power factors.

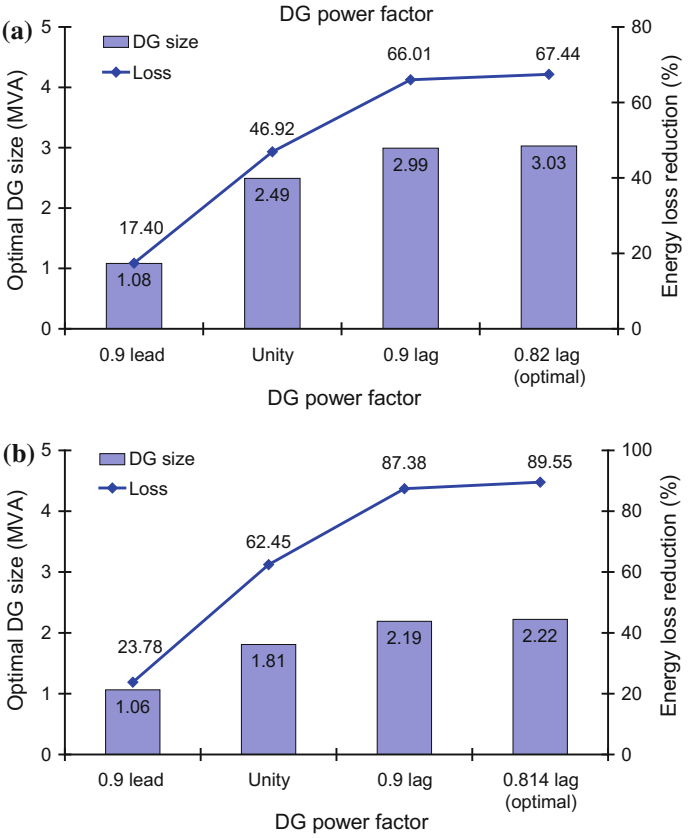


**Fig. 3.10** DG operation at different power factors: **a** 33-bus system and **b** 69-bus system

## 3.9 Conclusions

This chapter investigated the impact of dispatchable DG power factor operation (i.e., biomass) on distribution system losses. Such DG units are modelled as synchronous machines. It also presented an analytical approach to identify the size and power factor of DG units at various locations to minimise energy losses and a methodology to determine the best location. The approach is easily adapted to accommodate synchronous machine-based DG units under different operating conditions in terms of reactive power delivery capability. The results show that optimal power factor operation plays an important role in minimizing energy losses. DG operation at lagging power factors can produce a higher energy loss than that at leading power factors. It is also indicated that the 69 and 33-bus distribution systems can accommodate penetration levels of single dispatchable biomass DG up to 48 and 69%, respectively. However, this is not the case for non-dispatchable

renewable DG such as solar PV units, where a mismatch between load demand and PV generation exists, thus leading to a lower DG penetration level, as shown in the next chapter.

## References


1. Atwa YM, El-Saadany EF (2011) Probabilistic approach for optimal allocation of wind-based distributed generation in distribution systems. IET Renew Power Gener 5(1):79–88. doi:10.1049/iet-rpg.2009.0011
2. Katiraei F, Aguero JR (2011) Solar PV integration challenges. IEEE Power Energ Mag 9(3):62–71. doi:10.1109/mpe.2011.940579
3. IEEE 1547 Standard for interconnecting distributed resources with electric power systems, 2003. doi:10.1109/ieeestd.2003.94285
4. Pinheiro JMS, Dornellas CRR, Schilling MT, Melo ACG, Mello JCO (1998) Probing the new IEEE reliability test system (RTS-96): HL-II assessment. IEEE Trans Power Syst 13(1):171–176. doi:10.1109/59.651632
5. Elgerd IO (1971) Electric energy system theory: an introduction. McGraw-Hill Inc., New York
6. Hung DQ, Mithulananthan N, Bansal RC (2010) Analytical expressions for DG allocation in primary distribution networks. IEEE Trans Energy Convers 25(3):814–820. doi:10.1109/TEC.2010.2044414
7. Acharya N, Mahat P, Mithulananthan N (2006) An analytical approach for DG allocation in primary distribution network. Int J Electr Power Energy Syst 28(10):669–678. doi:10.1016/j.ijepes.2006.02.013
8. Hung DQ, Mithulananthan N, Bansal RC (2013) Analytical strategies for renewable distributed generation integration considering energy loss minimization. Appl Energy 105:75–85. doi:10.1016/j.apenergy.2012.12.023
9. Hung DQ, Mithulananthan N (2012) An optimal operating strategy of DG unit for power loss reduction in distribution systems. In: 2012 IEEE 7th international conference on industrial and information systems (ICIIS), 6–9 Aug 2012, pp 1–6. doi:10.1109/ICIInfS.2012.6304773
10. Hung DQ, Mithulananthan N (2014) Loss reduction and loadability enhancement with DG: a dual-index analytical approach. Appl Energy 115:233–241. doi:10.1016/j.apenergy.2013.11.010
11. Hung DQ, Mithulananthan N (2013) Multiple distributed generator placement in primary distribution networks for loss reduction. IEEE Trans Industr Electron 60(4):1700–1708. doi:10.1109/TIE.2011.2112316

# Chapter 4
# PV Integration

## 4.1 Introduction[1]

Depending on the location and technology of PV adopted, a power system would accommodate up to an estimated PV penetration level of 50% [1, 2]. However, the time-varying load model (i.e., time-varying voltage-dependent load model) may diversely affect the estimated PV penetration.

This chapter studies the penetration of PV units in a distribution system with several different types of time-varying load models. Here, a multiobjective index (*IMO*)-based analytical expression is proposed to identify the size of a PV-based DG unit with objectives of simultaneously reducing active and reactive power losses and voltage deviation. This expression is then adapted to place PV units while considering the characteristics of varying-time load models and probabilistic generation. This chapter also presents three different types of customers with dissimilar load patterns (i.e., industrial, residential and commercial) and a mix of all these customers, which are defined by time-varying voltage-dependent load models.

## 4.2 Load and Solar PV Modelling

### *4.2.1 Load Modelling*

The demand of the system under the study is assumed to follow different normalized daily load patterns (i.e., industrial, residential and commercial) with a peak of 1 p.u., as shown in Fig. 4.1 [3]. The time-varying voltage-dependent load model

[1]The work presented in this chapter was taken from the journal paper: D.Q. Hung, N. Mithulananthan, and Kwang Y. Lee, "Determining PV penetration for distribution systems with time-varying load models, *IEEE Transactions on Power Systems*, vol. 29, no. 1, pp. 3048–3057, November 2014.



N. Mithulananthan et al., *Intelligent Network Integration of Distributed Renewable Generation*, Green Energy and Technology,
DOI 10.1007/978-3-319-49271-1_4

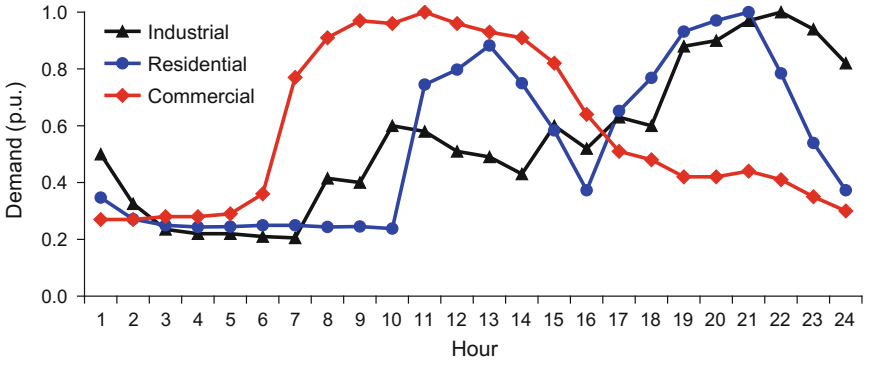


**Fig. 4.1** Normalized daily demand curve for various customers

or the time-varying load model defined in Sect. 2.2 is also considered in this work. For each load model, the load factor (*LF*) or the average load level of the system can be defined as the area under the load demand curve in p.u. divided by the total duration. This can be expressed as follows:

$$LF = \sum_{t=1}^{24} \frac{p.u.\ demand(t)}{24} \tag{4.1}$$

### 4.2.2 Solar PV Modelling

The solar irradiance for each hour of the day is modeled by the Beta Probability Density Function (PDF) based on historical data which have been collected for three years from the site (lat: 39.45, long: −104.65, California, USA) [4]. To obtain this PDF, a day is split into 24-h periods (*time segments*), each of which is 1 h and has its own solar irradiance PDF. From the collected historical data, the mean and standard deviation of the hourly solar irradiance of the day is calculated. It is assumed that each hour has 20 *states* for solar irradiance with a step of 0.05 kW/m$^2$. From the calculated mean and standard deviation, the PDF with 20 *states* for solar irradiance is generated for each hour of the day and the probability of each solar irradiance state is determined. Accordingly, the PV output power is obtained for that hour. The model is explained below.

The probability of the solar irradiance state $s$ during any specific hour can be calculated as follows [5]:

$$\rho(s) = \int_{s1}^{s2} f_b(s)ds \tag{4.2}$$

where $s_1$ and $s_2$ are the solar irradiance limits of state $s$; $f_b(s)$ is the Beta distribution function of $s$, which is calculated using Eq. (2.2).

The total expected output power (average output power) of a PV module across any specific period $t$, $P_{PV}(t)$ ($t$ = 1 h), can be obtained as a combination of Eqs. (4.2) and (2.3) [5]. This can be expressed as follows:

$$P_{PV}(t) = \int_0^1 P_{PV_o}(s)\rho(s)ds \tag{4.3}$$

For example, given the mean ($\mu$) and standard deviation ($\sigma$) of the hourly solar irradiance found in Table B.1 (Appendix B), the PDF for 20 solar irradiance states with an interval of 0.05 kW/m$^2$ for periods 8, 12 and 16 are generated using Eqs. (2.2) and (4.2), and plotted in Fig. 4.2. Obviously, as the solar irradiance is time and weather-dependent, different periods have different PDFs. The area under the curve of each hour is unity. Another example is that given the parameters of a PV module found in Table B.2 (Appendix B), the expected output of the PV module with respect to 20 solar irradiance states (Fig. 4.2) is calculated using Eq. (4.3) and plotted in Fig. 4.3. For period 8, the total expected output power, which is calculated as the area under the curve of that period (Fig. 4.3), is 53.08 W. As the period is assumed at 1 h, the PV module is expected to output at 53.08 Wh. Similarly, the expected PV outputs for periods 12 and 16 are found to be 129.96 and 73.42 Wh, respectively. It is observed from Fig. 4.3 that a difference in the expected PV output patterns exists among hours 8, 12 and 16.

The capacity factor of a PV module ($CF_{PV}$) can be defined as the average output power ($P_{PV}^{avg}$) divided by the rated power or maximum output ($P_{PV}^{\max}$) [5]:

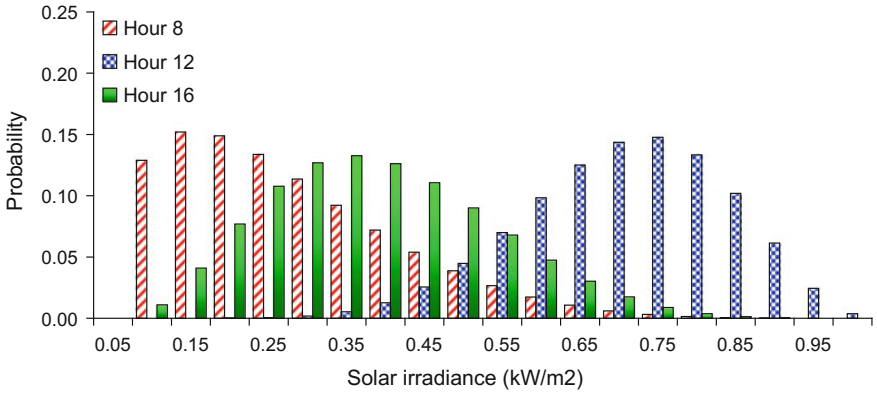


**Fig. 4.2** PDF for solar irradiance at hours 8, 12 and 16

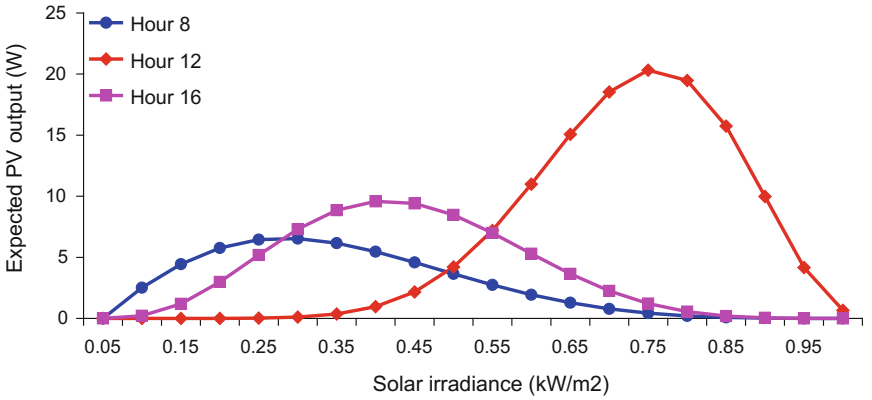


**Fig. 4.3** Expected output of a PV module at hours 8, 12 and 16

$$CF_{PV} = \frac{P_{PV}^{avg}}{P_{PV}^{\max}} \tag{4.4}$$

Once the average output power is calculated using (4.3) for each hour based on three years of the collected historical data as previously mentioned, the average and maximum output powers are obtained for the day. The $CF_{PV}$ is then obtained using (4.4).

The inverter-based PV technology [6, 7], which is capable of delivering active power and delivering or consuming reactive power, is adopted in this study. The relationship between the active and reactive power of a PV unit at bus $k$ ($P_{PV_k}$ and $Q_{PV_k}$) can be expressed as [8]:

$$Q_{PV_k} = a_k P_{PV_k} \tag{4.5}$$

where, $a_k = \pm \tan(\cos^{-1}(pf_{PV_k}))$; The parameter $a_k$ is positive for the PV unit supplying reactive power and negative for the PV unit consuming reactive power; and $pf_{PV_k}$ is the operating power factor of the PV unit at bus $k$.

### *4.2.3 Combined Generation-Load Model*

To incorporate the PV output powers as multistate variables in the problem formulation, the combined generation-load model reported in [5] is adopted in this study. The continuous PDF has been split into different states. As previously mentioned, each day has 24-h periods (*time segments*), each of which has 20 *states*

for solar irradiance with a step of 0.05 kW/m$^2$ for calculating the PV output powers. As the load demand is constant during each hour, its probability is unity. Therefore, the probability of any combination of the generation and load is the probability of the generation itself.

## 4.3 Impact Indices

In this study, three indices: active power loss, reactive power loss and voltage deviation are employed to describe the PV impacts on the distribution system. These indices play a critical role in PV planning and operations due to their significant impacts on utilities' revenue, power quality, and system stability and security. They are explained below.

### *4.3.1 Active Power Loss Index*

Figure 4.4a shows a $n$-branch radial distribution system without a PV unit. In the figure, $P_{bi}$ and $Q_{bi}$ are respectively the active and reactive power flow through branch $i$; $P_{Di}$ and $Q_{Di}$ are respectively the active and reactive load powers at bus $i$. The total power loss in the $n$-branch system without a PV unit ($P_L$) can be calculated as follows [9]:

$$P_L = \sum_{i=1}^{n} \frac{P_{bi}^2 + Q_{bi}^2}{|V_i|^2} R_i \tag{4.6}$$

where $R_i$ is the resistance of branch $i$; $|V_i|$ is the voltage magnitude at bus $i$. As illustrated in Fig. 4.4b, due to the active and reactive powers of the PV unit injected at bus $k$, the active and reactive powers flowing from the source to bus $k$ is reduced, whereas the power flows in the remaining branches are unchanged. Accordingly, the power loss defined by Eq. (4.6) can be rewritten as follows:

$$\begin{aligned} P_{L_{PV}} = & \sum_{i=1}^{k} \frac{(P_{bi} - P_{PV_k})^2}{|V_i|^2} R_i + \sum_{i=k+1}^{n} \frac{P_{bi}^2}{|V_i|^2} R_i \\ & + \sum_{i=1}^{k} \frac{(Q_{bi} - Q_{PV_k})^2}{|V_i|^2} R_i + \sum_{i=k+1}^{n} \frac{Q_{bi}^2}{|V_i|^2} R_i \end{aligned} \tag{4.7}$$

Substituting Eqs. (4.5) and (4.6) into Eq. (4.7), we obtain:

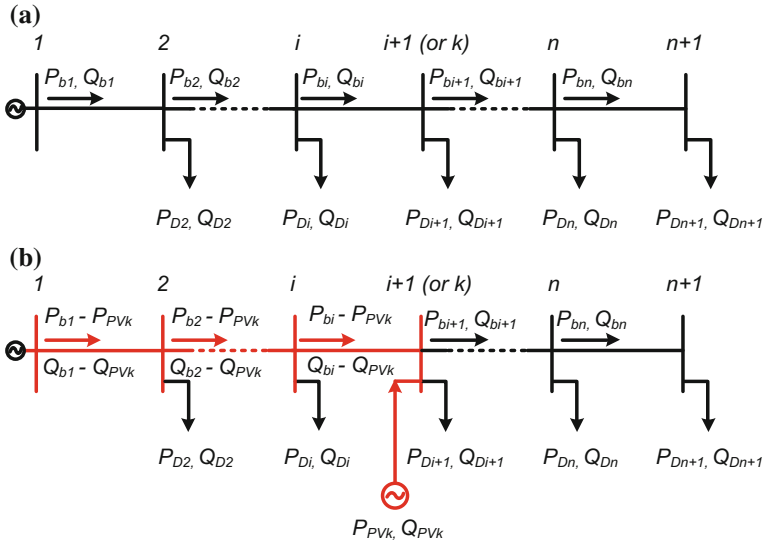


**Fig. 4.4** A radial distribution system: **a** without a PV unit and **b** with a PV unit

$$P_{L_{PV}} = \sum_{i=1}^{k} \frac{P_{PV_k}^2 - 2P_{bi}P_{PV_k}}{|V_i|^2} R_i + \sum_{i=1}^{k} \frac{a_k^2 P_{PV_k}^2 - 2Q_{bi}a_k P_{PV_k}}{|V_i|^2} R_i + P_L \tag{4.8}$$

The active power loss index (*ILP*) can be defined as the ratio of Eqs. (4.8) to (4.6), i.e. the power loss in the system with a PV unit divided by that without a PV unit, as follows:

$$ILP = \frac{PL_{PV}}{P_L} \tag{4.9}$$

### 4.3.2 Reactive Power Loss Index

The total reactive power loss ($Q_L$) in a radial distribution system with $n$ branches can be written as follows:

$$Q_L = \sum_{i=1}^{n} \frac{P_{bi}^2 + Q_{bi}^2}{|V_i|^2} X_i \tag{4.10}$$

where $X_i$ is the reactance of branch $i$. Similar to Eq. (4.8), when both $P_{PV_k}$ and $Q_{PV_k} = a_k P_{PV_k}$ are injected at bus $k$, Eq. (4.10) can be rewritten as follows:

$$Q_{L_{PV}} = \sum_{i=1}^{k} \frac{P_{PV_k}^2 - 2P_{bi}P_{PV_k}}{|V_i|^2} X_i + \sum_{i=1}^{k} \frac{a_k^2 P_{PV_k}^2 - 2Q_{bi}a_k P_{PV_k}}{|V_i|^2} X_i + Q_L \tag{4.11}$$

The reactive power loss index (*ILQ*) can be defined as the ratio of Eqs. (4.11) and (4.10) as follows:

$$ILQ = \frac{Q_{L_{PV}}}{Q_L} \tag{4.12}$$

### 4.3.3 Voltage Deviation Index

As shown in Fig. 4.4a, the voltage deviation (*VD*) along the branch from bus $i$ to bus $i + 1$, $(R_i + jX_i)$, can be expressed as follows [10]:

$$|VD_i| = \frac{|R_i P_{bi} + X_i Q_{bi}|}{|V_{i+1}|} \tag{4.13}$$

From Eq. (4.13), the total voltage deviation squared ($VD^2$) in the whole system with $n$ branches can be written as follows:

$$VD^2 = \sum_{i=1}^{n} \frac{(R_i P_{bi} + X_i Q_{bi})^2}{|V_{i+1}|^2} \tag{4.14}$$

When both $P_{PV_k}$ and $Q_{PV_k}$ are injected at bus $k$ (see Fig. 4.4b), Eq. (4.14) can be rewritten as follows:

$$\begin{aligned} VD_{PV}^2 = &\sum_{i=1}^{k} \frac{R_i^2 (P_{bi} - P_{PV_k})^2}{|V_{i+1}|^2} + \sum_{i=k+1}^{n} \frac{R_i^2 P_{bi}^2}{|V_{i+1}|^2} \\ &+ \sum_{i=1}^{k} \frac{X_i^2 (Q_{bi} - Q_{PV_k})^2}{|V_{i+1}|^2} + \sum_{i=k+1}^{n} \frac{X_i^2 Q_{bi}^2}{|V_{i+1}|^2} \\ &+ 2\sum_{i=1}^{k} \frac{R_i X_i (P_{bi} - P_{PV_k})(Q_{bi} - Q_{PV_k})}{|V_{i+1}|^2} + 2\sum_{i=k+1}^{n} \frac{R_i X_i P_{bi} Q_{bi}}{|V_{i+1}|^2} \end{aligned} \tag{4.15}$$

Substituting Eqs. (4.5) and (4.14) into Eq. (4.15), we obtain:

$$VD_{PV}^2 = \sum_{i=1}^{k} \frac{R_i^2 \left( P_{PV_k}^2 - 2P_{bi}P_{PV_k} \right)}{|V_{i+1}|^2} + \sum_{i=1}^{k} \frac{X_i^2 \left( a_k^2 P_{PV_k}^2 - 2Q_{bi}a_k P_{PV_k} \right)}{|V_{i+1}|^2} - 2\sum_{i=1}^{k} \frac{R_i X_i \left( P_{bi}a_k P_{PV_k} + Q_{bi}P_{PV_k} - a_k P_{PV_k}^2 \right)}{|V_{i+1}|^2} + VD^2 \tag{4.16}$$

Finally, the voltage deviation index (*IVD*) of a distribution system can be defined as the ratio of Eqs. (4.16) and (4.14) as follows:

$$IVD = \frac{VD_{PV}^2}{VD^2} \tag{4.17}$$

## 4.4 Multiobjective Index

When the PV unit is allocated for minimising either the active or reactive power loss (i.e., *ILP* or *ILQ,* respectively), this would potentially limit the PV penetration with a high voltage deviation. On the other hand, a high penetration level could be achieved when the PV unit is considered for reducing the voltage deviation (*IVD*) alone, but the system losses could be higher. To include all three, i.e. real power loss, reactive power loss and voltage deviation, in the analysis, a multiobjective index (*IMO*) can be defined as a combination of the *ILP*, *ILQ* and *IVD* with appropriate weighting factors:

$$IMO = \sigma_1 ILP + \sigma_2 ILQ + \sigma_3 IVD \tag{4.18}$$

where $\sum_{i=1}^{3} \sigma_i = 1.0 \wedge \sigma_i \in [0,\ 1.0]$. This can be performed as all impact indices are normalized with values between zero and one [11]. When a PV unit is not connected to the system (i.e., base case system), the *IMO* is the highest at one.

The weights are intended to give the relative importance to each aspect (i.e. real power loss reduction, reactive power loss reduction or voltage deviation) with PV allocation and it depends on the purpose of analysis (e.g., planning or operation) [11–14]. The determination of the proper weighting factors will also depend on the experience and concerns of the system planner. The PV installation has a significant impact on the active and reactive power losses and voltage profiles. The active power loss is currently one of the major concerns due to its impact on the distribution utilities' profit, while the reactive power loss and voltage profile are less

important than the active power loss. Considering these concerns and referring to previous reports in [11–14], this study assumes that the active power loss receives a significant weight of 0.5, leaving the reactive power loss and the voltage deviation of 0.25 each. However, the above weights can be adjusted based on the priority of distribution utilities.

As the solar irradiance is a random variable, the PV output power and its corresponding *IMO* are stochastic during each hour. The *IMO* can be formulated in the expected value. To calculate the *IMO*, the power flow is analyzed for each combined generation-load state. It is assumed that $IMO(s)$ is the expected *IMO* at solar irradiance $s$, the total expected *IMO* over any specific period $t$, $IMO(t)$ ($t$ = 1 h) can be formulated as a combination of Eqs. (4.2) and (4.18) as follows:

$$IMO(t) = \int_0^1 IMO(s)\rho(s)ds \tag{4.19}$$

The average *IMO* (*AIMO*) over the total period ($T$ = 24) in a system with a PV unit can be obtained from Eq. (4.19). This can be expressed as follows:

$$AIMO = \frac{1}{T}\int_0^T IMO(t)dt = \frac{1}{T}\sum_{t=1}^{T} IMO(t) \times \Delta t \tag{4.20}$$

where $\Delta t$ is the time duration or *time segment* of period $t$ (1 h in this study). The lowest *AIMO* implies the best PV allocation for reducing active and reactive power losses and enhancing voltage profiles.

## 4.5 Sizing PV

Most of the existing analytical methods have addressed DG allocation in distribution systems for reducing the active power loss as a single-objective [15–18]. This work proposes a new analytical expression based on the multiobjective index (*IMO*) as given by Eq. (4.18) for sizing a PV-based DG unit at a pre-defined power factor. Substituting Eqs. (4.9), (4.12) and (4.17) into Eq. (4.18), we get:

$$IMO = \frac{\sigma_1}{P_L}P_{LPV} + \frac{\sigma_2}{Q_L}Q_{LPV} + \frac{\sigma_3}{VD^2}VD_{PV}^2 \tag{4.21}$$

To find the minimum *IMO* value, the partial derivative of Eq. (4.21) with respect to $P_{PV_k}$ becomes zero:

$$\frac{\partial IMO}{\partial P_{PV_k}} = \frac{\sigma_1}{P_L}\frac{\partial P_{LPV}}{\partial P_{PV_k}} + \frac{\sigma_2}{Q_L}\frac{\partial Q_{LPV}}{\partial P_{PV_k}} + \frac{\sigma_3}{VD^2}\frac{\partial VD_{PV}^2}{\partial P_{PV_k}} = 0 \tag{4.22}$$

The partial derivatives of Eqs. (4.8), (4.11) and (4.16) with respect to $P_{PV_k}$ can be written as follows:

$$\frac{\partial P_{LPV}}{\partial P_{PV_k}} = -2A_k + 2C_k P_{PV_k} - 2B_k a_k + 2C_k a_k^2 P_{PV_k} \tag{4.23}$$

$$\frac{\partial Q_{LPV}}{\partial P_{PV_k}} = -2D_k + 2F_k P_{PV_k} - 2E_k a_k + 2F_k a_k^2 P_{PV_k} \tag{4.24}$$

$$\begin{aligned}\frac{\partial VD_{PV}^2}{\partial P_{PV_k}} = {} & 2G_k P_{PV_k} - 2H_k + 2I_k a_k^2 P_{PV_k} - 2J_k a_k \\ & - 2K_k a_k - 2L_k + 4M_k a_k P_{PV_k}\end{aligned} \tag{4.25}$$

where

$$A_k = \sum_{i=1}^{k} \frac{R_i P_{bi}}{|V_i|^2}; \quad B_k = \sum_{i=1}^{k} \frac{R_i Q_{bi}}{|V_i|^2}; \quad C_k = \sum_{i=1}^{k} \frac{R_i}{|V_i|^2}$$

$$D_k = \sum_{i=1}^{k} \frac{X_i P_{bi}}{|V_i|^2}; \quad E_k = \sum_{i=1}^{k} \frac{X_i Q_{bi}}{|V_i|^2}; \quad F_k = \sum_{i=1}^{k} \frac{X_i}{|V_i|^2}$$

$$G_k = \sum_{i=1}^{k} \frac{R_i^2}{|V_{i+1}|^2}; \quad H_k = \sum_{i=1}^{k} \frac{R_i^2 P_{bi}}{|V_{i+1}|^2}; \quad I_k = \sum_{i=1}^{k} \frac{X_i^2}{|V_{i+1}|^2}; \quad J_k = \sum_{i=1}^{k} \frac{X_i^2 Q_{bi}}{|V_{i+1}|^2}$$

$$K_k = \sum_{i=1}^{k} \frac{R_i X_i P_{bi}}{|V_{i+1}|^2}; \quad L_k = \sum_{i=1}^{k} \frac{R_i X_i Q_{bi}}{|V_{i+1}|^2}; \quad M_k = \sum_{i=1}^{k} \frac{R_i X_i}{|V_{i+1}|^2}$$

Substituting Eqs. (4.23), (4.24), (4.25) into Eq. (4.22), we get:

$$P_{PV_k} = \frac{\left[\begin{array}{l}\frac{\sigma_1}{P_L}(A_k + a_k B_k) + \frac{\sigma_2}{Q_L}(D_k + a_k E_k) \\ + \frac{\sigma_3}{VD^2}(H_k + a_k J_k + a_k K_k + L_k)\end{array}\right]}{\left[\begin{array}{l}\frac{\sigma_1}{P_L}\left(C_k + a_k^2 C_k\right) + \frac{\sigma_2}{Q_L}\left(F_k + a_k^2 F_k\right) \\ + \frac{\sigma_3}{VD^2}\left(G_k + a_k^2 I_k + 2a_k M_k\right)\end{array}\right]} \tag{4.26}$$

The power factor of a PV unit depends on the operating conditions and technology adopted. Given a $pf_{PV_k}$ or $a_k$ value, the active power size of a PV unit for the minimum *IMO* can be obtained from Eq. (4.26). The reactive power size is then obtained using Eq. (4.5).

## 4.6 Computational Procedure

In this section, a computational procedure is developed to allocate PV units for reducing the *AIMO* while considering the time-varying load models and probabilistic generation. To reduce the computational burden, the *IMO* is first minimised at the average load level as defined by Eq. (4.1) to specify the location of a PV unit. This average load level has a significantly larger duration than other loading levels (e.g., peak or low load levels). The size is then calculated at that location based on the probabilistic PV output curve by minimising the *AIMO* over all periods. The computational procedure is summarized in the following steps:

Step 1: Run power flow for the system without a PV unit at the average load level or at the system load factor (*LF*) using Eq. (4.1) and calculate the *IMO* using Eq. (4.18).

Step 2: Specify the location and size at a pre-defined power factor of a PV unit at the average load level only.

(a) Find the PV size at each bus ($P_{PV_k}^{avg}$) using Eq. (4.26).

(b) Place the PV unit obtained earlier at each bus and calculate the *IMO* for each case using Eq. (4.18).

(c) Locate the optimal bus at which the *IMO* is minimum with the corresponding size of the PV unit at the average load level ($P_{PV_k}^{avg}$) at that bus.

Step 3: Find the capacity factor of the PV unit ($CF_{PVk}$) using Eq. (4.4).

Step 4: Find the optimal size of the PV unit or its maximum output ($P_{PV_k}^{\max}$) at the optimal location obtained in *Step* 2 as follows, where depending on the patterns of demand and generation, an adjusted factor, $k_{PV}$ (e.g., 0.8, 0.9 or 1.1) could be used to achieve a better outcome:

$$P_{PV_k}^{\max} = k_{PV} \times \frac{P_{PV_k}^{avg}}{CF_{PV_k}} \tag{4.27}$$

Step 5: Find the PV output at the optimal location for period $t$ as follows, where $p.u.\ PV\ output(t)$ is the PV output in p.u. at period *t,* which is calculated using Eqs. (2.2), (2.3), (4.2), (4.3), and normalized:

$$P_{PVk}(t) = p.u.\ PV\ output(t) \times P_{PVk}^{\max} \tag{4.28}$$

Step 6: Run load flow with each PV output obtained in *Step* 5 for each state over all the periods of the day and calculate the *AIMO* using (4.20).

Step 7: Repeat *Steps* 4–6 by adjusting $k_{PV}$ in Eq. (4.27) until the minimum *AIMO* is obtained.

## 4.7 Example

### 4.7.1 Test Systems

The proposed approach was applied to 69- and 33-bus test distribution systems found in Figs. 2.3 and 2.2. Figures 4.5 and 4.6 present the 69- and 33-bus systems, respectively, which are incorporated with different load types (i.e., industrial, residential and commercial).

### 4.7.2 Load Modelling

As previously mentioned, three different types of customers with dissimilar load patterns (i.e., industrial, residential and commercial) and a mix of all these customers are defined by time-varying voltage-dependent load models. Five types of time-varying load models are considered in this study:

1. Time-varying mixed load model
2. Time-varying constant load model
3. Time-varying industrial load model
4. Time-varying residential load model
5. Time-varying commercial load model

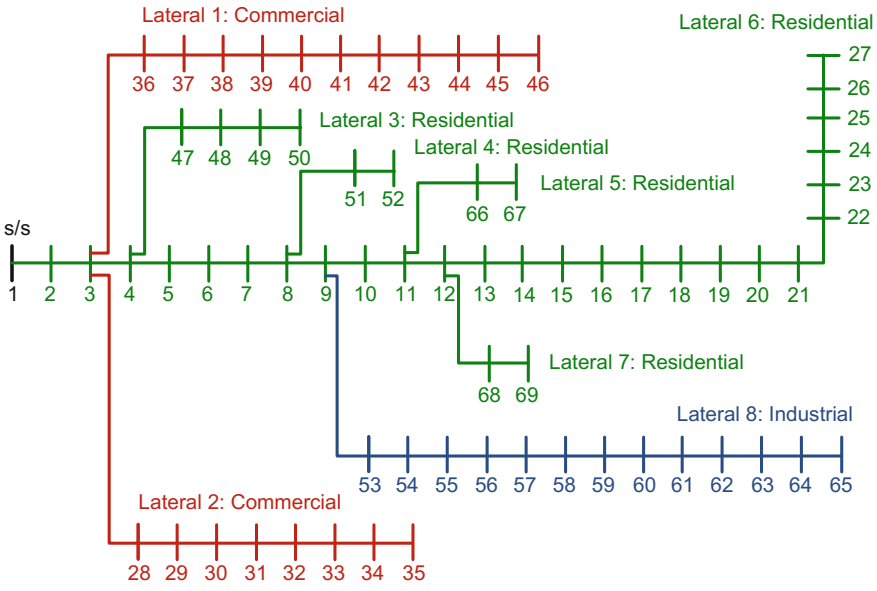


**Fig. 4.5** The 69-bus test distribution system

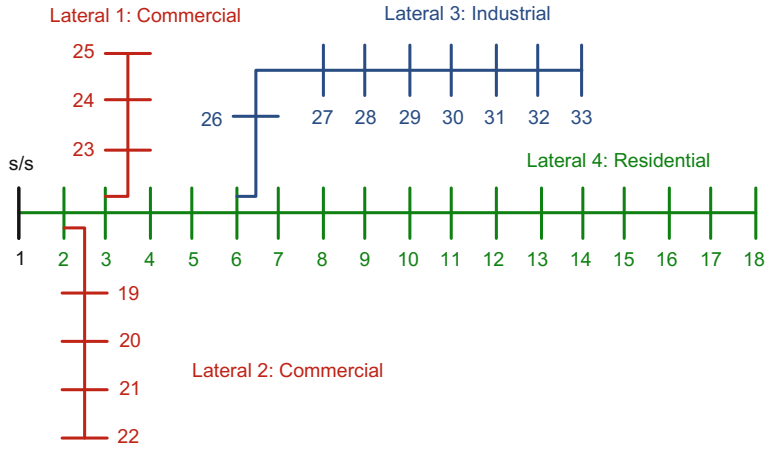


**Fig. 4.6** The 33-bus test distribution system

For both 69- and 33-bus systems, the loads are modeled by Eq. (2.1) by combining the time-varying demand patterns for industrial, residential and commercial loads. These loads are shown in Fig. 4.1 with the voltage-dependent load type with appropriate voltage exponents defined in Table 2.1, Chap. 2.

### *4.7.3 Solar PV Modelling*

The presented method can be applied to either solar farm or roof-top PV. However, the roof-top PV has been considered as an example to validate the proposed methodology in this work. It is assumed that a PV unit provides active and reactive power at a lagging power factor of 0.9 which is compliant with the new German grid code [19]. The mean and standard deviation (i.e., $\mu$ and $\sigma$, respectively) for each hour of a day are calculated using the hourly historical solar irradiance data collected for three years, as provided in Table B.1 (Appendix B) [4]. The characteristics of a PV module [20] employed for the PV model (2.3) can be found in Table B.2 (Appendix B). The solar irradiance $s$ is considered at an interval of 0.05 kW/m$^2$. Using Eqs. (2.2), (2.3), (4.2) and (4.3), the hourly expected output of the PV module is calculated and plotted in Fig. 4.7a–c. It is observed from these figures that a difference in the PV output patterns exists among hours 6–19. Actually, this is due to dependence of the PV output on the solar irradiance, ambient temperature and the characteristics of the PV module itself. The total expected output power for each hour can be calculated as a summation of all the expected output powers at that hour. Accordingly, the normalized expected PV output for the 24-h period day is plotted in Fig. 4.8.

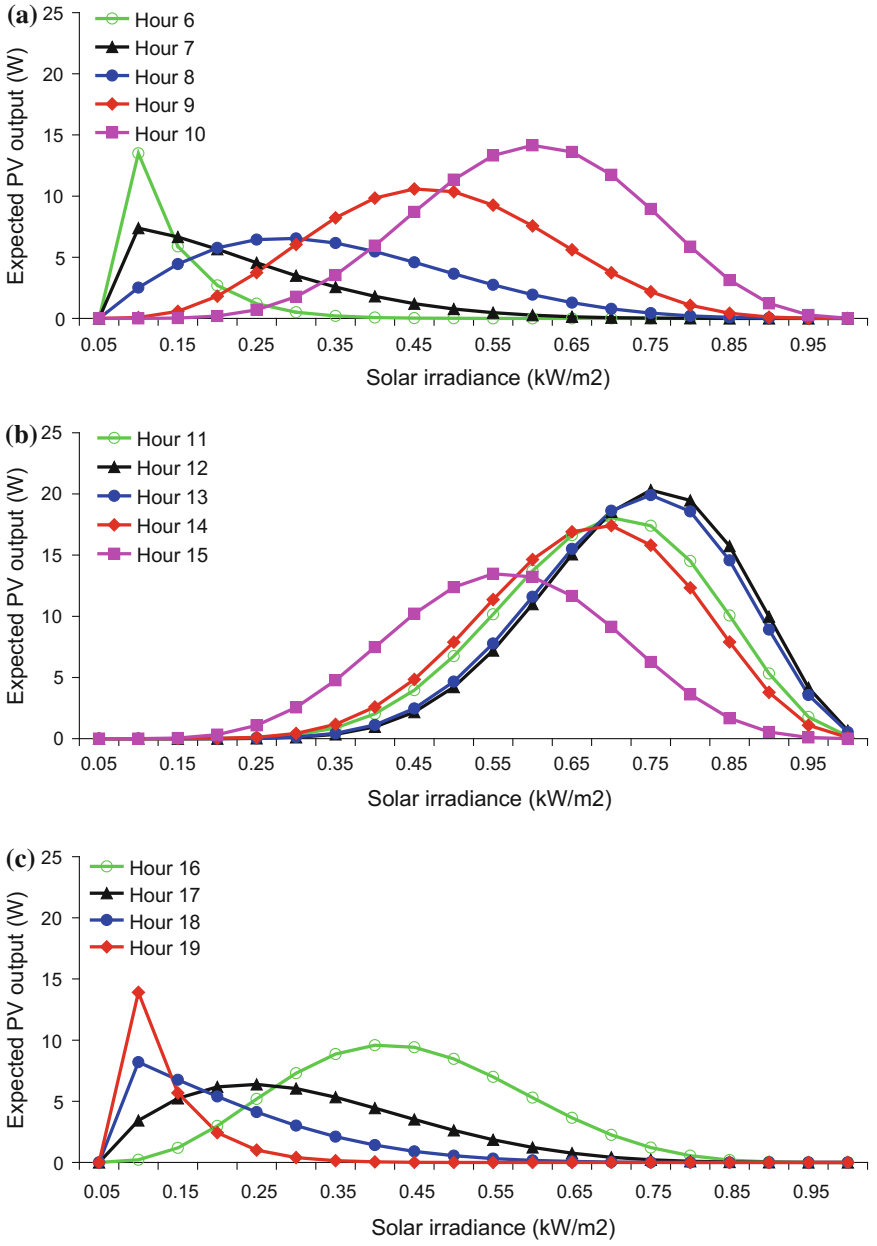


**Fig. 4.7** Expected PV output for hours: **a** 6–10, **b** 11–15 and **c** 16–19

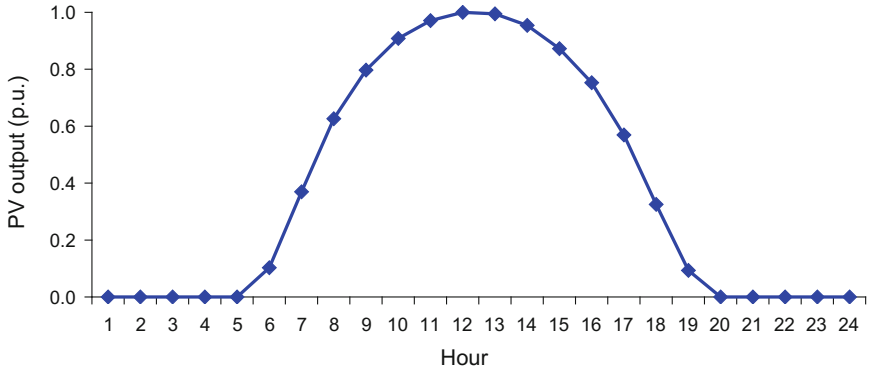


**Fig. 4.8** Normalized daily expected PV output

### *4.7.4 Location Selection*

As previously mentioned, to select the best location, after one power flow run for the base case system at average load level, a PV unit is sized at various buses using Eq. (4.26) and the corresponding multiobjective (*IMO*) for each bus is calculated. The best location at which the *IMO* is lowest is subsequently determined. Figure 4.9a shows the optimal sizes of a PV unit at various buses with the corresponding *IMO* values in the 69-bus system with the industrial load model. The sizes are significantly different in the range of 0.39–2.34 MW. It is observed from the figure that the best location is bus 61 where the *IMO* is lowest. Similarly, the best location is specified at bus 6 in the 33-bus system with the industrial load model, as depicted in Fig. 4.9b. It is noticed that given a fixed location due to resource availability and geographic limitations, the optimal size to which the *IMO* is lowest can be identified from the respective figures. For the other load models (i.e., constant, residential, commercial and mixed), the best locations are at buses 61 and 6 in the 69- and 33-bus systems, respectively. However, depending on the daily demand patterns and characteristic of systems, the locations may be different among load models.

### *4.7.5 Sizing with Respect to Indices*

For the 69-bus system, Fig. 4.10 shows the hourly expected outputs of a PV unit at bus 61 over one day (06:00 to 19:00) with different time-varying load models. These PV output patterns exactly follow the expected PV output curve depicted in Fig. 4.8. The maximum output of the PV unit for each load models, which is identified at hour 11, shows its optimum size. Figure 4.11 presents the expected *IMO* values, which are respectively obtained for the 69-bus system with the PV

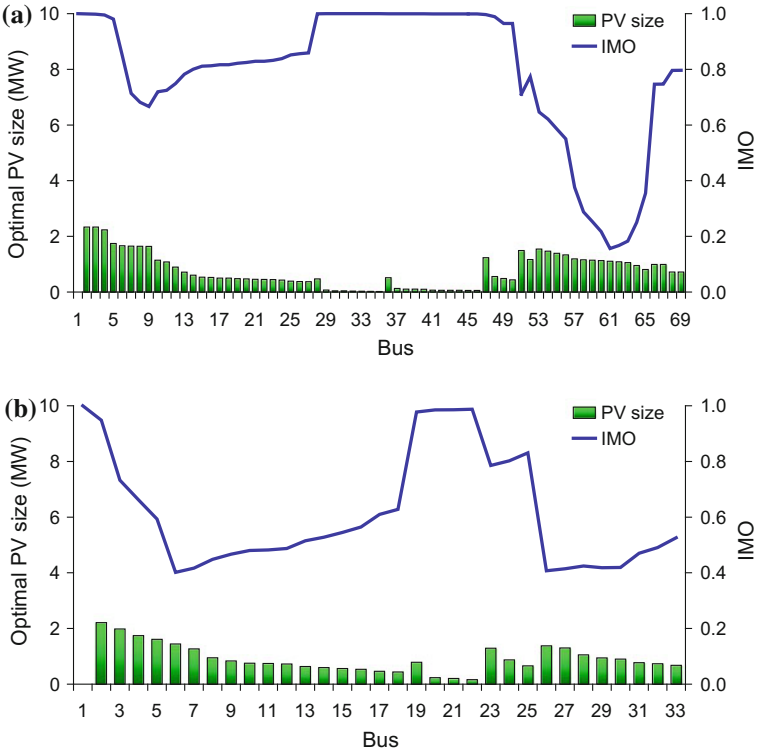


**Fig. 4.9** PV size with respect to IMO at various locations at average load level for the industrial load model: **a** 69-bus system and **b** 33-bus system

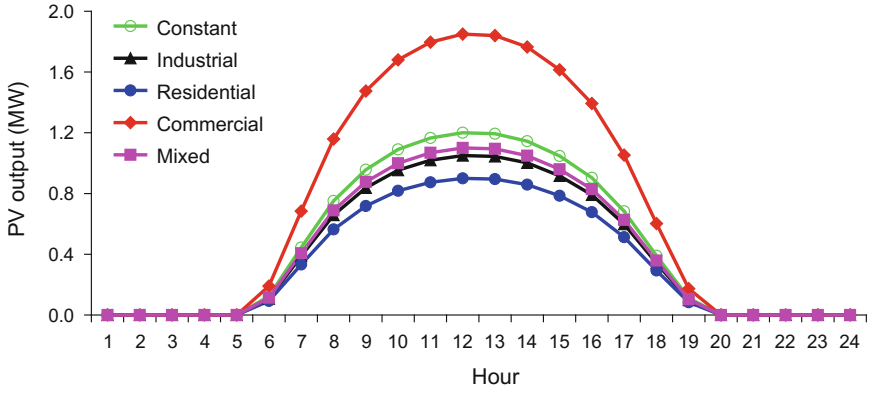


**Fig. 4.10** Hourly expected PV outputs at bus 61 for the 69-bus system for different time-varying load models

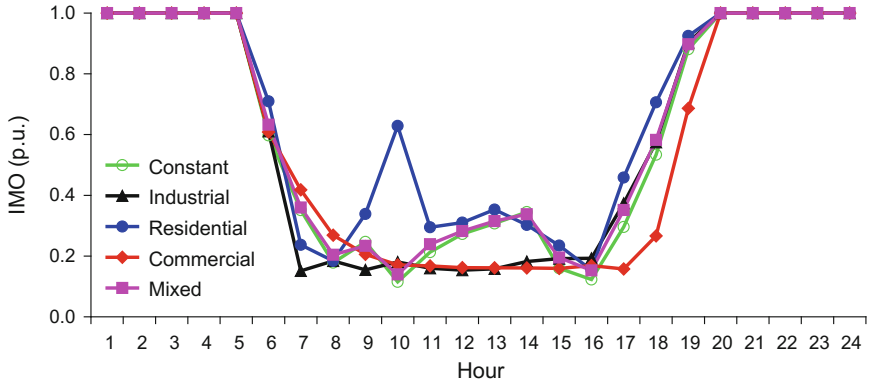


**Fig. 4.11** Hourly expected *IMO* curves for the 69-bus system with a PV unit at bus 61 for different time-varying load models

unit. At each period of the day, the *IMO* values in the system with the PV unit are substantially declined when compared to the system without the PV unit (*IMO* = 1 p.u.). This indicates that the PV installation positively affects the *IMO*. Figure 4.12 shows a comparison of the optimal PV size, and the averages of *IMO* and its components (*ILP*, *ILQ* and *IVD*) in the 69-bus system for different time-varying load models. As shown in Fig. 4.12, a significant difference in the optimal size of the PV unit is observed when different time-varying load models are considered. The PV size for the commercial load is remarkably larger than the industrial and residential loads. This is due to the fact that the commercial consumption and PV output availability (Figs. 4.1 and 4.11) almost occurred simultaneously during the day, while the industrial and residential customers had most of the consumption during the night. It is revealed from Fig. 4.12 that the maximum PV size is determined for the commercial load, whereas the minimum PV size is identified for the residential load. In addition, the size of the PV unit for the

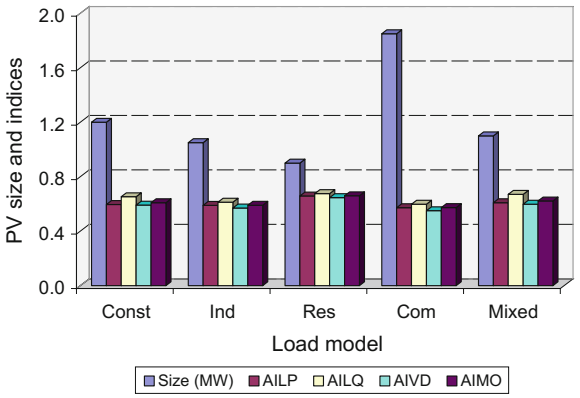


**Fig. 4.12** PV size and indices for the 69-bus system with a PV unit at bus 61 for different time-varying load models

**Table 4.1** PV allocation in the 69- and 33-bus systems

| Load models | 69-bus system | | | 33-bus system | | |
|---|---|---|---|---|---|---|
| | Bus | Size (MW) | *AIMO* | Bus | Size (MW) | *AIMO* |
| Constant | 61 | 1.20 | 0.609 | 6 | 1.80 | 0.737 |
| Industrial | 61 | 1.05 | 0.590 | 6 | 1.55 | 0.722 |
| Residential | 61 | 0.90 | 0.660 | 6 | 1.15 | 0.770 |
| Commercial | 61 | 1.85 | 0.573 | 6 | 2.50 | 0.716 |
| Mixed | 61 | 1.10 | 0.622 | 6 | 1.65 | 0.754 |

time-varying constant load model is roughly 9.09% bigger than the time-varying mixed load model. A similar trend has been observed for the 33-bus system.

Table 4.1 shows a summary and comparison of the results of PV allocation obtained in the 69- and 33-bus systems with different time-varying load models. The results include the optimum bus, size and penetration of the PV unit and corresponding *AIMO* for each load model. Differences in the location, size and penetration exist among the load models. For the 69-bus system, the minimum and maximum *AIMO* values are respectively 0.573 (p.u.) for the commercial load model and 0.660 (p.u.) for the residential load model. A similar trend is observed for the 33-bus system. The lowest *AIMO* is 0.716 (p.u.) for the commercial load model, whereas the highest *AIMO* is 0.770 (p.u.) for the residential load model.

### *4.7.6 PV Penetration and Energy Losses*

Figure 4.13 shows the PV penetration levels in the 69- and 33-bus systems with different time-varying load models. *First*, it is observed that the time-varying load models adopted have a diverse impact on the penetration level. In the 69-bus system, the penetration levels are 32.59% for the commercial load model and 19.55 and 17.38% for the industrial and residential load models, respectively. This is because the PV generation pattern (Fig. 4.7) matches better with the commercial demand than the industrial and residential demand curves (Fig. 4.1). Similarly, in the 33-bus system, the penetration levels are 45.23% for the commercial load model and 29.64 and 22.80% for the industrial and residential load models, respectively. *Secondly*, it is shown from Fig. 4.13 that there is a difference in the PV penetration between the time-varying constant and mixed load models in both test systems. In the 69-bus system, the PV penetration is 22.18% for the time-varying constant load model, whereas this value is 20.34% for the time-varying mixed load model. Similarly, in the 33-bus system, the PV penetration levels are 34.18 and 31.33% for the time-varying constant and mixed load models, respectively. *Finally*, it is also revealed that the system load characteristics play a crucial role in determining the PV penetration. For each load model, the PV penetration in the 69-bus system is lower than the 33-bus system, as shown in Fig. 4.13.

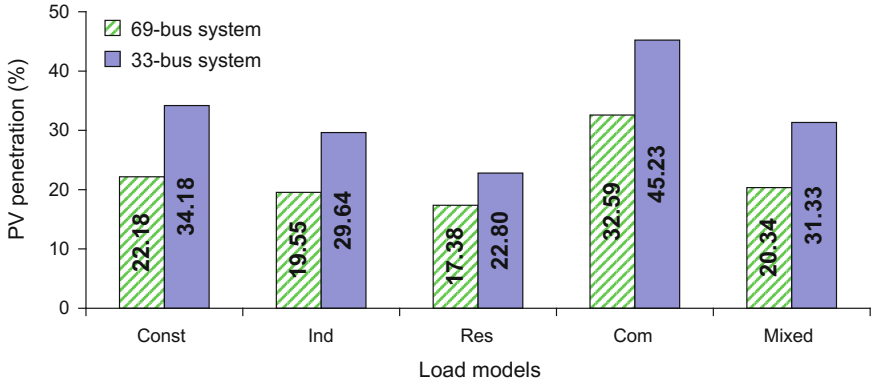


**Fig. 4.13** PV penetration levels in the 69- and 33-bus systems

**Table 4.2** Energy loss reduction over a day for 69 and 33-bus systems

| Load models | 69-bus system | | | 33-bus system | | |
|---|---|---|---|---|---|---|
| | $E_L$ (MWh) | $E_{LPV}$ (MWh) | $\Delta E$ (%) | $E_L$ (MWh) | $E_{LPV}$ (MWh) | $\Delta E$ (%) |
| Constant | 1.87 | 1.32 | 29.54 | 1.73 | 1.25 | 28.13 |
| Industrial | 1.56 | 1.11 | 28.50 | 1.51 | 1.18 | 21.32 |
| Residential | 1.49 | 1.01 | 32.28 | 1.45 | 1.11 | 23.33 |
| Commercial | 1.68 | 0.52 | 68.90 | 1.63 | 0.81 | 50.20 |
| Mixed | 1.54 | 1.08 | 29.79 | 1.43 | 1.04 | 27.58 |

Table 4.2 shows a summary and comparison of the energy loss of the system without and with the PV unit over a day ($E_L$ and $E_{LPV}$, respectively) for different time-varying load models. The daily energy loss is calculated as a sum of all hourly power losses over the day. For each load model, it is observed that the energy loss of the system with the PV unit is significantly reduced when compared to that of the system without the PV unit. In addition, due to inclusion of the active and reactive load voltage exponents in the mixed load model, the energy losses with and without the PV unit for this model are respectively lower than the constant load model. Table 4.2 also shows the results of the energy loss reduction of the two systems ($\Delta E$) for all load models. In both systems, the maximum loss reduction is observed in the commercial load, whereas the minimum value is obtained in the industrial customer. This is due to the fact that the PV generation matches better with the commercial load than the industrial customer, as previously mentioned.

## 4.8 Conclusions

This chapter presented an analytical approach to determine the penetration of PV units in a distribution system with different types of time-varying load models. In this approach, an *IMO*-based analytical expression was proposed to identify the size of PV units, which are capable of supplying active and reactive power, with objectives of simultaneously reducing active and reactive power losses and voltage deviation. The analytical expression was then adapted to accommodate PV units while considering the characteristics of time-varying voltage-dependent load models and probabilistic generation. The Beta PDF model was used to describe the probabilistic nature of solar irradiance. The results indicated that the time-varying load models play a critical role in determining the PV penetration in any distribution system.

For the residential load model, a poor match between the generation and demand leads to relatively low PV penetration levels, roughly 17 and 23% in the 69- and 33-bus systems, respectively. Similarly, for the industrial load, due to a mismatch between the generation and demand, the 69- and 33-bus systems can accommodate PV penetration levels of approximately 20 and 30%, respectively. In contrast, for the commercial load model, a good match between the demand and generation results in higher penetration levels at around 33 and 45% in the respective 69- and 33-bus systems. In addition, a practical load model which is defined as a time-varying mixed load model of residential, industrial and commercial types was examined. It was observed that the PV penetration in the time-varying mixed load model is lower than the time-varying constant load model. This study recommends that the time-varying mixed load model should be used for determining the penetration of PV units in a distribution network.

## References

1. Eftekharnejad S, Vittal V, Heydt GT, Keel B, Loehr J (2013) Impact of increased penetration of photovoltaic generation on power systems. IEEE Trans Power Syst 28(2):893–901. doi:10.1109/tpwrs.2012.2216294
2. Whitaker C, Newmiller J, Ropp M, Norris B (2008) Distributed photovoltaic systems design and technology requirements. Sandia National Laboratories. https://www1.eere.energy.gov/solar/pdfs/distributed_pv_system_design.pdf
3. Lopez E, Opazo H, Garcia L, Bastard P (2004) Online reconfiguration considering variability demand: applications to real networks. IEEE Trans Power Syst 19(1):549–553. doi:10.1109/tpwrs.2003.821447
4. SolarAnywhere. Available: https://solaranywhere.com/
5. Atwa YM, El-Saadany EF, Salama MMA, Seethapathy R (2010) Optimal renewable resources mix for distribution system energy loss minimization. IEEE Trans Power Syst 25(1):360–370. doi:10.1109/TPWRS.2009.2030276
6. Turitsyn K, Sulc P, Backhaus S, Chertkov M (2011) Options for control of reactive power by distributed photovoltaic generators. Proc IEEE 99(6):1063–1073. doi:10.1109/JPROC.2011.2116750

7. Albuquerque FL, Moraes AJ, Guimarães GC, Sanhueza SMR, Vaz AR (2010) Photovoltaic solar system connected to the electric power grid operating as active power generator and reactive power compensator. Sol Energy 84(7):1310–1317. doi:10.1016/j.solener.2010.04.011
8. Hung DQ, Mithulananthan N, Bansal RC (2010) Analytical expressions for DG allocation in primary distribution networks. IEEE Trans Energy Convers 25(3):814–820. doi:10.1109/TEC.2010.2044414
9. Injeti SK, Prema Kumar N (2013) A novel approach to identify optimal access point and capacity of multiple DGs in a small, medium and large scale radial distribution systems. Int J Electr Power Energy Syst 45(1):142–151. doi:10.1016/j.ijepes.2012.08.043
10. Viawan FA, Karlsson D (2007) Combined local and remote voltage and reactive power control in the presence of induction machine distributed generation. IEEE Trans Power Syst 22(4):2003–2012. doi:10.1109/tpwrs.2007.907362
11. Singh D, Verma KS (2009) Multiobjective optimization for DG planning with load models. IEEE Trans Power Syst 24(1):427–436. doi:10.1109/TPWRS.2008.2009483
12. Ochoa LF, Padilha-Feltrin A, Harrison GP (2006) Evaluating distributed generation impacts with a multiobjective index. IEEE Trans Power Delivery 21(3):1452–1458. doi:10.1109/TPWRD.2005.860262
13. El-Zonkoly AM (2011) Optimal placement of multi-distributed generation units including different load models using particle swarm optimisation. IET Gener Transm Distrib 5(7):760–771. doi:10.1049/iet-gtd.2010.0676
14. Ochoa LF, Padilha-Feltrin A, Harrison GP (2008) Evaluating distributed time-varying generation through a multiobjective index. IEEE Trans Power Delivery 23(2):1132–1138. doi:10.1109/TPWRD.2008.915791
15. Hung DQ, Mithulananthan N, Bansal RC (2010) Analytical expressions for DG allocation in primary distribution networks. IEEE Trans Energy Convers 25(3):814–820. doi:10.1109/TEC.2010.2044414
16. Caisheng W, Nehrir MH (2004) Analytical approaches for optimal placement of distributed generation sources in power systems. IEEE Trans Power Syst 19(4):2068–2076. doi:10.1109/tpwrs.2004.836189
17. Gözel T, Hocaoglu MH (2009) An analytical method for the sizing and siting of distributed generators in radial systems. Electr Power Syst Res 79(6):912–918. doi:10.1016/j.epsr.2008.12.007
18. Acharya N, Mahat P, Mithulananthan N (2006) An analytical approach for DG allocation in primary distribution network. Int J Electr Power Energy Syst 28(10):669–678. doi:10.1016/j.ijepes.2006.02.013
19. Samadi A, Ghandhari M, Söder L (2012) Reactive power dynamic assessment of a PV system in a distribution grid. Energy Procedia 20:98–107. doi:10.1016/j.egypro.2012.03.012
20. Hung DQ, Mithulananthan N, Lee KY (2014) Determining PV penetration for distribution systems with time-varying load models. IEEE Trans Power Syst 29(6):3048–3057. doi:10.1109/tpwrs.2014.2314133

# Chapter 5
# PV and BES Integration

## 5.1 Introduction

As discussed in Chap. 4, PV units can be allocated to minimize energy losses and enhance voltage profiles in distribution systems. However, the high penetration of this intermittent renewable source together with demand variations has introduced many challenges to distribution systems such as power fluctuations, reverse power flows, voltage rises, high losses and low voltage stability [1]. Consequently, generated power curtailment, dump loads and dispatchable BES systems have been utilized together with intermittent renewable DG units (i.e., wind and solar) to eliminate the intermittency, reduce power fluctuations and avoid any violation of the system constraints [2].

This chapter studies the integration of PV and BES units in a commercial distribution system for reducing energy loss and enhancing voltage stability. In this chapter, each nondispatchable PV unit is converted into a dispatchable source with a combination of PV and BES units. Multiobjective index (*IMO*)-based analytical expressions are presented to capture the size and power factor of the combined PV and BES units. A Self-Correction Algorithm (SCA) is also reported for sizing multiple PV and BES units while considering the time-varying demand and probabilistic generation.

## 5.2 Load and Generation Modelling

### *5.2.1 Load Modelling*

The demand of the system under the study is assumed to follow a 24-h daily commercial load curve as shown in Fig. 4.1. The time-varying commercial load model as defined in Sect. 2.2 is also considered in this work.



N. Mithulananthan et al., *Intelligent Network Integration of Distributed Renewable Generation*, Green Energy and Technology,
DOI 10.1007/978-3-319-49271-1_5

### 5.2.2 PV Modelling

The PV unit considered is a nondispatchable and probabilistic source and its modelling is described in Sect. 4.2.2. The fact is that capacitors have been traditionally utilized to deliver reactive power or correct power factors for loss reduction and voltage stability enhancement. However, they are not smooth in controlling voltages and not flexible to compensate for transient events due to the impact of intermittent renewable energy resources [3, 4]. As a fast response device, the inverter-based PV unit has the capability to control reactive power or power factors for loss minimization and voltage regulation while supplying energy as a primary purpose [3, 4]. This study considers that a PV unit is associated with two types of converters (type 1 and type 2) for comparison.

- Type 1 is capable of operating at any desired power factor (lagging/leading) to deliver active power and inject or absorb reactive power over all periods [3–5].
- Type 2 can deliver active power only (i.e., unity power factor) as per the standard IEEE 1547 [6].

### 5.2.3 BES Modelling

The Battery Energy Storage (BES) unit is modelled as a dispatchable source described in Sect. 2.3.4. The BES energy variation at bus $k$ in period $t$ can be expressed as [7]:

$$\begin{aligned} E_{BESk}(t) &= E_{BESk}(t-1) - \frac{P_{BESk}^{DISCH}(t)}{\eta_d}\Delta t, \, for \, P_{BESk}(t) > 0 \\ E_{BESk}(t) &= E_{BESk}(t-1) - \eta_c P_{BESk}^{CH}(t)\Delta t, \, for \, P_{BESk}(t) \le 0 \end{aligned} \tag{5.1}$$

where $E_{BESk}$ is the total energy stored in the BES unit; $P_{BESk}^{CH}$ and $P_{BESk}^{DISCH}$ are respectively the charge and discharge power of the BES unit; $\eta_c$ and $\eta_d$ are respectively the charge and discharge efficiencies of the BES unit; $\Delta t$ is the time duration of period $t$.

The lower and upper bounds of the BES unit should be satisfied as follows [8]:

$$E_{BES_k}^{\min} \le E_{BES_k}(t) \le E_{BES_k}^{\max} \tag{5.2}$$

where $E_{BES_k}^{\min}$ and $E_{BES_k}^{\max}$ are respectively the lower and upper bounds of the energy in the BES unit. In this research, the lower and upper bounds are assumed to be 20 and 90% of the installed capacity of the BES unit, respectively [8, 9].

## 5.3 Conceptual Design

Figure 5.1a, b shows the proposed conceptual model of a grid-connected PV and BES system (PV-BES). This system is intended to be installed on the rooftop areas of commercial buildings. The idea is to convert each nondispatchable PV unit to a dispatchable one with a combination of PV and BES units to retain the system active and reactive power losses for each load level at the lowest levels. This combination can produce a daily amount of dispatchable energy, $E_{(PV\,+\,BES)}$. Here, in a 24-h day cycle, the PV unit is generating an $E_{PV}$ amount of energy. A portion of this energy is delivered to the grid, $E_{PV}^{GRID}$. The redundant energy of the PV unit is used to charge the BES unit, $E_{BES}^{CH}$ rather than curtailing it when the PV output is high during the day. This stored energy is then discharged to the grid, $E_{BES}^{DISCH}$ when the PV output is small or zero during the night. The PV and BES units are placed in the same location to avoid network energy losses during the charge of the BES unit. The daily energy amount of a combination of PV and BES units over the total period ($T$ = 24 h) at bus $k$ can be written as:

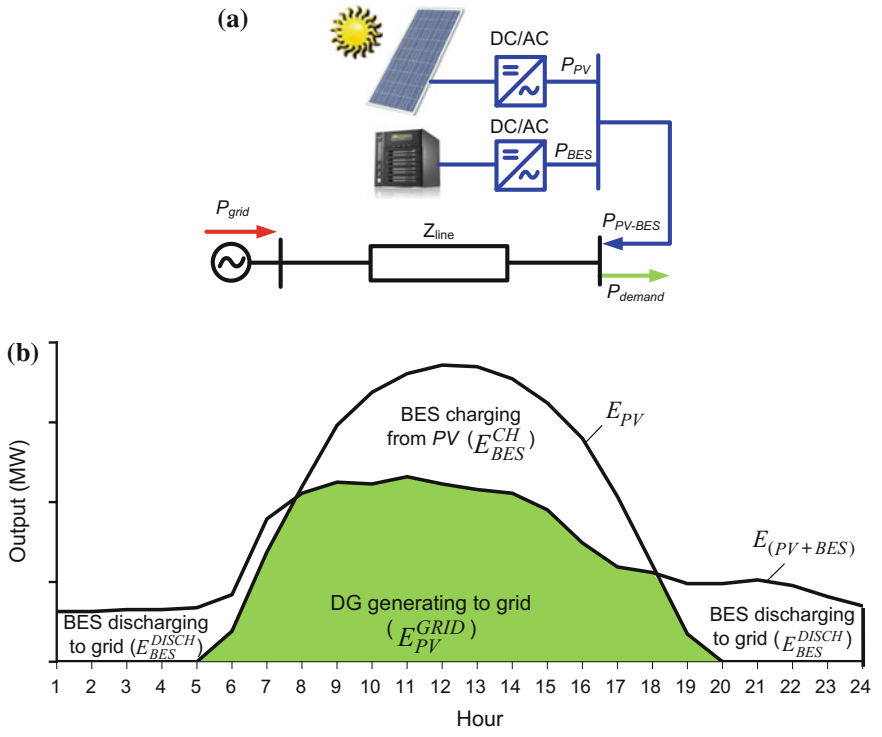


**Fig. 5.1** Conceptual model of grid-connected PV-BES system. **a** Connection diagram and **b** Charging and discharging characteristics of BES and PV outputs

$$E_{(PV+BES)_k} = \int_0^T P_k(t)dt = \sum_{t=1}^{24} P_k(t)\Delta t \tag{5.3}$$

where $P_k(t)$ is the active power output of the combination of PV and BES units at bus $k$ at period $t$ across a given day. The power factor of PV and BES units are optimally dispatched for each 1-h period. From the utility perspective, this model can reduce energy loss and enhance voltage stability, which are respectively related to active and reactive power loss indices as explained below.

## 5.4 Impact Indices

### 5.4.1 Active Power Loss Index

When a mix of PV and BES units, $(PV + BES)$ is injected both active power $(P_k)$ and reactive power $(Q_k)$ at bus $k$, Eq. (4.6) can be rewritten as follows:

$$\begin{aligned} P_{L(PV+BES)} = &\sum_{i=1}^{k} \frac{(P_{bi} - P_k)^2}{|V_i|^2} R_i + \sum_{i=k+1}^{n} \frac{P_{bi}^2}{|V_i|^2} R_i \\ &+ \sum_{i=1}^{k} \frac{(Q_{bi} - Q_k)^2}{|V_i|^2} R_i + \sum_{i=k+1}^{n} \frac{Q_{bi}^2}{|V_i|^2} R_i \end{aligned} \tag{5.4}$$

Let $a_k = \pm\tan(\cos^{-1}(pf_k))$; $a_k$ is positive for the PV-BES mix injecting reactive power and $a_k$ is negative for the PV-BES mix consuming reactive power; $pf_k$ is the operating power factor of the PV-BES mix at bus $k$, the relationship between $P_k$ and $Q_k$ at bus $k$ can be expressed as:

$$Q_k = a_k P_k \tag{5.5}$$

From Eqs. (4.6), Eqs. (5.4) and (5.5), we obtain:

$$P_{L(PV+BES)} = \sum_{i=1}^{k} \frac{P_k^2 - 2P_{bi}P_k}{|V_i|^2} R_i + \sum_{i=1}^{k} \frac{a_k^2 P_k^2 - 2Q_{bi}a_k P_k}{|V_i|^2} R_i + P_L \tag{5.6}$$

Finally, the active power loss index ($ILP$) is defined as the ratio of Eqs. (5.6) and (4.6) as follows:

$$ILP = \frac{P_{L(PV+BES)}}{P_L} \tag{5.7}$$

where the total active power loss ($P_L$) in a radial distribution system with $n$ branches can be calculated using Eq. (4.6).

### 5.4.2 Reactive Power Loss Index

Similar to Eq. (5.6), when a mix of PV and BES units, $(PV + BES)$ is injected both $P_k$ and $Q_k = a_k P_k$ at bus $k$, Eq. (4.10) can be rewritten as follows:

$$Q_{L(PV+BES)} = \sum_{i=1}^{k} \frac{P_k^2 - 2P_i P_k}{|V_i|^2} X_i + \sum_{i=1}^{k} \frac{a_k^2 P_k^2 - 2Q_i a_k P_k}{|V_i|^2} X_i + Q_L \tag{5.8}$$

Finally, the reactive power loss index ($ILQ$) is defined as the ratio of Eqs. (5.8) and (4.10) as follows:

$$ILQ = \frac{Q_{L(PV+BES)}}{Q_L} \tag{5.9}$$

where the total reactive power loss ($Q_L$) in a radial distribution system with $n$ branches can be calculated as Eq. (4.10).

## 5.5 Multiobjective Index

The multiobjective index ($IMO$) is a combination of the $ILP$ and $ILQ$ indices, respectively related to energy loss and voltage stability by assigning a weight to each index. The $IMO$ index that can be utilized to assess the performance of a distribution system with PV and BES can be expressed as follows:

$$IMO = \sigma_1 ILP + \sigma_2 ILQ \tag{5.10}$$

where $\sum_{i=1}^{2} \sigma_i = 1.0 \wedge \sigma_i \in [0,\ 1.0]$. This can be performed since all impact indices are normalized (values between zero and one) [10]. When hybrid PV and BES systems are not connected to the system (i.e., base case system), the $IMO$ is the highest at one.

These weights are intended to give relative importance to each impact index for the connection of hybrid PV-BES systems and depend on the required analysis (e.g., planning and operation) [10–13]. Determination of suitable values for the weights will also rely on the experience and concerns of engineers. The integration of hybrid PV-BES systems has a significant impact on the energy loss and voltage stability of distribution networks. Currently, the energy loss is one of the major concerns at the distribution system due to its impact on the utilities' profit, while the

voltage stability is less important than the energy loss. Therefore, the weight for the energy loss should be higher than that for the voltage stability. If there is an increasing concern on voltage stability due to high intermittent renewable penetration and an increase in loads and system security, the weights can be adjusted based on the priority. Considering the above current concerns and referring to previous research papers [10–13], this study assumes that the active power loss related to energy loss receives a significant weight of 0.7, leaving the reactive power loss related to voltage stability at a weight of 0.3.

The *IMO* at period *t*, $IMO(t)$ is obtained from Eq. (5.10). Hence, the average multiobjective index (*AIMO*) over the total period ($T$ = 24 h) in a distribution system with an interval ($\Delta t$) of 1 h can be expressed as follows:

$$AIMO = \frac{1}{T}\int_0^T IMO(t)dt = \frac{1}{24}\sum_{t=1}^{24} IMO(t)\Delta t \tag{5.11}$$

The lowest *AIMO* implies the best PV and BES allocation for energy loss reduction and voltage stability enhancement. The objective function defined by the *AIMO* in Eq. (5.11) is subject to technical constraints as follows. The bus voltages ($V_k$) must remain within acceptable limits in all periods.

$$V_{\min} \le V_k(t) \le V_{\max} \tag{5.12}$$

## 5.6 Energy Loss and Voltage Stability

### 5.6.1 Energy Loss

The active power loss at each period $t$, $P_{loss}(t)$ can be obtained from Eq. (4.6) without a PV-BES unit or Eq. (5.6) with a PV-BES unit. Hence, the total annual energy loss ($E_{loss}$) over the total period ($T$ = 24 h) in a distribution system with a time duration ($\Delta t$) of 1-h can be expressed as:

$$E_{loss} = 365\int_0^T P_{loss}(t)dt = 365\sum_{t=1}^{24} P_{loss}(t)\Delta t \tag{5.13}$$

### 5.6.2 Voltage Stability

The static voltage stability can be analyzed using the relationship between the receiving Power ($P$) and the Voltage (V) at a certain bus in a distribution or

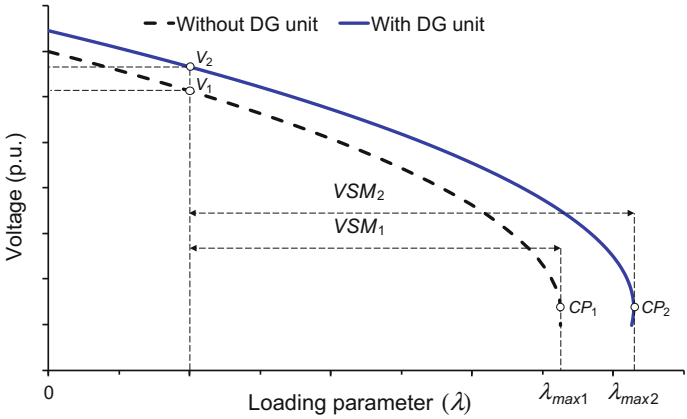


**Fig. 5.2** Hybrid PV-BES system impact on maximum loadability and voltage stability margin [15, 16]

transmission system, as illustrated in Fig. 5.2. This curve is popularly referred to as *P-V* curve or "Nose Curve" and obtained using the Continuation Power Flow (CPF) technique [14]. The Critical Point (*CP)* or the voltage collapse point in the curve represents the maximum loading ($\lambda_{max}$) of the system. The Voltage Stability Margin (*VSM*) is defined as the distance from an operating point to the critical point. Even though system may not be operating closer to the collapse point due to lower voltage limits and exceeding feeder current limits, *P-V* curves indicate approximate and relative stability margins. As shown in Fig. 5.2, the scaling factor of the load demand at a certain operating point ($\lambda$) varies from zero to $\lambda_{max}$. When a hybrid PV-BES system is integrated in the system appropriately, overall loss reduces, considering charging and discharging of BES. Accordingly, the $V_1$ and $CP_1$ enhance to $V_2$ and $CP_2$, respectively. Hence, the maximum loadability increases from $\lambda_{max1}$ to $\lambda_{max2}$ as defined as follows [15, 16]. The voltage stability margin subsequently improves from $VSM_1$ to $VSM_2$.

$$P_D = \lambda P_{Do};\ Q_D = \lambda Q_{Do} \tag{5.14}$$

where $P_{Do}$ and $Q_{Do}$ correspond to the initial active and reactive power demands, respectively.

## 5.7 Proposed Analytical Expressions

This section presents analytical expressions based on the multiobjective index (*IMO*) defined by Eq. (5.10) to calculate the size and power factor of a mix of PV and BES units.

Substituting Eqs. (5.7) and (5.9) into Eq. (5.10), we obtain:

$$IMO(P_k, a_k) = \frac{\sigma_1}{P_L} P_{L(PV+BES)} + \frac{\sigma_2}{Q_L} Q_{L(PV+BES)} \tag{5.15}$$

As given in Eq. (5.15), the *IMO* variation is a function of the PV-BES penetration level related to variables $P_k$ and $a_k$(or $pf_k$: the power factor of the PV-BES mix at bus $k$). At the minimum *IMO*, the partial derivative of Eq. (5.15) with respect to both variables at bus $k$ becomes zero.

$$\frac{\partial IMO}{\partial P_k} = \frac{\sigma_1}{P_L} \frac{\partial P_{L(PV+BES)}}{\partial P_k} + \frac{\sigma_2}{Q_L} \frac{\partial Q_{L(PV+BES)}}{\partial P_k} = 0 \tag{5.16}$$

$$\frac{\partial IMO}{\partial a_k} = \frac{\sigma_1}{P_L} \frac{\partial P_{L(PV+BES)}}{\partial a_k} + \frac{\sigma_2}{Q_L} \frac{\partial Q_{L(PV+BES)}}{\partial a_k} = 0 \tag{5.17}$$

The derivative of Eqs. (5.6) and (5.8) with respect to $P_k$ can be expressed as follows:

$$\frac{\partial P_{L(PV+BES)}}{\partial P_k} = -2A_k + 2B_k P_k - 2C_k a_k + 2B_k a_k^2 P_k \tag{5.18}$$

$$\frac{\partial Q_{L(PV+BES)}}{\partial P_k} = -2D_k + 2E_k P_k - 2a_k F_k + 2a_k^2 E_k P_k \tag{5.19}$$

where

$$A_k = \sum_{i=1}^{k} \frac{R_i P_{bi}}{|V_i|^2};\ B_k = \sum_{i=1}^{k} \frac{R_i}{|V_i|^2};\ C_k = \sum_{i=1}^{k} \frac{R_i Q_{bi}}{|V_i|^2}$$

$$D_k = \sum_{i=1}^{k} \frac{X_i P_{bi}}{|V_i|^2};\ E_k = \sum_{i=1}^{k} \frac{X_i}{|V_i|^2};\ F_k = \sum_{i=1}^{k} \frac{X_i Q_{bi}}{|V_i|^2}$$

Substituting Eqs. (5.18) and (5.19) into Eq. (5.16), we get:

$$P_k = \frac{\sigma_1(A_k + C_k a_k)Q_L + \sigma_2(D_k + a_k F_k)P_L}{\sigma_1(B_k + B_k a_k^2)Q_L + \sigma_2(E_k + E_k a_k^2)P_L} \tag{5.20}$$

The derivative of Eqs. (5.6) and (5.8) with respect to $a_k$ can be expressed as follows:

$$\frac{\partial P_{L(PV+BES)}}{\partial a_k} = -2C_k P_k + 2B_k a_k P_k^2 \tag{5.21}$$

$$\frac{\partial Q_{L(PV+BES)}}{\partial a_k} = -2F_k P_k + 2a_k E_k P_k^2 \tag{5.22}$$

Substituting Eqs. (5.21) and (5.22) into Eq. (5.17), we obtain:

$$a_k = \frac{\sigma_1 C_k Q_L + \sigma_2 F_k P_L}{P_k(\sigma_1 B_k Q_L + \sigma_2 E_k P_L)} \tag{5.23}$$

The relationship between the power factor of a PV-BES unit ($pf_k$) and variable $a_k$ at bus $k$ can be expressed as follows:

$$pf_k = \cos\left(\tan^{-1}(a_k)\right) \tag{5.24}$$

At the minimum *IMO*, the optimal size and power factor at bus $k$, period $t$ (i.e., $P_k(t)$ and $pf_k(t)$, respectively) can be obtained from Eqs. (5.20), (5.23) and (5.24) as:

$$P_k(t) = \frac{\sigma_1 A_k(t) Q_L(t) + \sigma_2 D_k(t) P_L(t)}{\sigma_1 B_k(t) Q_L(t) + \sigma_2 E_k(t) P_L(t)} \tag{5.25}$$

$$pf_k(t) = \cos\left(\tan^{-1}\left(\frac{\sigma_1 C_k(t) Q_L(t) + \sigma_2 F_k(t) P_L(t)}{\sigma_1 A_k(t) Q_L(t) + \sigma_2 D_k(t) P_L(t)}\right)\right) \tag{5.26}$$

The optimal size and power factor of a single PV-BES unit for each period can be calculated using Eqs. (5.25) and (5.26), respectively. When multiple PV-BES units are considered, a Self Correction Algorithm (SCA) developed below is employed.

## 5.8 Self-Correction Algorithm

### *5.8.1 Sizing PV-BES*

This section presents an algorithm to size multiple PV-BES units, which are known as a combination of PV and BES units, at a number of pre-specified buses to minimize the active and reactive power losses at each load level. As reported in Sect. 5.2.1, each PV-BES unit is placed at the same bus. Here, the PV-BES unit is modelled as a dispatchable source. The algorithm includes two tasks. The *first task* is to calculate the approximate size and power factor of the PV-BES unit using Eqs. (5.25) and (5.26) at pre-specified buses, respectively. The *second task* is to re-calculate the size and power factor of each PV-BES unit obtained previously using Eqs. (5.25) and (5.26), respectively. The *second task* is repeated until the difference between the last and previous *IMO* values is reached to a pre-defined tolerance (zero in this study). The algorithm involves the following steps:

Step 1: Set buses (based on resource availability and other constraints) to install PV-BES units.
Step 2: Run power flow for the first period and calculate the size and power factor of each PV-BES unit for each bus using Eqs. (5.25) and (5.26), respectively. Find the *IMO* for each case using Eq. (5.10). Locate the bus where the *IMO* is the lowest with the corresponding size and power factor. Update the load data with the PV-BES unit obtained at this bus. Repeat *Step* 2 for the rest of the selected buses.
Step 3: Re-calculate the size and power factor by repeating *Step* 2 until the difference between the last and previous *IMO* values is reached to zero.
Step 4: Repeat *Step*s 2 to 3 for the rest periods. Calculate the *AIMO* using Eq. (5.11).

The above algorithm is developed to place PV-BES units considering the optimal power factor. This algorithm can be modified to allocate PV-BES units with a pre-specified power factor as well. When the power factor is pre-specified, the algorithm is similar to the above with exception that in *Step* 2, the size of the PV-BES unit for each bus is determined using Eq. (5.20) rather than Eq. (5.25). After the size of the combination of the PV-BES unit is found for each bus, two additional analyses explained below are implemented to capture the individual size of the PV and BES units for each selected bus.

### 5.8.2 Sizing PV

As shown in Fig. 5.1a, b, the daily charging and discharging energies at bus $k$ is obtained from the hourly input and output power of the BES unit.

$$E_{BES_k}^{CH} = \int_0^T P_{BES_k}^{CH}(t)dt = \sum_{t=1}^{24} P_{BES_k}^{CH}(t)\Delta t \tag{5.27}$$

$$E_{BES_k}^{DISCH} = \int_0^T P_{BES_k}^{DISCH}(t)dt = \sum_{t=1}^{24} P_{BES_k}^{DISCH}(t)\Delta t \tag{5.28}$$

The total output energies of the PV-BES mix and PV unit at bus $k$ is respectively calculated as follows:

$$E_{(PV+BES)_k} = E_{PV_k}^{GRID} + E_{BES_k}^{DISCH} \tag{5.29}$$

$$E_{PV_k} = E_{PV_k}^{GRID} + E_{BES_k}^{CH} \tag{5.30}$$

where $E_{PV_k}^{GRID}$ is the amount of PV energy delivered to the grid at bus $k$. The charging and discharging energy of the BES unit at bus $k$ with a round-trip efficiency ($\eta_{BES} = \eta_c \times \eta_d$) is expressed as:

$$E_{BES_k}^{DISCH} = \eta_{BES} E_{BES_k}^{CH} \tag{5.31}$$

The total output energy of the PV unit at bus $k$ can be obtained from Eqs. (5.29), (5.30) and (5.31) as follows:

$$E_{PV_k} = \frac{E_{(PV+BES)_k} - (1 - \eta_{BES}) E_{PV_k}^{GRID}}{\eta_{BES}} \tag{5.32}$$

The maximum power generation of the PV unit during a specific period over a 24-h day cycle is utilized to specify the power rating or optimal size of the PV unit at bus $k$.

$$P_{PV_k} = k_{PV}^{unit} E_{PV_k} \tag{5.33}$$

where $k_{PV}^{unit} = \frac{P_{PV}^{unit}}{E_{PV}^{unit}}$, $P_{PV}^{unit}$ is the maximum output of a PV module unit, and $E_{PV}^{unit}$ is the amount of PV generated energy over a 24-h day. Assuming $\eta_{BES} = 1$, i.e., $E_{PV_k} = E_{(PV+BES)_k}$, the initial PV size is calculated from Eq. (5.33) as $P'_{PV_k} = k_{PV}^{unit} E_{(PV+BES)_k}$, and $E_{PV_k}^{GRID'}$ is then obtained from Fig. 5.1a, b, for example. When $\eta_{BES}$ is less than unity, $P_{PV_k}$ increases. However, as demonstrated in the simulation results, $E_{PV_k}^{GRID}$ rises insignificantly compared to $E_{PV_k}^{GRID'}$. Hence, the optimal PV size is obtained from Eqs. (5.32) and (5.33) as follows:

$$P_{PV_k} = k_{PV}^{unit} \left( \frac{E_{(PV+BES)_k} - (1 - \eta_{BES}) E_{PV_k}^{GRID'}}{\eta_{BES}} \right) \tag{5.34}$$

### 5.8.3 Sizing BES

The optimal size of a BES unit at bus $k$ is calculated with respect to the power rating ($P_{BES_k}$) and energy capacity ($E_{BES_k}$) such that it can accommodate all redundant energy of the PV unit that needs to be curtailed to maintain the system loss for each period at the lowest level. The maximum charging and discharging power during a specific period across a 24-h day cycle is utilized to specify the power rating of the BES unit. The maximum charging energy during this cycle is used to determine the energy capacity of the BES unit.

## 5.9 Example

### 5.9.1 Test System

The proposed methodology was applied to the 33-bus distribution system depicted in Fig. 3.1. The system demand follows a commercial load curve illustrated in Fig. 5.1. It is assumed that operating voltages are from 0.95 to 1.05 p.u. The hourly expected output of the PV module is plotted in Fig. 4.8. Three PV units are assumed to be allocated at buses 12, 20 and 24. Sodium-sulfur BES unit considered has a round-trip efficiency of 77%. To demonstrate the effectiveness of the methodology, the following scenarios are considered.

- Scenario 1: Three PV-BES units that can generate both active and reactive power at optimal power factor for each period, as proposed in this chapter.
- Scenario 2: Three PV-BES units that can deliver active power only (i.e., unity power factor) for all periods as per the standard IEEE 1547 [6].

### 5.9.2 Sizing PV and BES Units

Figure 5.3a, b, c shows the results of PV-BES placement with optimal power factor dispatch at buses 12, 20 and 24 for Scenario 1. The number of PV-BES units can be limited due to the availability of PV resources and geographic limitations. The output and power factor of PV-BES units are optimally dispatched for each 1-h period across a 24-h day cycle such that the system can achieve the lowest *IMO* for each period. As shown in Fig. 5.3a, PV-BES units 1, 2 and 3 correspond to the PV-BES units located at buses 12, 20 and 24 respectively. The output curves of these PV-BES units follow the commercial load demand pattern in Fig. 4.1 as the PV-BES units are dispatchable sources. It can be seen from Fig. 5.3b that the power factor of PV-BES unit 1 at bus 12 is dispatched for each period across a 24-h day in the range of 0.860 and 0.867 (lagging). For PV-BES unit 2 at bus 20, the power factor varies from 0.899 to 0.901 (lagging). Similarly, the power factor of PV-BES unit 3 at bus 24 varies between 0.872 and 0.876 (lagging). Figure 5.3c shows the *ILP*, *ILQ* and *IMO* values for each period related to the active power loss, reactive power loss and multiobjective indices, respectively after the three PV-BES units are installed in the system. Significant reductions in the indices *ILP*, *ILQ* and *IMO* show the positive effect of three PV-BES units placement on the system. At each period, the *ILP* is lower than the *ILQ*, indicating that the system can benefit more from reducing the active power loss than the reactive power loss. Similar results have been obtained for Scenario 2 (i.e., the PV-BES unit is capable of delivering active power only).

Table 5.1 summaries the results of PV-BES placement for Scenarios 1 and 2, including the optimal size and power factor for each location. The optimal size of

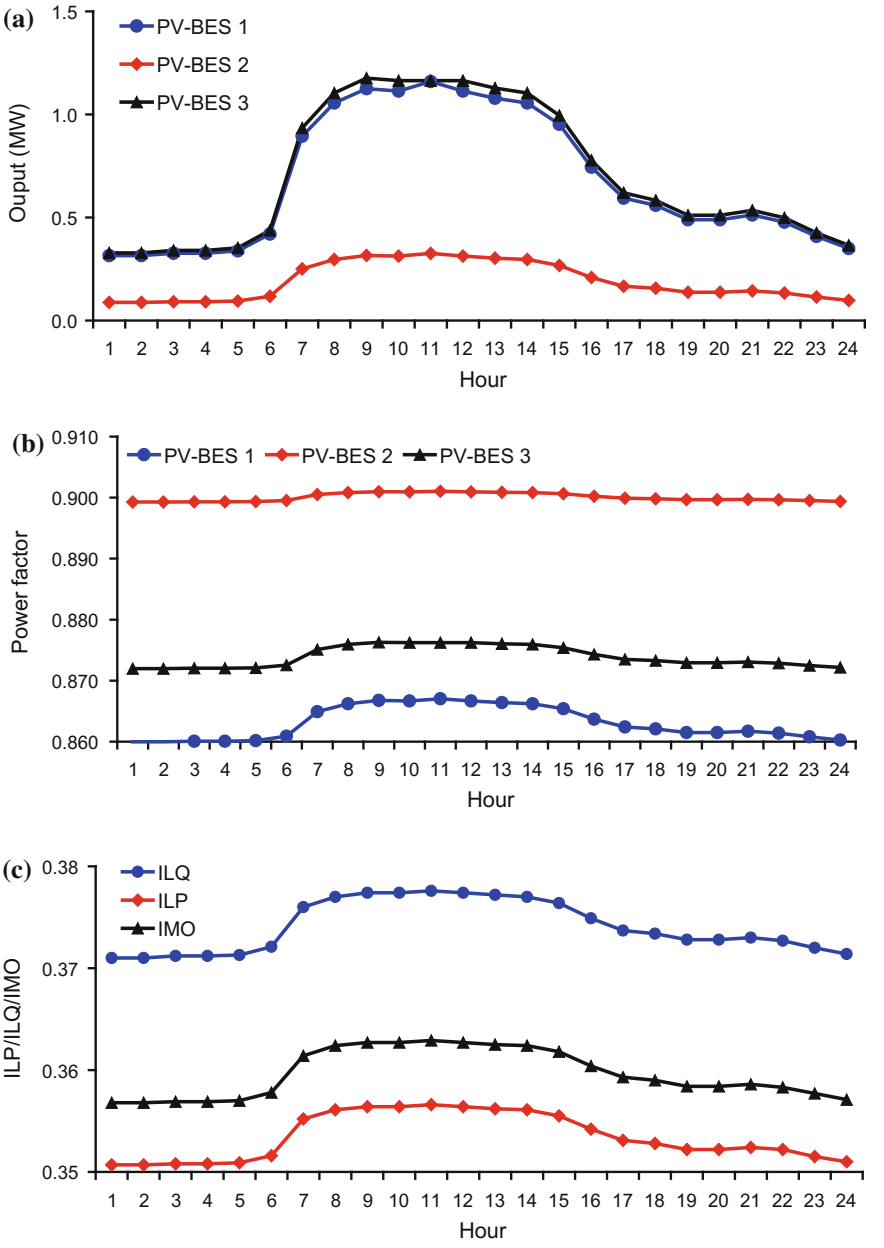


**Fig. 5.3** Daily PV-BES outputs, power factor and index curves for Scenario 1: **a** PV-BES outputs, **b** Power factor of PV-BES units, **c** Indices with three PV-BES units

**Table 5.1** PV-BES placement with optimal lagging and unity power factors

| Scenario | Bus | Size (MW) | Power factor | *AILP* | *AILQ* | *AIMO* |
|---|---|---|---|---|---|---|
| 1 | 12 | 1.160 | 0.867 | 0.3484 | 0.3691 | 0.3546 |
| | 20 | 0.326 | 0.901 | | | |
| | 24 | 1.164 | 0.876 | | | |
| 2 | 12 | 1.155 | 1.000 | 0.5150 | 0.5255 | 0.5181 |
| | 20 | 0.327 | 1.000 | | | |
| | 24 | 1.167 | 1.000 | | | |

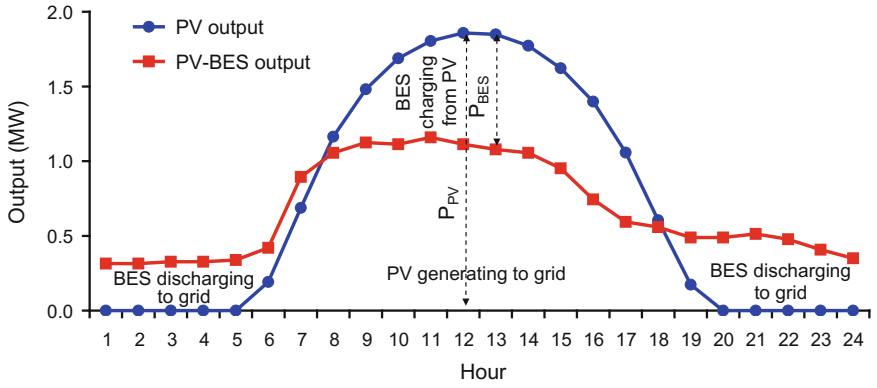


**Fig. 5.4** Daily charging and discharging curves of BES unit at bus 12 for Scenario 1

each PV-BES unit, which corresponds to its maximum output at hour 11 is obtained from Fig. 5.3a. Table 5.1 also shows the *AILP*, *AILQ* and *AIMO* values, which correspond to the average active power loss, average reactive power loss and average multiobjective indices over 24 h across the day, respectively. It can be seen from Table 5.1 that in Scenario 1, the power factors of the PV-BES units at buses 12, 20 and 24 are different at 0.867, 0.901 and 0.876 (lagging), respectively. It is also observed from the table that operation of the PV-BES units with power factor dispatch for each period in Scenario 1 can make a significant contribution to minimising the *AIMO* when compared to that with unity power factor in Scenario 2.

Figure 5.4 presents the hourly-expected PV output at bus 12 for Scenario 1 with optimal power factor dispatch. This curve exactly follows the expected PV output curve in Fig. 3.2. The maximum output of each PV unit that is identified at hour 12 indicates its optimum size. The figure also shows the amount of energy that the PV unit can generate versus the amount of PV-BES energy accommodated by the network to retain the loss for each period at the lowest level. The sum of the hourly differences between these two patterns identifies the amount of energy charged and discharged by the BES unit. The amount of PV energy that needs to be curtailed to remain the minimum energy loss is stored into the BES unit. This stored energy

**Table 5.2** Sizing PV and BES units at optimal lagging power factor (Scenario 1)

| Bus | 12 | 20 | 24 | Total |
|---|---|---|---|---|
| PV size (MW) | 1.858 | 0.526 | 1.952 | 4.336 |
| PV size (MVAr) | 1.068 | 0.253 | 1.075 | 2.396 |
| BES power rating (MW) | 0.770 | 0.221 | 0.813 | 1.804 |
| BES power rating (MVAr) | 0.443 | 0.106 | 0.448 | 0.997 |
| BES energy capacity (MWh) | 5.750 | 1.655 | 6.139 | 13.544 |

portion is then discharged to the grid following the PV-BES output curve to keep the lowest energy loss as well. The maximum difference found at hour 13 gives the maximum power of the charging energy or the power rating of the BES unit ($P_{BES}$). The maximum charging energy over a 24-h day cycle is used to calculate the capacity of the BES unit ($E_{BES}$). The charging and discharging time of the BES unit can be identified from Fig. 5.4. Similar results have been found for the PV-BES units at buses 20 and 24 in Scenario 1 (optimal power factor) and buses 12, 20 and 24 in Scenario 2 (unity power factor) as well.

Tables 5.2 and 5.3 summarize the results of the size of PV units and the power rating and energy capacity of BES units for each location in Scenarios 1 and 2, respectively. It is observed from the tables that the similarity in the size of the PV units in MW, the power rating of the BES units in MW and the energy capacity of the BES units in MWh exist between Scenarios 1 and 2. However, as previously mentioned, the PV-BES units in Scenario 1 deliver both active and reactive power at optimal lagging power factor for each period across a 24-h day (see Fig. 5.3b), as proposed in this chapter, whereas the PV-BES units in Scenario 2 only supply active power over all periods as per the standard IEEE 1547 [6]. Particularly, as shown in Table 5.2, the total size of the PV units is 4.336 MW of the active power and 2.396 MVAr of the reactive power. The total active and reactive power ratings of the BES units are 1.804 MW and 0.997 MVAr, respectively and the total energy capacity of the BES units over the day is 13.544 MWh. In this scenario, the BES units also either absorb or inject the required amount of reactive power for each hour of the day. For Scenario 2, as shown in Table 5.3, the total active power size of the PV units is 4.336 MW. The total active power rating of the BES units is 1.803 MW and the total energy capacity of the BES units over the day is 13.549 MWh. Unlike Scenario 1, in this Scenario, as the BES units operate at unity power factor, there is no reactive power delivered or absorbed by these units.

### *5.9.3 Energy Loss and Voltage Stability*

Figures 5.5 and 5.6 show the results of energy loss and *PV* curve-based voltage stability margin of the system with and without the PV-BES units, respectively. The

**Table 5.3** Sizing PV and BES units at unity power factor (Scenario 2)

| Bus | 12 | 20 | 24 | Total |
|---|---|---|---|---|
| PV size (MW) | 1.858 | 0.526 | 1.952 | 4.336 |
| BES power rating (MW) | 0.773 | 0.220 | 0.810 | 1.803 |
| BES energy capacity (MWh) | 5.786 | 1.648 | 6.115 | 13.549 |

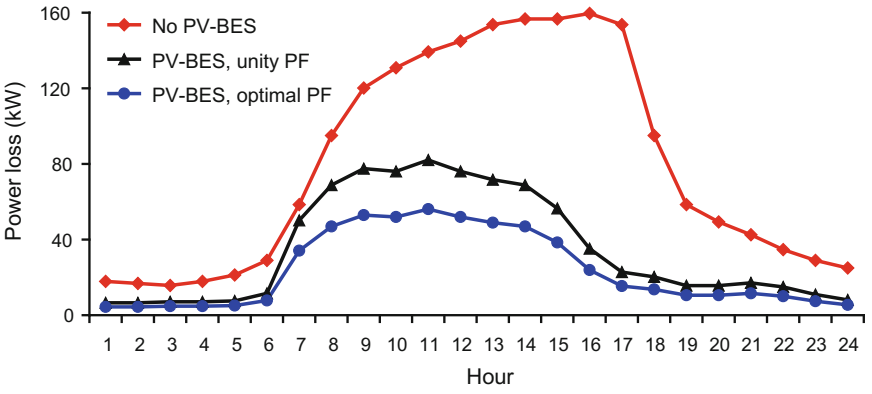


**Fig. 5.5** PV-BES impact on energy loss

power factors of the PV-BES units is set at unity in compliance with the current standard IEEE 1547 [6] and optimally dispatched for each period as proposed in this chapter. It is observed from the figures that operation of the PV-BES units with optimal power factor dispatch (Scenario 1) can significantly reduce energy loss and better enhance voltage stability when compared to that with unity power factor (Scenario 2).

As illustrated in Fig. 5.5, the system power loss for Scenario 1 with optimal power factor dispatch for each period is rather lower than that for Scenario 2 with unity power factor. Table 5.4 summarizes the results of the annual energy losses of the system for all scenarios. Before PV-BES insertion (i.e., for the base case scenario), the annual energy loss is 701.33 MWh. After PV-BES installation, Scenario 1 obtains a maximum energy loss reduction of 70.44%, whereas Scenario 2 achieves an energy loss reduction of 56.55% only.

As shown in Fig. 5.6, $V$ is the normal operating point voltages ($\lambda = 1$), $\lambda_{max}$ is the maximum loading, *VSM* is the static voltage stability margin that is defined as the distance from the operating point to a voltage collapse point or a critical point (*CP*), $\Delta VSM$ is an increase in the voltage stability margin. In Scenario 1, when three PV-BES units generate an amount of 2.65 MW at their optimal power factors found in Table 5.1, the normal operating point voltage at the weakest point (bus 18) improves from $V_0$ (without PV-BES units) to $V_1$ (with PV-BES units). The maximum loading increases from $\lambda_{max0}$ (without PV-BES units) to $\lambda_{max1}$ (with PV-BES units). Hence, the voltage stability margin in Scenario 1 ($\Delta VSM_1$) is enhanced by

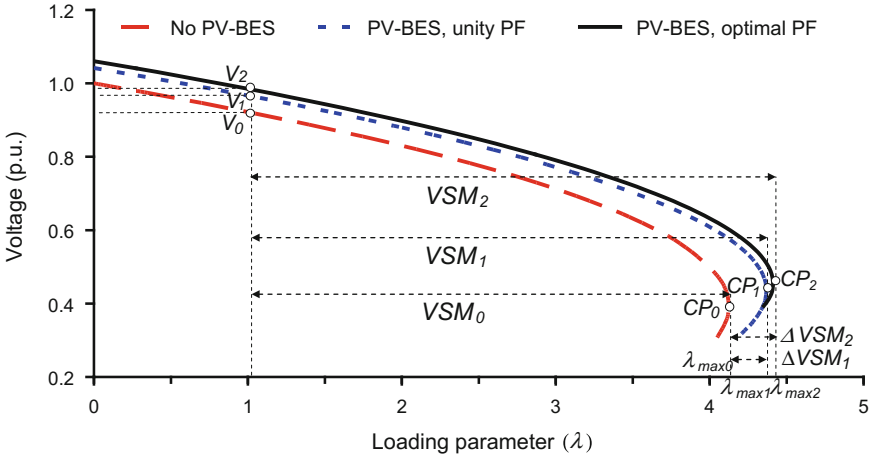


**Fig. 5.6** PV-BES impact on maximum loadability and voltage stability margin

**Table 5.4** Energy loss and voltage stability

| Scenario | Annual energy loss | Annual loss reduction | Voltage stability | | |
|---|---|---|---|---|---|
| | (MWh) | (%) | $V$ (p.u.) | $\lambda_{max}$ (p.u.) | $\Delta VSM$ (p.u.) |
| Base case | 701.33 | | 0.9175 | 4.1217 | |
| 1 | 207.31 | 70.44 | 0.9878 | 4.4120 | 0.2903 |
| 2 | 304.72 | 56.55 | 0.9663 | 4.3673 | 0.2456 |

roughly 0.29 p.u. Similarly, the $\Delta VSM_2$ in Scenario 2 is increased by approximately 0.25 p.u. These results are summarized in Table 5.4. It is obvious that the combination of the PV and BES units with optimal power factor dispatch for each period (Scenario 1) achieves a larger *VSM* value than that with unity power factor (Scenario 2).

Figure 5.7 presents the voltage profiles for scenarios: without the PV-BES units (base case scenario) and with the PV-BES units at the optimal and unity power factors (i.e., Scenarios 1 and 2, respectively) at the extreme periods where the voltage profiles are worst. Without the PV-BES units, the extreme period is specified at the peak period 11 as depicted in Fig. 5.7, at which the voltages at several buses are under the lower limit of 0.95 p.u. With the PV-BES units, by considering the combination of the demand and PV-BES output curves, the extreme period is identified at the peak period 11. Moreover, it is observed from Fig. 5.7 that after the PV-BES units are integrated, at the extreme periods the voltage profiles improve significantly. The voltage profile in Scenario 1 is better than that in Scenario 2.

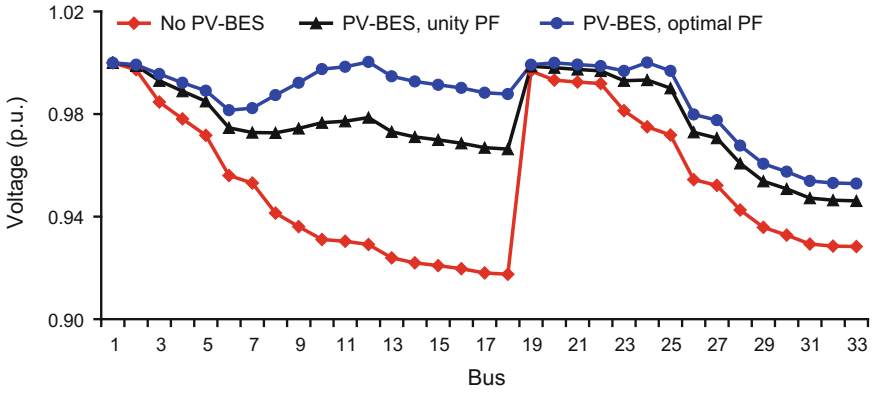


**Fig. 5.7** Voltage profiles at extreme periods for all scenarios

## 5.10 Conclusions

This chapter presented a methodology to accommodate a combination of PV and BES units for reducing energy loss and enhancing voltage stability in distribution systems. In this methodology, each nondispatchable PV unit is converted into a dispatchable source with a combination of PV and BES units. *IMO*-based analytical expressions were presented to calculate the size and power factor of the PV-BES combination. A self-correction algorithm was also reported to size multiple PV and BES units while considering the time-varying demand and probabilistic generation. The power factors are optimally dispatched at each load level. The Beta PDF model was employed to describe the probabilistic nature of solar irradiance. The results indicated that the model can support high PV penetration associated with an efficient usage of BES sources. Operation of PV and BES units with optimal power factor dispatch for each load level can significantly reduce energy losses and better enhance voltage stability when compared to that with unity power factor, which currently follows the standard IEEE 1547. This result implies that the standards and regulatory frameworks regarding PV planning and operations need to be revised appropriately to avail maximum loss reduction and voltage stability enhancement.

**Acknowlegments** The work presented in this chapter was taken from the journal paper: D.Q. Hung, N. Mithulananthan, and R.C. Bansal, "Integration of PV and BES units in commercial distribution systems considering energy losses and voltage stability", *Applied Energy,* volume 113, pages 1162-1170, January 2014.

## References


1. Katiraei F, Aguero JR (2011) Solar PV integration challenges. IEEE Power Energ Mag 9 (3):62–71. doi:10.1109/mpe.2011.940579
2. Omran WA, Kazerani M, Salama MMA (2011) Investigation of methods for reduction of power fluctuations generated from large grid-connected photovoltaic systems. IEEE Trans Energy Convers 26(1):318–327. doi:10.1109/tec.2010.2062515
3. Yeh HG, Gayme DF, Low SH (2012) Adaptive VAr control for distribution circuits with photovoltaic generators. IEEE Trans Power Syst 27(3):1656–1663. doi:10.1109/tpwrs.2012.2183151
4. Turitsyn K, Sulc P, Backhaus S, Chertkov M (2011) Options for control of reactive power by distributed photovoltaic generators. Proc IEEE 99(6):1063–1073. doi:10.1109/JPROC.2011.2116750
5. Albuquerque FL, Moraes AJ, Guimarães GC, Sanhueza SMR, Vaz AR (2010) Photovoltaic solar system connected to the electric power grid operating as active power generator and reactive power compensator. Sol Energy 84(7):1310–1317. doi:10.1016/j.solener.2010.04.011
6. IEEE 1547 Standard for interconnecting distributed resources with electric power systems, 2003. doi:10.1109/ieeestd.2003.94285
7. Chen SX, Gooi HB, Wang MQ (2012) Sizing of energy storage for microgrids. IEEE Transactions on Smart Grid 3(1):142–151. doi:10.1109/tsg.2011.2160745
8. Gabash A, Pu L (2012) Active-reactive optimal power flow in distribution networks with embedded generation and battery storage. IEEE Trans Power Syst 27(4):2026–2035. doi:10.1109/tpwrs.2012.2187315
9. Gabash A, Li P (2013) Flexible optimal operation of battery storage systems for energy supply networks. IEEE Trans Power Syst 28(3):2788–2797. doi:10.1109/tpwrs.2012.2230277
10. Singh D, Verma KS (2009) Multiobjective optimization for DG planning with load models. IEEE Trans Power Syst 24(1):427–436. doi:10.1109/TPWRS.2008.2009483
11. Ochoa LF, Padilha-Feltrin A, Harrison GP (2006) Evaluating distributed generation impacts with a multiobjective index. IEEE Trans Power Deliv 21(3):1452–1458. doi:10.1109/TPWRD.2005.860262
12. Ochoa LF, Padilha-Feltrin A, Harrison GP (2008) Evaluating distributed time-varying generation through a multiobjective index. IEEE Trans Power Deliv 23(2):1132–1138. doi:10.1109/TPWRD.2008.915791
13. El-Zonkoly AM (2011) Optimal placement of multi-distributed generation units including different load models using particle swarm optimisation. IET Gener Trans Distrib 5(7):760–771. doi:10.1049/iet-gtd.2010.0676
14. Canizares CA, Alvarado FL (1993) Point of collapse and continuation methods for large AC/DC systems. IEEE Trans Power Syst 8(1):1–8. doi:10.1109/59.221241
15. Ettehadi M, Ghasemi H, Vaez-Zadeh S (2013) Voltage stability-based DG placement in distribution networks. IEEE Trans Power Deliv 28(1):171–178. doi:10.1109/tpwrd.2012.2214241
16. Al Abri RS, El-Saadany EF, Atwa YM (2013) Optimal placement and sizing method to improve the voltage stability margin in a distribution system using distributed generation. IEEE Trans Power Syst 28(1):326–334. doi:10.1109/tpwrs.2012.2200049

# Chapter 6
# PV and EV Integration

## 6.1 Introduction

The widespread adoption of PV sources has a harmful effect on the power quality, especially the voltage rise that occurs due to reverse power flows when the generation of PV exceeds the local demand [1]. On the other hand, the distribution system would potentially face excessive voltage drops due to high EV penetration, especially the simultaneous charging of a large number of EV units during the peak demand [2].

This chapter presents an analytical method to accommodate EV charging stations for a commercial distribution system with PV units. In this method, an analytical approach is presented to size and operate charging stations to minimize voltage deviations while considering the probabilistic characteristics of PV generation and EV charging loads. Such stations are employed to deliver active power to aggregated EVs while offering a capability of hourly reactive power or power factor control.

## 6.2 Network Modeling

### *6.2.1 Commercial System Modeling*

The grid model under this study is a distribution network, which supplies electricity to commercial loads (e.g., university campuses, business centers and government offices). Rooftop solar PV units are located at commercial buildings and interfaced with the grid through converters. EV charging stations are installed in parking lots within a workplace and connected to the grid. Such stations are intended to charge various types of EV-40 as shown in Table 6.1 [3], where all EVs are assumed to have a 40-mile maximum all-electric range. EVs are a type of plug-in hybrid vehicles



N. Mithulananthan et al., *Intelligent Network Integration of Distributed Renewable Generation*, Green Energy and Technology,
DOI 10.1007/978-3-319-49271-1_6

**Table 6.1** Battery parameters for four types of EV-40

| EV models | Share of each type (%) | Capacity (kWh) | Consumption (kWh/mile) |
|---|---|---|---|
| Compact sedan | 60.85 | 13.02 | 0.3255 |
| Full-size sedan | 11.94 | 14.42 | 0.3605 |
| Mid-size SUVs or pickup | 13.10 | 17.50 | 0.4375 |
| Full-size SUVs or pickup | 14.11 | 20.30 | 0.5075 |

which can work on battery-based electricity and torque from internal combustion engines. The main system components can be modelled as described below.

### 6.2.2 Load Modeling

This study adopts the time-varying voltage-dependent load model reported in Sect. 2.2. The demand of the system under study is assumed to follow a normalized daily commercial load pattern presented in Sect. 4.2.1, Chap. 4.

### 6.2.3 Solar PV Modeling

A forecasting model of PV outputs detailed in Sect. 4.2.2 is adopted in this study to generate a daily probabilistic PV generation curve. In this model, the Beta Probability Density Function (PDF) is used to describe the hourly solar irradiance for the day, based on historical data that have been collected for three years. To obtain such a PDF, a day is split into 24-h periods (time segments), each of which is one hour and has its own solar irradiance PDF. From the collected historical data, the mean and standard deviation values of the hourly solar irradiance of the day is estimated. Each hour is assumed to have 20 states for solar irradiance with an interval of 0.05 kW/m$^2$. From the estimated mean and standard deviation, the PDF with 20 states for solar irradiance is then generated for each hour of the day and the probability of each solar irradiance state is calculated. Finally, the solar irradiance state is further converted into the PV output power based on the characteristics of the PV module, which can be found in [4].

### 6.2.4 EV Modelling [5]

To forecast hourly energy consumption for aggregated EV units, which will arrive at a workplace and return home, a day is split into 24-h periods. The energy

consumption of EV units for each hour of the day is calculated based on the travel distance. The arrival time is described using a normal distribution. The normal charging level of 1.44 kW is considered [3]. Finally, the daily EV charging load profile is estimated based on the energy consumption, arrival time and charging level of EV units.

#### 6.2.4.1 Energy Consumption

The travel distance of EV units can be described using a lognormal distribution function as follows:

$$f_{dist}(d) = \frac{1}{d\sigma_d\sqrt{2\pi}}e - \frac{(\ln d - \mu_d)^2}{2\sigma_d^2} \tag{6.1}$$

where $d$ is the total distance in mile driven by an EV unit; $\mu_d = 3.37$ and $\sigma_d = 0.5$ are respectively the mean and standard deviation [6]. Using the statistic distribution fitting toolbox in MATLAB and Monte Carlo simulation with 10,000 samples, the PDF of the travel distance is generated. The mean and standard deviation values of the distribution are estimated at 32.90 miles and 17.46 miles, respectively.

The state of charge (SOC) is defined as the percentage of energy remaining in the battery of a vehicle upon arrival. To extend the battery life, the lower and upper limits of the SOC are set at 10 and 80%, respectively. As a type of plug-in hybrid electric vehicles, EVs are capable of working on electricity and gas using battery and internal combustion engines, respectively. To avoid over-discharge, EV units use gas when the SOC is below the lower limit. The SOC depends on the travel distance and maximum range of an EV. Given the mileage of an EV, the SOC at the beginning of a recharging cycle can be calculated as follows [3]:

$$SOC = \begin{cases} 100 \times \left(1 - \frac{d}{d_r}\right), & d \le d_r \\ 0 & d > d_r \end{cases} \tag{6.2}$$

where $d_r$ is the maximum EV range (mile). The energy required to fully charge the EV battery ($E_b$) can be written as follows:

$$E_b = \frac{(1 - SOC) \times BC}{\eta} \tag{6.3}$$

where $BC$ corresponds to 70% of the battery capacity (kWh) for each type of PHEVs, which is estimated as a difference of the lower and upper bounds of the SOC that were previously set at 10 and 80%, respectively; $\eta$ is the charging efficiency (%), which is assumed to be 90%.

#### 6.2.4.2 EV Arrival Time

The PDF can be described using a normal distribution function as follows:

$$f_{arr}(t) = \frac{1}{\sigma_{arr}\sqrt{2\pi}} \exp - \frac{(t - \mu_{arr})^2}{2\sigma_{arr}^2} \tag{6.4}$$

where $\mu_{arr} = 9$ and $\sigma_{arr} = 1.5$ are respectively the mean and standard deviation of EV arrival time [6].

#### 6.2.4.3 EV Charging Load Profile

A method detailed in [3] is adopted in this work. The profile is estimated based on the energy consumption, arrival time and charging level, as described earlier. The total energy at any particular time is calculated as a sum of the energy needed by EVs which arrive at that time and which have arrived earlier but have not been fully charged yet.

#### 6.2.4.4 EV Charging Station

The inverter-based EV charging station is utilized to charge a number of EVs while regulating reactive power. The relationship between the active and reactive power of a EV charging station at bus $i$ ($P_{CS_i}$ and $Q_{CSi}$) can be expressed as follows [7]:

$$Q_{CS_i} = a_i P_{CS_i} \tag{6.5}$$

where, $a_i = \pm \tan(\cos^{-1}(pf_{CSi}))$, $a_i$ is positive for the charging station supplying reactive power, and negative for the charging station consuming reactive power; $pf_{CSi}$ is the operating power factor of the charging station at bus $i$, which is dispatchable or controllable. Given a daily EV charging load curve, the power factor can be dispatched at each solar irradiance state over all periods of the day. To control $Q_{CSi}$ without disturbing $P_{CS_i}$, $Q_{CSi}$ is constrained by $|Q_{CSi}| \leq \sqrt{S_{CSi}^2 - P_{CSi}^2}$, where $S_{CSi}$ is the apparent power of the charging station at bus $i$ [8].

## 6.3 Voltage Deviation

Considering Fig. 4.4a, one can found that the voltage deviation ($VD_i$) along the branch from bus $i$ to bus $i + 1$, ($R_i + jX_i$) can be described as follows:

$$VD_i = V_i \angle \delta_i - V_{i+1} \angle \delta_{i+1} = (R_i + jX_i)I_i \tag{6.6}$$

where $I_i = \frac{P_{bi} - jQ_{bi}}{V_i^*}$ is the current flowing the branch from bus $i$ to bus $i + 1$. The apparent power loss of this branch ($S_{Li}$) can be estimated as follows:

$$S_{Li} = I_i^2 \times (R_i + jX_i). \tag{6.7}$$

Substituting Eq. (6.7) into Eq. (6.6), we obtain:

$$VD_i = \sqrt{S_{Li} \times (R_i + jX_i)} \tag{6.8}$$

It is obvious from Eq. (6.8) that as the component of $(R_i + jX_i)$ is constant, to minimize the voltage deviation, the problem can be formulated as minimizing the apparent power loss.

## 6.4 Power Losses

The total apparent power loss in a distribution system without EV and PV units (i.e., $S_L$) can be expressed as follows:

$$S_L = \sqrt{P_L^2 + Q_L^2} \tag{6.9}$$

where $P_L$ and $Q_L$ are the total active and reactive power losses in the distribution system without EV and PV units which are calculated using Eqs. (3.1) and (3.2), respectively.

This study considers that a charging station is used to charge aggregated EVs parked in a parking lot while regulating reactive power and PV units are assumed to generate active power only. The size of an EV charging station is estimated as the total power consumption needed by the aggregated EV units. The active and reactive power injections at bus $i$, where the charging station and PV units are connected, can be expressed as follows:

$$P_i = P_{PVi} - P_{CSi} - P_{Di} \tag{6.10}$$

$$Q_i = -Q_{CSi} - Q_{Di} = -a_i P_{CSi} - Q_{Di} \tag{6.11}$$

where $a_i$ is defined as Eq. (3.3); $P_{PVi}$ is the active power injection from the PV unit at bus $i$; $P_{CSi}$ and $a_i$ are variables while the $P_{PVi}$ is known.

Substituting Eqs. (6.10) and (6.11) into Eqs. (3.1) and (3.2), we can obtain the total active and reactive power losses with the aggregated EV and PV unit (i.e., $P'_L$ and $Q'_L$) as follows:

$$P'_L = \sum_{i=1}^{N}\sum_{j=1}^{N}\left[\begin{array}{l}\alpha_{ij}\big((P_{PVi}-P_{CSi}-P_{Di})P_j+(-a_iP_{CSi}-Q_{Di})Q_j\big)\\ \quad+\beta_{ij}\big((-a_iP_{CSi}-Q_{Di})P_j-(P_{PVi}-P_{CSi}-P_{Di})Q_j\big)\end{array}\right] \tag{6.12}$$

$$Q'_L = \sum_{i=1}^{N}\sum_{j=1}^{N}\left[\begin{array}{l}\gamma_{ij}\big((P_{PVi}-P_{CSi}-P_{Di})P_j+(-a_iP_{CSi}-Q_{Di})Q_j\big)\\ \quad+\xi_{ij}\big((-a_iP_{CSi}-Q_{Di})P_j-(P_{PVi}-P_{CSi}-P_{Di})Q_j\big)\end{array}\right]. \tag{6.13}$$

Finally, the total apparent power loss with the EV and PV unit (i.e., $S'_L$) can be derived from Eqs. (6.12) and (6.13) as follows:

$$S'_L = \sqrt{P'^2_L + Q'^2_L}. \tag{6.14}$$

## 6.5 Apparent Power Loss Index

The apparent power loss index of the system (i.e., *ILS*) can be calculated as the ratio of Eqs. (6.14) and (6.9) as

$$ILS = \frac{\sqrt{P'^2_L + Q'_L}}{\sqrt{P^2_L + Q^2_L}} \tag{6.15}$$

It is noted from Eq. (6.15) that without charging stations, the *ILS* is unity. With charging stations, the *ILS* is less than one showing that charging stations have a positive impact on the apparent power loss of the system, whereas the index is more than one indicating that they have a negative impact on that loss.

As the solar irradiance is a random variable, the PV output power and its corresponding *ILS* as defined by Eq. (6.15) are stochastic during each hour. The *ILS* can be formulated in the expected value. To calculate the *ILS*, the power flow is analyzed for each combined generation-load state [9]. As previously assumed, each day has 24-h periods (time segments), each of which has 20 states for solar irradiance. As the load and EV consumption are constant during each hour, the probability for each is unity. As a result, the probability of any combination of the PV generation, load and EV consumption is the probability of the generation itself. It is assumed that $ILS(s)$ is the expected *ILS* at solar irradiance $s$, the total expected *ILS* over any specific period $t$, $ILS(t)$ ($t$ = 1 h) can be formulated as

$$ILS(t) = \int_0^1 ILS(s)\rho(s)ds \tag{6.16}$$

where $\rho(s)$ is the probability of the solar irradiance state $s$ in a specific period (1 h).

The average *ILS* (*AILS*) over the total period ($T = 24$) in a system with the charging station can be obtained from Eq. (6.16) as

$$AILS = \frac{1}{T}\int_{0}^{T} ILS(t)dt = \frac{1}{T}\sum_{t=1}^{T} ILS(t) \times \Delta t \tag{6.17}$$

where $\Delta t$ is the time duration or time segment of period $t$. The lowest *AILS* implies the best charging station allocation to minimize apparent power losses and enhance voltage profiles.

## 6.6 Sizing EV Charging Stations

The apparent power loss of the system is minimum if the derivative of Eq. (6.15) with respect to $P_{CSi}$ and $a_i$ becomes zero.

$$\frac{\partial ILS}{\partial P_{CSi}} = \frac{1}{S_L}\left(\frac{P'_L}{S'_L} \times \frac{\partial'_L}{\partial P_{CSi}} + \frac{Q'_L}{S'_L} \times \frac{\partial Q'_L}{\partial P_{CSi}}\right) = 0. \tag{6.18}$$

$$\frac{\partial ILS}{\partial a_i} = \frac{1}{S_L}\left(\frac{P'_L}{S'_L} \times \frac{\partial P'_L}{\partial a_i} + \frac{Q'_L}{S'_L} \times \frac{\partial Q'_L}{\partial a_i}\right) = 0. \tag{6.19}$$

With EV charging stations and PV units in the system, the ratio of the active to apparent power losses will be changed from the base case value. However, a number of simulations that have been done in the study show that this change is negligible. A similar result has been observed for the ratio of reactive and apparent power losses. Hence, Eqs. (6.18) and (6.19) can be approximately rewritten as follows:

$$\frac{\partial ILS}{\partial P_{CSi}} = \frac{1}{S_L}\left(\frac{P_L}{S_L} \times \frac{\partial P'_L}{\partial P_{CSi}} + \frac{Q_L}{S_L} \times \frac{\partial Q'_L}{\partial P_{CSi}}\right) = 0 \tag{6.20}$$

$$\frac{\partial ILS}{\partial a_i} = \frac{1}{S_L}\left(\frac{P_L}{S_L} \times \frac{\partial P'_L}{\partial a_i} + \frac{Q_L}{S_L} \times \frac{\partial Q'_L}{\partial a_i}\right) = 0 \tag{6.21}$$

The derivatives of Eqs. (6.12) and (6.13) with respect to $P_{CSi}$ and $a_i$ can be written as follows:

$$\frac{\partial P'_L}{\partial P_{CSi}} = -2\sum_{j=1}^{N}\left[\alpha_{ij}\left(P_j + a_i Q_j\right) + \beta_{ij}\left(a_i P_j - Q_j\right)\right] \tag{6.22}$$

$$\frac{\partial Q'_L}{\partial P_{CSi}} = -2\sum_{j=1}^{N}\left[\gamma_{ij}\left(P_j + a_i Q_j\right) + \xi_{ij}\left(a_i P_j - Q_j\right)\right] \tag{6.23}$$

$$\frac{\partial P'_L}{\partial a_i} = -2P_{CSi}\sum_{j=1}^{N}\left[\alpha_{ij}Q_j + \beta_{ij}P_j\right] \tag{6.24}$$

$$\frac{\partial Q'_L}{\partial a_i} = -2P_{CSi}\sum_{j=1}^{N}\left[\gamma_{ij}Q_j + \xi_{ij}P_j\right]. \tag{6.25}$$

Substituting Eqs. (6.22) and (6.23) into Eq. (6.20), we get:

$$\begin{aligned} &2\frac{P_L}{S_L}\sum_{j=1}^{N}\left[\alpha_{ij}\left(P_j + a_i Q_j\right) + \beta_{ij}\left(a_i P_j - Q_j\right)\right] \\ &\quad + 2\frac{Q_L}{S_L}\sum_{j=1}^{N}\left[\gamma_{ij}\left(P_j + a_i Q_j\right) + \xi_{ij}\left(a_i P_j - Q_j\right)\right] = 0. \end{aligned} \tag{6.26}$$

Equation (6.26) can be rearranged as follows:

$$\begin{aligned} &\frac{P_L}{S_L}[\alpha_{ii}(P_i + a_i Q_i) + A_i + a_i B_i] \\ &\quad + \frac{Q_L}{S_L}[\gamma_{ii}(P_i + a_i Q_i) + C_i + a_i D_i] = 0 \end{aligned} \tag{6.27}$$

where

$$A_i = \sum_{\substack{j=1 \\ j\neq i}}^{N}\left(\alpha_{ij}P_j - \beta_{ij}Q_j\right); \quad B_i = \sum_{\substack{j=1 \\ j\neq i}}^{N}\left(\alpha_{ij}Q_j + \beta_{ij}P_j\right);$$

$$C_i = \sum_{\substack{j=1 \\ j\neq i}}^{N}\left(\gamma_{ij}P_j - \xi_{ij}Q_j\right); \quad D_i = \sum_{\substack{j=1 \\ j\neq i}}^{N}\left(\gamma_{ij}Q_j + \xi_{ij}P_j\right)$$

Substituting Eqs. (3.4) and (3.5) into Eq. (6.27), we get:

$$P_{CSi} = \frac{\left[\begin{array}{l}\left(\frac{P_L}{S_L}\alpha_{ii} + \frac{Q_L}{S_L}\gamma_{ii}\right)\left(P_{PVi} - P_{Di} - a_i Q_{Di}\right) \\ \quad + \frac{P_L}{S_L}\left(A_i + a_i B_i\right) + \frac{Q_L}{S_L}\left(C_i + a_i D_i\right)\end{array}\right]}{\left(a_i^2 + 1\right)\left(\frac{P_L}{S_L}\alpha_{ii} + \frac{Q_L}{S_L}\gamma_{ii}\right)}. \tag{6.28}$$

Similarly, substituting Eqs. (6.24) and (6.25) into Eq. (6.21), we obtain:

$$2\frac{P_L}{S_L}\sum_{j=1}^{N}\left(\alpha_{ij}Q_j+\beta_{ij}P_j\right)+2\frac{Q_L}{S_L}\sum_{j=1}^{N}\left(\gamma_{ij}Q_j+\xi_{ij}P_j\right)=0. \tag{6.29}$$

Equation (6.29) can be rearranged as follows:

$$\frac{P_L}{S_L}(\alpha_{ii}Q_i+B_i)+\frac{Q_L}{S_L}(\gamma_{ii}Q_i+D_i)=0. \tag{6.30}$$

Substituting Eq. (3.5) into Eq. (6.30), we get:

$$a_i=-\frac{Q_{Di}}{P_{CSi}}-\frac{\frac{P_L}{S_L}B_i+\frac{Q_L}{S_L}D_i}{P_{CSi}\left(\frac{P_L}{S_L}\alpha_{ii}+\frac{Q_L}{S_L}\gamma_{ii}\right)}. \tag{6.31}$$

Given a $P_{PVi}$ value, at the minimum *ILS*, the $P_{EVi}$ and $a_i$ can be derived from Eqs. (6.28) and (6.31) as follows:

$$P_{CSi}=P_{PVi}-P_{Di}+\frac{\frac{P_L}{S_L}A_i+\frac{Q_L}{S_L}C_i}{\frac{P_L}{S_L}\alpha_{ii}+\frac{Q_L}{S_L}\gamma_{ii}} \tag{6.32}$$

$$a_i=\frac{\left(\frac{P_L}{S_L}\alpha_{ii}+\frac{Q_L}{S_L}\gamma_{ii}\right)Q_{Di}+\left(\frac{P_L}{S_L}B_i+\frac{Q_L}{S_L}D_i\right)}{\left(\frac{P_L}{S_L}\alpha_{ii}+\frac{Q_L}{S_L}\gamma_{ii}\right)(P_{Di}-P_{PVi})-\left(\frac{P_L}{S_L}A_i+\frac{Q_L}{S_L}C_i\right)}. \tag{6.33}$$

The "dispatchable" power factor of the charging station at bus $i$ ($pf_{CSi}$) can be derived from Eq. (6.33) as

$$pf_{CSi}=\cos\left(\tan^{-1}(a_i)\right). \tag{6.34}$$

## 6.7 Computational Procedure

In order to specify the location of the EV charging station, the *ILS* is first minimized at the average load level, which has a significant impact on the overall apparent power loss. Its size is then calculated at that location based on the EV charging load curve by minimizing the *AILS* over all periods as given by Eq. (6.15). The power factor or reactive power of the charging station is optimally dispatched at each state over all periods of a day. The procedure includes the following steps:

Step 1 Analyse power flow for the network including PV units without EV charging at the average load level and estimate the *ILS* using Eq. (6.15).

Step 2 Determine the location, size and power factor of the EV charging station at the average load level.

(a) Specify the size and power factor at each bus ($P_{EVi}$) using (6.32) and (6.34), respectively.
(b) Place the charging station obtained earlier at each bus and calculate the *ILS* for each case using Eq. (6.15).
(c) Allocate the optimal bus where the *ILS* is minimum with the corresponding size of the charging station at that bus.

Step 3 Specify the EV load at the optimal location for time segment $t$ as below, where $SF_{CS}(t)$ is the scaling factor of the EV load at time period $t$. Here, depending on demand patterns, an adjusted factor, $k_{EV}$ (e.g., 0.8, 0.9 or 1.1) could be utilized to achieve a better outcome.

$$P_{CSi}(t) = k_{CS} \times P_{CSi} \times SF_{CS}(t). \tag{6.35}$$

Step 4 Perform power flow for the system with each EV load obtained in Step 3 for each combined generation-load state over all the hour periods of a day as described in Section III.C. Find the power factor of the charging station for each state over all the hour periods using Eq. (6.34). Calculate the *AILS* using Eq. (6.17).

Step 5 Repeat Steps 3–4 by adjusting $k_{CS}$ in Eq. (6.35) until the minimum *AILS* is obtained.

## 6.8 Example

### 6.8.1 Test Systems

The 33-bus test distribution system as shown in Fig. 6.1 is used to validate the proposed approach. It has a peak demand of 3715 kW and 2300 kVAr. The complete data of this system can be found in [10]. The operating voltage limits are assumed to be ±6% of the nominal value in compliance with Australian standards AS 60038 [11]. The proposed approach has been simulated in MATLAB environment.

### 6.8.2 Load Modeling

It is assumed that the demand of the 33-bus system follows a normalized daily commercial load pattern with the time-varying load model, as shown in Fig. 6.2 [12]. The total daily energy consumption of the system is 58.82 MWh.

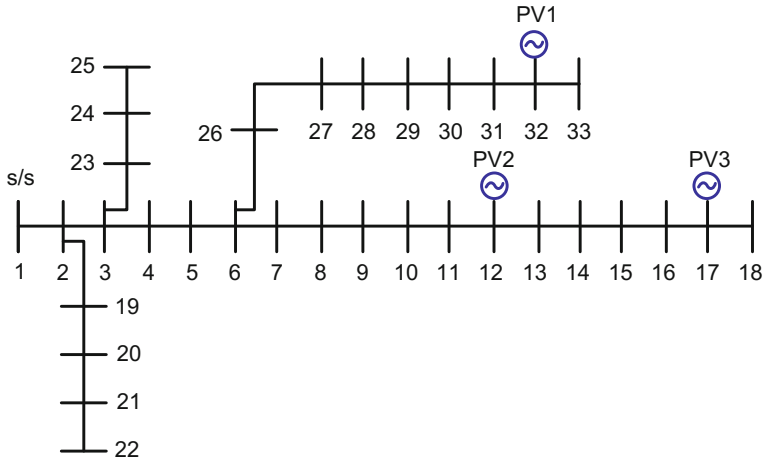


**Fig. 6.1** The 33-bus test distribution system

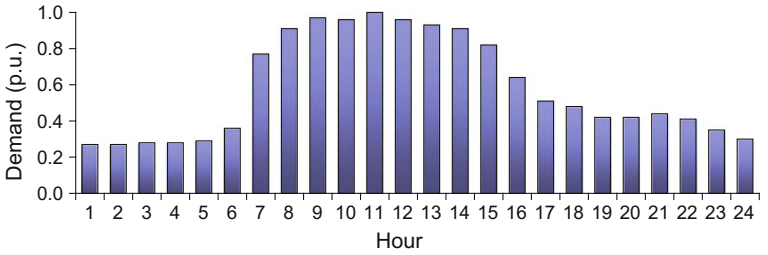


**Fig. 6.2** Normalized hourly commercial load demand

### *6.8.3 PV Modeling*

The assumption is that three PV units operating at unity power factor are allocated at buses 12, 17 and 32. Each PV unit is assumed to generate at a capacity of 1 MW. The mean and standard deviation of solar irradiance, which are estimated using the hourly historical solar irradiance data collected for three years, can be found in Table B.1, Appendix B [10]. Using the PV model explained in Sect. 6.2.3, the solar irradiance data, and the characteristics of the PV module found in Table B.2, Appendix B [12], the PDF of the PV output for each hour is estimated and plotted in Fig. 6.3a–c. The total daily energy generated by the three PV units is 18.01 MWh, which corresponds to a penetration level of 34.76% when compared to the total system load demand as estimated earlier.

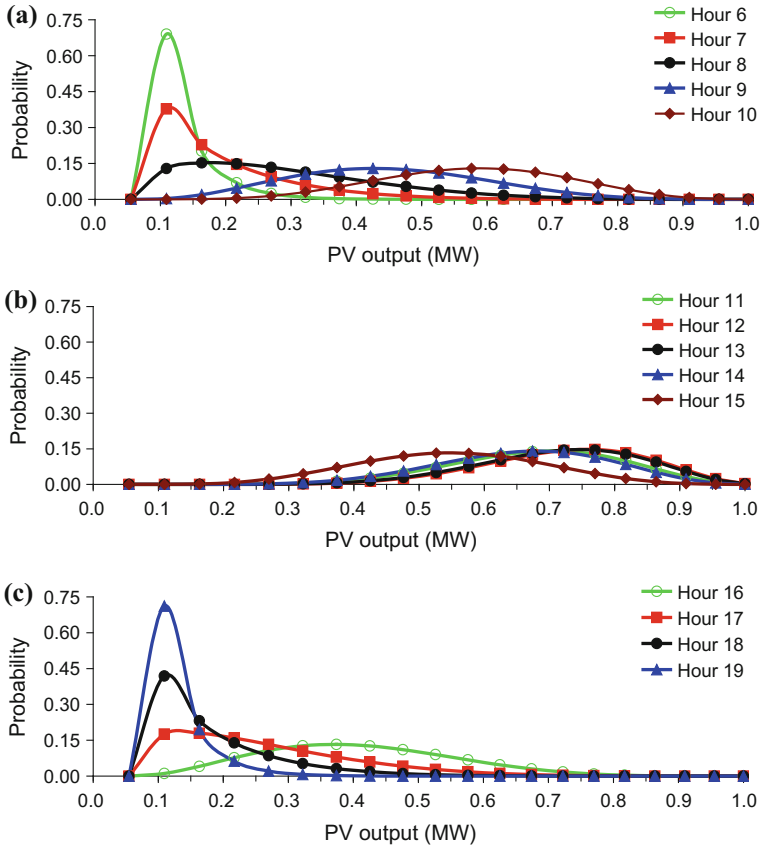


**Fig. 6.3** The PDFs of each PV for hours: **a** 6–10, **b** 11–15, and **c** 16–19

### *6.8.4 EV Modeling*

Using the model and data in Sect. 6.2.4, the PDFs of daily aggregated EV charging load consumption connected to a parking lot is calculated and plotted in Fig. 6.4.

### *6.8.5 Location Selection*

As previously described, to determine the best location, the EV charging station is sized at various buses using Eqs. (6.32) and (6.34) and the corresponding apparent power loss index (*ILS*) using Eq. (6.15) for each bus is estimated. The best location where the *ILS* is lowest is then identified. Figure 6.5 shows the optimum sizes and power factors of the charging stations at various buses with the corresponding *ILS*

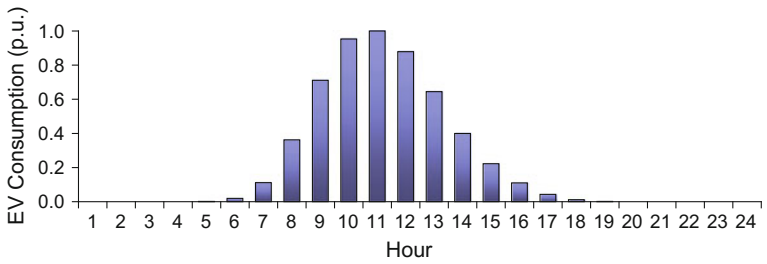


**Fig. 6.4** Normalized hourly EV energy consumption at a parking lot

values in the 33-bus system. The sizes are significantly different in the range of minus (−) 0.642 MW to plus (+) 0.376 MW. The positive size indicates that the charging station is being connected to EVs and working as a load that is consuming the active power from the grid. In contrast, the negative size shows that the charging station is being connected to EVs and working as a generator that is delivering the active power from EVs to the grid. It is noted that the charging station is considered in this study to charge EVs or consume the active power from the grid; however, the results of the charging station that discharges or delivers the active power are also provided in this subsection for comparison purposes. The leading power factors indicate that the charging station supplies reactive power as the existing system lacks local reactive power support as the PV units provide active power only. It is observed from Fig. 6.5 that the charging stations in which the EV units absorb the power are allocated close to the PV connection points (i.e., buses 12, 17 and 32). These charging stations locally consume the power from the PV generation. This can avoid network losses during the charging progress of the EV units. Hence, the *ILS* values for the EVs located at those buses are almost lower than the others that are placed close to the source and deliver power to the grid. Another observation is that the power factors are rather different among buses. It is assumed that the EV charging station consumes active power only while regulating reactive power at each hour of the day to retain the minimum *ILS*. Accordingly, it can be seen from Fig. 6.5 that the best location is bus 17 where the *ILS* is lowest. At this bus, the optimum size and power factor of the EV charging station is found to be 0.376 MW and 0.82 (leading), respectively.

### *6.8.6 Sizing EV Charging Stations*

Figure 6.6 shows the hourly energy consumption pattern of the aggregated EV units connected to the charging station at bus 17 over a day. This curve exactly follows the corresponding normalized daily energy consumption of the EV units as illustrated in Fig. 6.4. The maximum EV consumption, which is identified at 11th hour period, shows the optimal active power size of the EV charging station

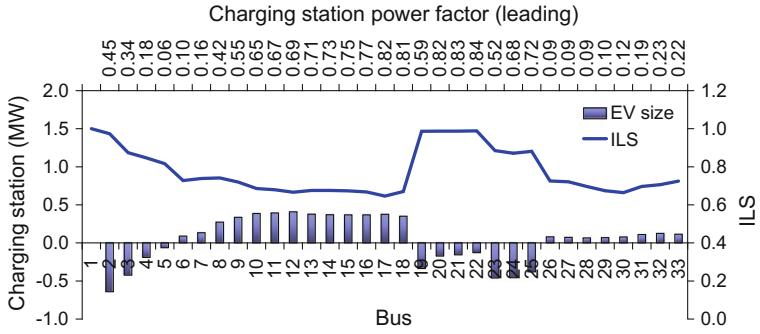


**Fig. 6.5** Sizing EV charging stations with respect to *ILS*

(0.376 MW). This size is calculated as the total aggregated energy consumption of all the EV units connected to the parking lot. Similarly, the maximum reactive power size of the charging station is 0.268 MVAr which is specified at hour period 11 as well. Figure 6.6 also presents the reactive power or power factor dispatch of the EV charging station at each hour period over the day to retain the *ILS* at the lowest level. As shown in Fig. 6.6, at periods 5–19, the EV charging station absorbs active power while delivering reactive power required by the grid. In the absence of EV charging at periods 1–4 and 20–24, the charging station supplies reactive power to support the grid as well.

Figure 6.7a–c shows the PDFs of the *ILS* of the system with the EV charging station with a dispatchable power factor at bus 17. It is observed from the figure that a difference in the *ILS* patterns exist among hours 6–19. This dissimilarity is due to dependence of the *ILS* on the uncertainty of the PV outputs and variability of the load demand and the EV consumption over the day as illustrated in Figs. 6.2, 6.3 and 6.4. Figure 6.8 presents the expected *ILS* values over the 24-h day, which is obtained for the system before and after the EV charging station connected. The total expected *ILS* for each hour period is calculated using (18). At each hour of the day, the *ILS* values for the system with the charging station operation at a dispatchable power factor (PF) (i.e., reactive power dispatch) are lower than the system

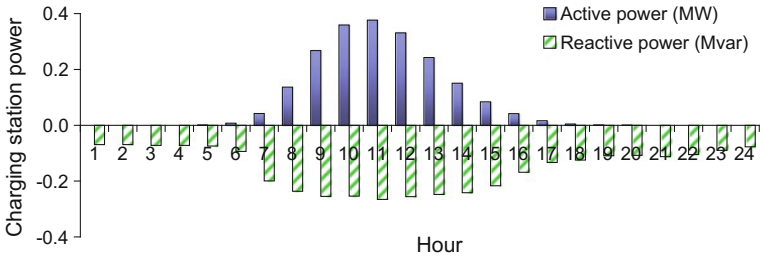


**Fig. 6.6** Hourly power consumption and reactive power dispatch

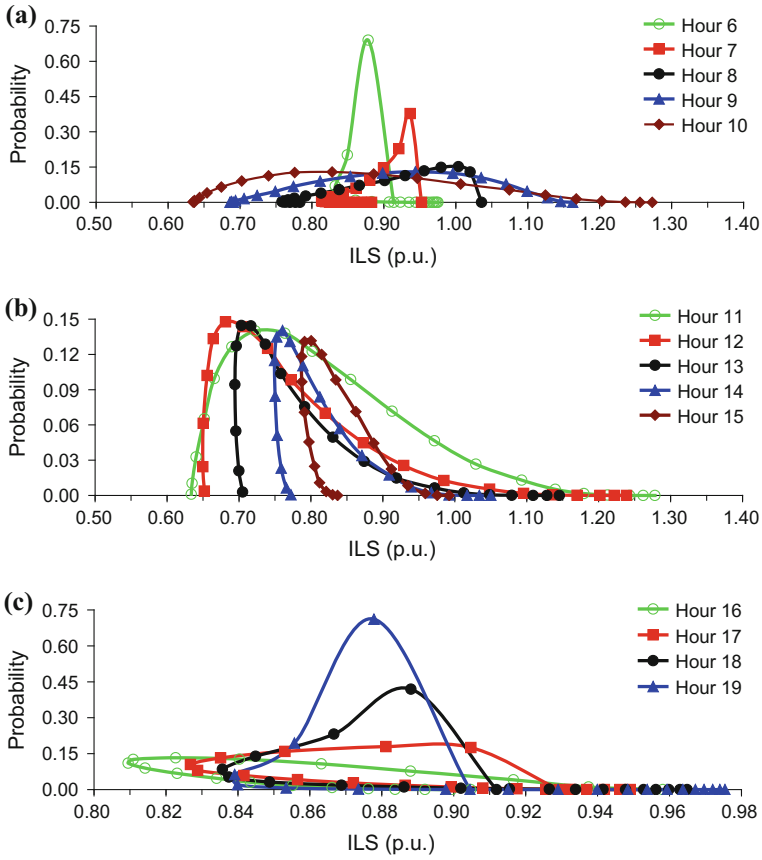


**Fig. 6.7** The PDFs of the *ILS* with the EV charging station with a dispatchable power factor at bus 17 for hours: **a** 6–10, **b** 11–15, and **c** 16–19

without the EVs (*ILS* = 1 p.u.). This indicates that the charging station has a positive impact on the *ILS* value. On the other hand, Fig. 6.8 also shows the *ILS* for the charging station operation at unity power factor (i.e., without reactive power dispatch). It can be seen from this figure that the *ILS* is lower than unity at each of periods 10–17 due to the EVs consuming the redundancy of the PV generation. In contrast, at periods 6–9, the *ILS* at each period is larger than unity due to the EVs absorbing a portion of the energy from the grid. In general, it is revealed from Fig. 6.9 that the EV charging station with reactive power or power factor dispatch obtains an *ILS* value at each hour lower than that with unity power factor.

Table 6.2 presents a summary of the results of EV charging station adoption with a dispatchable power factor (Scenario 1) and unity power factor (Scenario 2) in the system. These results include the optimal bus and size of the EV charging station and corresponding *AILS* for each scenario. The *AILS* is calculated using Eq. (6.17). Differences in the size and *AILS* are observed between the two

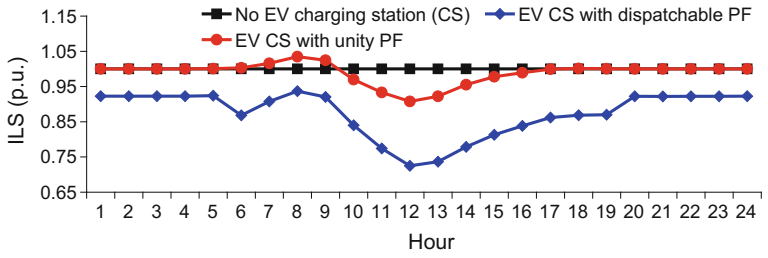


**Fig. 6.8** Hourly expected *ILS* curve

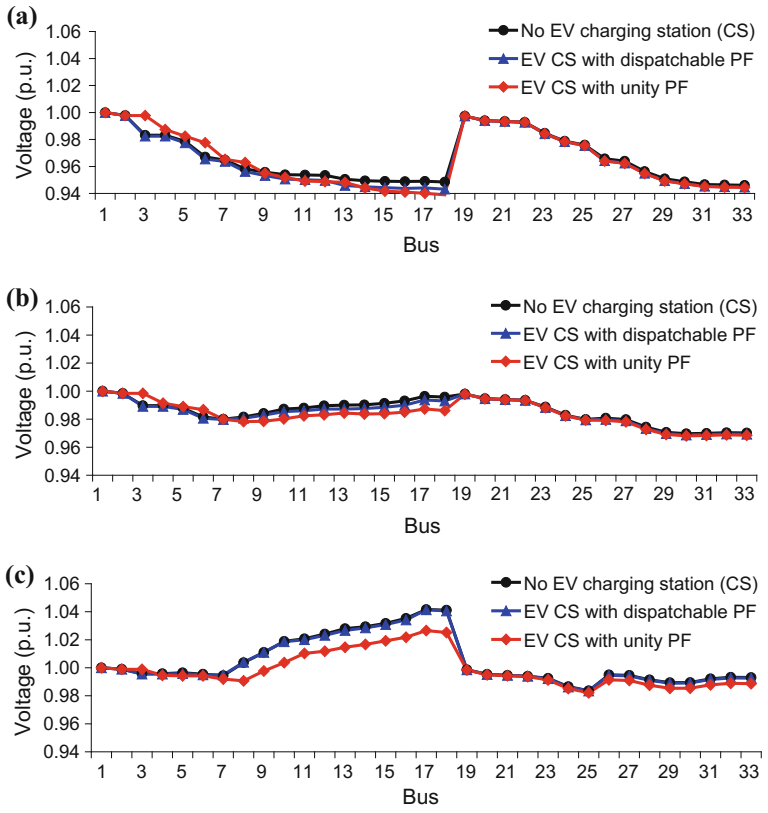


**Fig. 6.9** The voltage distributions of the system at heavy load period (11 am): **a** minimum voltage, **b** mean voltage, and **c** maximum voltage

scenarios. The size of the EV adopted in Scenario 1 is 0.376 MW which is larger than Scenario 2 at 0.209 MW. The *AILS* value is 0.874 p.u. for Scenario 1 while this value is 0.989 p.u. for Scenario 2. The above differences are due to the fact that the charging station in Scenario 1 charges a number of EV units while regulating

**Table 6.2** EV adoption with dispatchable and unity power factors

| Scenario | Power factor | Bus | Size (MW) | Capacity (MWh) | No. of EVs | *AILS* (p. u.) |
|---|---|---|---|---|---|---|
| 1 | Dispatchable | 17 | 0.376 | 2.06 | 261 | 0.874 |
| 2 | Unity | 17 | 0.209 | 1.14 | 145 | 0.989 |

the reactive power over the 24-h day. In contrast, the EV charging only is considered in Scenario 2. Table 6.2 also shows the number of EV units charging in the parking lot, which is estimated as the size of the charging station for each scenario divided by the power rating of each outlet at 1.44 kW. The total energy needed to charge the aggregated EVs is 2.06 and 1.14 MWh for Scenarios 1 and 2, respectively.

### *6.8.7 EV Impacts on Voltage Profiles and Energy Losses*

Figure 6.9a–c presents the probabilistic distribution of voltage profiles for scenarios: without charging station and with charging station operating at a dispatchable power factor and unity power factor. These outcomes were evaluated based on the location and size of the EV charging station obtained earlier for all the scenarios. Each scenario shows the distribution of the minimum, mean and maximum voltages at all buses in the whole system at the heavy load period (11 am). For the mean voltage distribution shown in Fig. 6.9b, the maximum voltage deviation is approximately 3% for all the scenarios when compared to the nominal voltage of 1 p.u. However, a significantly larger deviation is found for the minimum voltage distribution at roughly 6% (Fig. 6.9a). Similarly, the deviation is around 4% for the maximum voltage distribution (Fig. 6.9c). The differences in the maximum voltage deviation, which were observed between the mean voltage distribution and the others as previously mentioned, are due to the intermittency and variations of the PV generation illustrated in Fig. 6.3. Moreover, it can be seen from Fig. 6.9a that in the absence of the EV charging, the voltage profiles at a few buses are rather close to the lower limit of 0.94 p.u. due to the system experiencing the peak load at hour period 11. In the presence of the EV charging, the voltages are found to be closer to the lower limit due to the addition of excessive EV charging to the system at that period. However, they are still within the acceptable limits. An attempt to increase the size of the EV charging stations in both scenarios leads to further drops in voltages at a large number of buses, below the lower limit. The above observations show that it is necessary to evaluate the PDFs of voltage profiles when EV charging stations are adopted in the system with PV units.

Figure 6.10 shows the PDFs of voltages at the EV charging station connection point (bus 17). As previously mentioned in Table 6.2, the penetration of the EV in Scenario 1 with a dispatchable power factor (0.376 MW) is higher than the Scenario 2 with unity power factor (0.209 MW). However, the voltage distribution

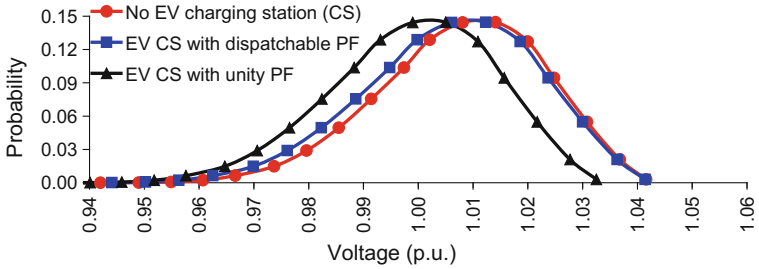


**Fig. 6.10** The PDFs of voltages at bus 17 at 11 am

**Table 6.3** Impact of EV adoption on energy losses

| Scenario | Power factor | Before EV (MWh) | After EV (MWh) | Reduction (%) |
|---|---|---|---|---|
| 1 | Dispatchable | 1.17 | 0.99 | 15.38 |
| 2 | Unity | 1.17 | 1.15 | 1.71 |

in Scenario 1 is rather close to that in the scenario without EV charging stations when compared to Scenario 2. This shows that the power factor or reactive power dispatch from the charging station in Scenario 1 has a positive impact on voltage drops and support high EV penetration.

Table 6.3 shows a summary and comparison of the energy losses over the 24-h day before and after the EV charging station connected to the grid for Scenario 1 with a dispatchable power factor and Scenario 2 with unity power factor. The total energy loss over the day is estimated as a sum of all hourly expected power losses of that day that consider the uncertainty of the PV outputs. It is observed from the table that without the EV charging station, the energy loss of the base case system including the three PV units is 1.17 MWh. With the EV charging station, due to inclusion of the power factor dispatch over the day in Scenario 1, the loss reduction of the system is 15.38%, which is higher than scenario 2 at 1.71%.

## 6.9 Conclusions

This chapter reported an analytical approach to adopt plug-in hybrid EV charging stations that can support reactive power for a commercial distribution system with PV units. In this approach, expressions based on an apparent power loss index were presented to identify the size of EV charging stations that are capable of consuming active power with a dispatchable power factor or reactive power dispatch for lowering voltage deviations. Such charging stations were used to charge a number of aggregated EV units in a public parking lot. The presented expressions were then adapted to accommodate charging stations while considering the time-varying voltage-dependent load models and the probability of PV generation and EV

charging. Probability density functions were employed to describe the probabilistic characteristics of solar irradiance and EV travel habits (i.e., arrival time and travel distance). The power factor or reactive power of charging stations is dispatched at each period over a 24-h day to deliver reactive power to the grid. The results indicated that the locations of EV charging stations were found close to PV connection points. Another indication was that charging station operation at a dispatchable power factor can reduce probabilistic voltage drops and energy losses significantly while supporting high EV penetration when compared to that at unity power factor.

## References


1. Turitsyn K, Sulc P, Backhaus S, Chertkov M (2011) Options for control of reactive power by distributed photovoltaic generators. Proc IEEE 99(6):1063–1073. doi:10.1109/JPROC.2011.2116750
2. Richardson P, Flynn D, Keane A (2012) Optimal charging of electric vehicles in low-voltage distribution systems. IEEE Trans Power Syst 27(1):268–279. doi:10.1109/tpwrs.2011.2158247
3. Darabi Z, Ferdowsi M (2011) Aggregated impact of plug-in hybrid electric vehicles on electricity demand profile. IEEE Trans Sustain Energy 2(4):501–508. doi:10.1109/tste.2011.2158123
4. Teng JH, Luan SW, Lee DJ, Huang YQ (2013) Optimal charging/discharging scheduling of battery storage systems for distribution systems interconnected with sizeable PV generation systems. IEEE Trans Power Syst 28(2):1425–1433. doi:10.1109/tpwrs.2012.2230276
5. Hung DQ, Dong ZY, Trinh H (2016) Determining the size of PHEV charging stations powered by commercial grid-integrated PV systems considering reactive power support. Appl Energy 183:160–169. doi:10.1016/j.apenergy.2016.08.168
6. Ma T, Mohammed O (2014) Optimal charging of plug-in electric vehicles for a car park infrastructure. IEEE Trans Ind Appl 50(4):2323–2330. doi:10.1109/tia.2013.2296620
7. Hung DQ, Mithulananthan N, Bansal RC (2010) Analytical expressions for DG allocation in primary distribution networks. IEEE Trans Energy Convers 25(3):814–820. doi:10.1109/TEC.2010.2044414
8. Falahi M, Hung-Ming C, Ehsani M, Le X, Butler-Purry KL (2013) Potential power quality benefits of electric vehicles. IEEE Trans Sustain Energy 4(4):1016–1023. doi:10.1109/tste.2013.2263848
9. Caisheng W, Nehrir MH (2004) Analytical approaches for optimal placement of distributed generation sources in power systems. IEEE Trans Power Syst 19(4):2068–2076. doi:10.1109/tpwrs.2004.836189
10. SolarAnywhere. Available: https://solaranywhere.com/
11. Standard Voltages, Australia Std. AS 60038-2012, 2012
12. Hung DQ, Mithulananthan N, Lee KY (2014) Determining PV penetration for distribution systems with time-varying load models. IEEE Trans Power Syst 29(6):3048–3057. doi:10.1109/tpwrs.2014.2314133

# Chapter 7
# Biomass Integration—A Cost Benefit Analysis

## 7.1 Introduction

Chapters 3–6 presented approaches to integrate renewable DG units and its operating strategies for energy loss reduction and voltage stability enhancement in distribution systems. However, the size of DG units obtained from existing studies may not match the standard sizes available in the market. In this chapter, analytical expressions are presented based on a multi-objective index (IMO) to determine the optimal power factor for reducing energy losses and enhancing voltage stability in industrial distribution systems over a given planning horizon. Here, new analytical expressions are developed to efficiently capture the optimal power factor of each DG unit with a commercial standard size to ease the computational burden. In this study, it is assumed that DG units are owned and operated by distribution utilities. To make the work comprehensive, in addition to the analytical expressions presented to specify the optimal power factor, a benefit-cost analysis is carried out in this work to determine the optimal location, total size and number of DG units. The total benefit as a sum of energy sales, energy loss reduction, network upgrade deferral and emission reduction is compared to the total cost including capital, operation and maintenance costs.

## 7.2 Load and DG Modelling

### *7.2.1 Load Modelling*

The system considered under the study is assumed to follow the industrial load duration curve as shown in Fig. 7.1, including four discrete load bands (maximum, normal, medium and minimum) that change as the load grows over a planning hori-



N. Mithulananthan et al., *Intelligent Network Integration of Distributed Renewable Generation*, Green Energy and Technology,
DOI 10.1007/978-3-319-49271-1_7

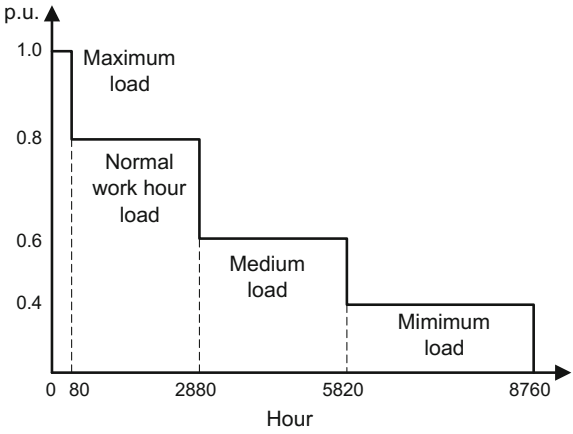


**Fig. 7.1** Nominalised load duration curve

zon. The load factor or average load level of the system over the base year, $LF_{base}$ can be defined as the ratio of the area under load curve to the total duration (four load bands: 8760 h). That means $LF_{base} = \sum_{t=1}^{8760} \frac{p.u.\ load(t)}{8760}$, where $p.u.\ load(t)$ is the demand in p.u. at period $t$. Assuming the growth rate of demand a year ($\delta$), the load factor or average load level of the system over a given planning horizon ($Ny$), $LF$ can be calculated as:

$$LF = \frac{1}{Ny} \sum_{y=1}^{Ny} \sum_{t=1}^{8760} \frac{p.u.load(t)}{8760} \times (1+\delta)^{y} \tag{7.1}$$

The time-varying industrial load model defined in Sect. 2.2 is considered in this work.

### 7.2.2 DG Modelling

As described in Sect. 2.3.1, gas-turbine engines fuelled by biogas produced from biomass materials are adopted in this work. The biogas can be considered as natural gas standards. As a synchronous generator, the biomass gas turbine-based DG unit is capable of delivering active power and injecting or absorbing reactive power. It is assumed that the DG units offer constant output powers at their rated capacities. Given $P_{DGi}$ and $Q_{DGi}$ values which correspond to the active and reactive power of a DG unit injected at bus $i$, the power factor of the DG unit at bus $i$ ($pf_{DGi}$) can be expressed as follows:

$$pf_{DGi} = \frac{P_{DGi}}{\sqrt{P_{DGi}^2 + Q_{DGi}^2}} \tag{7.2}$$

## 7.3 Impact Indices

Active and reactive power loss indices have been used to evaluate the impact of DG inclusion in a distribution system [1–4]. These indices play a critical role in DG planning and operations due to their significant impacts on utilities' revenue, power quality, system stability and security, and environmental efficiency. In this work, the active and reactive power loss indices are utilized for reducing power losses and enhancing voltage stability.

### *7.3.1 Active Power Loss Index*

Substituting Eqs. (3.4) and (3.5) into Eq. (3.1), in Chap. 3, one can obtain the total active power loss with a DG unit ($P_{LDG}$) as follows:

$$P_{LDG} = \sum_{i=1}^{N}\sum_{j=1}^{N}\left[\begin{array}{l}\alpha_{ij}\big((P_{DGi} - P_{Di})P_j + (Q_{DGi} - Q_{Di})Q_j\big) \\ +\beta_{ij}\big((Q_{DGi} - Q_{Di})P_j - (P_{DGi} - P_{Di})Q_j\big)\end{array}\right] \tag{7.3}$$

The active power loss index (*ILP*) is defined as the ratio of Eqs. (7.3) and (3.1) as follows:

$$ILP = \frac{P_{LDG}}{P_L} \tag{7.4}$$

### *7.3.2 Reactive Power Loss Index*

Substituting Eqs. (3.4) and (3.5) into Equation into Eq. (3.2), in Chap. 3, one can obtain the total reactive power loss with DG unit ($Q_{LDG}$) as follows:

$$Q_{LDG} = \sum_{i=1}^{N}\sum_{j=1}^{N}\left[\begin{array}{l}\gamma_{ij}\big((P_{DGi} - P_{Di})P_j + (Q_{DGi} - Q_{Di})Q_j\big) \\ +\xi_{ij}\big((Q_{DGi} - Q_{Di})P_j - (P_{DGi} - P_{Di})Q_j\big)\end{array}\right] \tag{7.5}$$

The reactive power loss index (*ILQ*) is defined as the ratio of Eqs. (7.5) and (3.2) as follows:

$$ILQ = \frac{Q_{LDG}}{Q_L} \tag{7.6}$$

## 7.4 Multiobjective Index

The multiobjective index (*IMO*) is a combination of the *ILP* and *ILQ* impact indices, which are respectively related to energy loss and voltage stability by giving a weight to each impact index. This *IMO* index can be expressed by Eq. (7.7) which is subject to the constraint on the pre-specified apparent power of DG capacity $(S_{DGi})$ through a relationship between $P_{DGi}$ and $Q_{DGi}$. That means:

$$IMO = \sigma_1 ILP + \sigma_2 ILQ \tag{7.7}$$

subject to $S_{DGi}^2 = P_{DGi}^2 + Q_{DGi}^2$

where $\sum_{i=1}^{2} \sigma_i = 1.0 \wedge \sigma_i \in [0,\ 1.0]$. This can be performed as all impact indices are normalized with values between zero and one [4]. When DG units are not connected to the system (i.e., base case system), the *IMO* is highest, at unity. As described in Sect. 7.3.3, this study assumes that the active power loss related to energy loss receives a significant weight of 0.7, leaving the weight associated with the reactive power loss (and also static voltage stability) at 0.3.

The lowest *IMO* implies the best DG allocation for energy loss reduction and voltage stability enhancement. The objective function defined by the *IMO* in Eq. (7.7) is subject to technical constraints described below.

## 7.5 Technical Constraints

The maximum DG penetration, which is calculated as the total capacity of DG units, is limited to less than or equal to a sum of the total system demand and the total system loss.

$$\sum_{i=2}^{N} P_{DGi} \leq \sum_{i=2}^{N} P_{Di} + P_L; \sum_{i=2}^{N} Q_{DGi} \leq \sum_{i=2}^{N} Q_{Di} + Q_L \tag{7.8}$$

where $P_L$ and $Q_L$ are respectively calculated using Eqs. (3.1) and (3.2).

The voltage at each bus is maintained close to the nominal voltage.

$$V_i^{\min} \leq V_i \leq V_i^{\max} \tag{7.9}$$

where $V_i^{\min}$ and $V_i^{\max}$ are respectively the lower and upper bounds of the voltage at bus $i$, $V_i = 1$ p.u. (substation nominal voltage).

The thermal capacity of circuit $n$ $\left(S_n^{\max}\right)$ is less than the maximum apparent power transfer $(S_n)$.

$$|S_n| \leq S_n^{\max} \tag{7.10}$$

## 7.6 Energy Loss and Voltage Stability

### 7.6.1 Energy Loss

The total active power loss of a system with a DG unit at each period $t$, $P_{loss}(t)$ can be obtained from Eq. (7.3). Here, the total period duration of a year is 8760 h, which are calculated as a sum of all the total period durations of all the load levels throughout a year as shown in Fig. 7.1. The total annual energy loss in a distribution system can be calculated as $ALoss_y = \sum_{t=1}^{8760} P_{loss}(t)$. Hence, the total energy loss over a given planning horizon ($Ny$), $E_{Loss}$ can be expressed as:

$$E_{Loss} = \sum_{y=1}^{Ny} \sum_{t=1}^{8760} P_{loss}(y,t) \times \Delta t \tag{7.11}$$

where $\Delta t$ is 1 h, which is the time duration of period $t$.

### 7.6.2 Voltage Stability

As described in Sect. 5.6.2, static voltage stability in a power system can be analyzed using a P–V curve, which is obtained using the continuation power flow method [5]. As the power from DG units are injected appropriately in the system, the *VSM* increases. The power of the load demands increases by a scaling factor $(\lambda)$ as defined by Eq. (5.14).

## 7.7 Benefit and Cost Analysis

### 7.7.1 Utility's Benefit

The present value benefit ($B$) in $ given to a utility to encourage DG connection over a planning horizon from owning and sitting its own DG units can be expressed as follows:

$$B = \sum_{y=1}^{Ny} \frac{R_y + LI_y + EI_y}{(1+d)^y} + ND \sum_{i=2}^{N} P_{DGi} \tag{7.12}$$

where all annual values are discounted at the rate $d$; $R_y$ is the annual energy sales ($/year); $LI_y$ is the loss incentive ($/year); $EI_y$ is the emission incentive ($/year); $ND$ is the network deferral benefit ($/kW); $P_{DGi}$ is the total DG capacity connected at bus $i$ (kW); and $N_y$ is the planning horizon (years). The $LI_y$ can be written as [6, 7]:

$$LI_y = CLoss_y\left(TLoss_y - ALoss_y\right)$$

where $CLoss_y$ is the loss value ($/MWh), $ALoss_y$ is the actual annual energy loss of the system with DG units (MWh), and $TLoss_y$ is the target level of the annual energy loss of the system without DG units (MWh).

When DG units are integrated into the grid for primary energy supply purposes, the environmental benefit as a result of reducing the usage of fossil fuel energy resources could be obtained. The $EI_y$ including the emission produced by the electricity purchased from the grid and DG units can be formulated as [8]:

$$EI_y = CE_y\left(TE_y - AE_y\right)$$

where $CE_y$ is the cost of each ton of generated $CO_2$ ($/Ton$CO_2$); $AE_y$ is the actual annual emission of a system with DG units (Ton$CO_2$); $TE_y$ is the target level of the annual emission of the system without DG unit (Ton$CO_2$).

### 7.7.2 Utility's Cost

The present value cost ($C$) in $ incurred by a distribution utility over a planning horizon can be expressed as [6, 7]:

$$C = \sum_{y=1}^{Ny} \frac{OM_y}{(1+d)^y} + C_{DG} \sum_{i=2}^{N} P_{DGi} \tag{7.13}$$

where $OM_y$ is the annual operation, maintenance and fuel costs ($/year) in year y; $C_{DG}$ is the capital cost of a DG unit ($/kW).

### 7.7.3 Benefit-Cost Ratio Analysis

The benefit to cost ratio (*BCR*) can be expressed as follows:

$$BCR = \frac{B}{C} \tag{7.14}$$

where the $B$ and $C$ are calculated using Eqs. (7.12) and (7.13), respectively. The decision for the optimal location, size and number of DG units is obtained when the *BCR* as given by Eq. (7.14) is highest.

## 7.8 Optimal Power Factor

As discussed in Chap. 4, it becomes necessary to study the optimal power factor of DG units for minimising power losses to which the active and reactive power injections of each DG unit are optimized simultaneously. On the other hand, in practice, the choice of the best DG capacity may follow commercial standard sizes available in the market or be limited by energy resource availability. Given such a pre-specified DG capacity, the DG power factor can be optimally calculated by adjusting the active and reactive power sizes at which the *IMO* as defined by Eq. (7.7) can reach a minimum level. Using the Lagrange multiplier method, we can mathematically convert the constrained problem defined by Eq. (7.7) into an unconstrained one as follows:

$$L(P_{DGi}, Q_{DGi}, \lambda_i) = \sigma_1 ILP + \sigma_2 ILQ + \lambda_i\left(S_{DGi}^2 - P_{DGi}^2 - Q_{DGi}^2\right) \tag{7.15}$$

where $\lambda_i$ is the Lagrangian multiplier.

Substituting Eqs. (7.4) and (7.6) into Eq. (7.15), we obtain:

$$L = \frac{\sigma_1}{P_L} P_{LDG} + \frac{\sigma_2}{Q_L} Q_{LDG} + \lambda_i\left(S_{DGi}^2 - P_{DGi}^2 - Q_{DGi}^2\right) \tag{7.16}$$

The necessary conditions for the optimization problem, given by Eq. (7.16), state that the derivatives with respect to control variables $P_{DGi}$, $Q_{DGi}$ and $\lambda_i$ become zero.

$$\frac{\partial L}{\partial P_{DGi}} = \frac{\sigma_1}{P_L}\frac{\partial P_{LDG}}{\partial P_{DGi}} + \frac{\sigma_2}{Q_L}\frac{Q_{LDG}}{\partial P_{DGi}} - 2\lambda_i P_{DGi} = 0 \tag{7.17}$$

$$\frac{\partial L}{\partial Q_{DGi}} = \frac{\sigma_1}{P_L}\frac{\partial P_{LDG}}{\partial Q_{DGi}} + \frac{\sigma_2}{Q_L}\frac{Q_{LDG}}{\partial Q_{DGi}} - 2\lambda_i Q_{DGi} = 0 \tag{7.18}$$

$$\frac{\partial L}{\partial \lambda_i} = P_{DGi}^2 + Q_{DGi}^2 - S_{DGi}^2 = 0 \tag{7.19}$$

The derivative of Eqs. (7.3) and (7.5) with respect to $P_{DGi}$ and $Q_{DGi}$ are given as:

$$\frac{\partial P_{LDG}}{\partial P_{DGi}} = 2\sum_{j=1}^{N}\left[\alpha_{ij}P_j - \beta_{ij}Q_j\right] = 2\alpha_{ii}P_i + 2A_i \tag{7.20}$$

$$\frac{\partial Q_{LDG}}{\partial P_{DGi}} = 2\sum_{j=1}^{N}\left[\gamma_{ij}P_j - \xi_{ij}Q_j\right] = 2\gamma_{ii}P_i + 2C_i \tag{7.21}$$

$$\frac{\partial P_{LDG}}{\partial Q_{DGi}} = 2\sum_{j=1}^{N}\left[\alpha_{ij}Q_j + \beta_{ij}P_j\right] = 2\alpha_{ii}Q_i + 2B_i \tag{7.22}$$

$$\frac{\partial Q_{LDG}}{\partial Q_{DGi}} = 2\sum_{j=1}^{N}\left[\gamma_{ij}Q_j + \xi_{ij}P_j\right] = 2\gamma_{ii}Q_i + 2D_i \tag{7.23}$$

where

$$A_i = \sum_{\substack{j=1\\ j\neq i}}^{N}\left(\alpha_{ij}P_j - \beta_{ij}Q_j\right); B_i = \sum_{\substack{j=1\\ j\neq i}}^{N}\left(\alpha_{ij}Q_j + \beta_{ij}P_j\right);$$

$$C_i = \sum_{\substack{j=1\\ j\neq i}}^{N}\left(\gamma_{ij}P_j - \xi_{ij}Q_j\right); D_i = \sum_{\substack{j=1\\ j\neq i}}^{N}\left(\gamma_{ij}Q_j + \xi_{ij}P_j\right)$$

Substituting Eqs. (7.20) and (7.21) into Eq. (7.17), we obtain:

$$\frac{2\sigma_1}{P_L}\left[\alpha_{ii}P_i + A_i\right] + \frac{2\sigma_2}{Q_L}\left[\gamma_{ii}P_i + C_i\right] - 2\lambda_i P_{DGi} = 0 \tag{7.24}$$

Substituting Eq. (3.4) into Eq. (7.24), we obtain:

$$P_{DGi} = \frac{P_{Di}Y_i - \frac{\sigma_1 A_i}{P_L} - \frac{\sigma_2 C_i}{Q_L}}{Y_i - \lambda_i} \tag{7.25}$$

where

$$Y_i = \frac{\sigma_1 \alpha_{ii}}{P_L} + \frac{\sigma_2 \gamma_{ii}}{Q_L}$$

Similarly, substituting Eqs. (7.22) and (7.23) into Eq. (7.18), we obtain:

$$\frac{2\sigma_1}{P_L}[\alpha_{ii}Q_i + B_i] + \frac{2\sigma_2}{Q_L}[\gamma_{ii}Q_i + D_i] - 2\lambda_i Q_{DGi} = 0 \tag{7.26}$$

Substituting Eq. (3.5) into Eq. (7.26), we obtain Eq. (7.27), where $Y_i$ is given in Eq. (7.25).

$$Q_{DGi} = \frac{Q_{Di}Y_i - \frac{\sigma_1 B_i}{P_L} - \frac{\sigma_2 D_i}{Q_L}}{Y_i - \lambda_i} \tag{7.27}$$

Substituting Eqs. (7.25) and (7.27) into Eq. (7.19), we obtain:

$$Y_i - \lambda_i = \pm \frac{1}{S_{DGi}} \sqrt{\left(P_{Di}Y_i - \frac{\sigma_1 A_i}{P_L} - \frac{\sigma_2 C_i}{Q_L}\right)^2 + \left(Q_{Di}Y_i - \frac{\sigma_1 B_i}{P_L} - \frac{\sigma_2 D_i}{Q_L}\right)^2} \tag{7.28}$$

Substituting Eq. (7.28) into Eqs. (7.25) and (7.27), we obtain:

$$P_{DGi} = \pm \frac{\left(P_{Di}Y_i - \frac{\sigma_1 A_i}{P_L} - \frac{\sigma_2 C_i}{Q_L}\right) S_{DGi}}{\sqrt{\left(P_{Di}Y_i - \frac{\sigma_1 A_i}{P_L} - \frac{\sigma_2 C_i}{Q_L}\right)^2 + \left(Q_{Di}Y_i - \frac{\sigma_1 B_i}{P_L} - \frac{\sigma_2 D_i}{Q_L}\right)^2}} \tag{7.29}$$

$$Q_{DGi} = \pm \frac{\left(Q_{Di}Y_i - \frac{\sigma_1 B_i}{P_L} - \frac{\sigma_2 D_i}{Q_L}\right) S_{DGi}}{\sqrt{\left(P_{Di}Y_i - \frac{\sigma_1 A_i}{P_L} - \frac{\sigma_2 C_i}{Q_L}\right)^2 + \left(Q_{Di}Y_i - \frac{\sigma_1 B_i}{P_L} - \frac{\sigma_2 D_i}{Q_L}\right)^2}} \tag{7.30}$$

It is observed from Eq. (7.29) that $P_{DGi}$ can be positive or negative, depending on the characteristic of system loads. However, the load power factor of a distribution system without reactive power compensation is normally in the range from 0.7 to 0.95 lagging (inductive load). $P_{DGi}$ is assumed to be positive in this study, i.e., the DG unit delivers active power. $Q_{DGi}$ can be positive or negative, as given by Eq. (7.30). $Q_{DGi}$ can be positive with inductive loads or negative with capacitive loads (i.e., the DG unit injects or absorbs reactive power).

Given a $S_{DGi}$ value is pre-defined, the optimal $P_{DGi}$ and $Q_{DGi}$ values are respectively calculated using Eqs. (7.29) and (7.30) to minimize the *IMO* as defined

by Eq. (7.7), after running only one power flow for the base-case system. Accordingly, the optimal power factor ($pf_{DGi}$) value is specified using Eq. (7.2). Any power factors other than the optimal $pf_{DGi}$ value will lead to a higher *IMO*.

## 7.9 Computational Procedure

DG units are considered to be placed at an average load level (*LF*), defined by Eq. (7.1), over a given planning horizon, which has the most positive impact on the *IMO*. This also reduces the computational burden and the search space. The energy loss given by Eq. (7.11) is calculated by a multiyear multiperiod power flow analysis over the planning horizon. The computational procedure is explained for each step as follows:

1. *Step 1*: Set the apparent power of DG units ($S_{DGi}$) and the maximum number of buses to connect DG units.
2. *Step 2*: Run power flow for the system without DG units at the average load level over the planning horizon (*LF*) using Eq. (7.1).
3. *Step 3*: Find the optimal power factor of each DG unit for each bus using Eq. (7.2). Calculate the *IMO* for each case using Eq. (7.7) with DG unit.
4. *Step 4*: Locate the optimal bus for DG installation at which the *IMO* is the lowest with the corresponding optimal size and power factor at that bus.
5. *Step 5*: Run multiyear multiperiod power flow with the DG size obtained in *Step 4* over the planning horizon. Calculate the energy loss and its corresponding *BCR* using Eqs. (7.11) and (7.14), respectively.
6. *Step 6*: Repeat *Steps 3–5* until "the maximum number of buses is reached". These buses are defined as "a set of candidate buses". Continue to connect DG units to "these candidate buses" by repeating *Steps 3–5*.
7. *Step 7:* Stop if any of the violations of the constraints (Sect. 8.3.3) occurs or the last iteration *BCR* is smaller than the previous iteration one. Obtain the results of the previous iteration.

## 7.10 Example

### *7.10.1 Test System*

The methodology presented above was applied to an 11 kV 69-bus radial distribution system that is fed by a 6 MVA 33/11 kV transformer, as depicted in Fig. 2.3 [9]. The total active and reactive power of the system at the average load level defined by Eq. (7.1) is 3.35 MW and 2.30 MVAr, respectively.

**Table 7.1** Economic input data

| | |
|---|---|
| Gas turbine-based DG capacity [6] | 0.8 MVA |
| Investment cost [6] | $976/kW |
| Operation and maintenance and fuel costs [6] | $46/MWh |
| Electricity sales [6] | $76/MWh |
| Loss incentive [6] | $78/MWh |
| Network upgrade deferral benefit for deferral of transformer upgrades [6] | $407/kW of DG |
| Emission factor of grid [8] | 0.910 Ton$CO_2$/MWh |
| Emission factor of 1 MVA gas engine [8] | 0.773 Ton$CO_2$/MWh |
| Emission cost [8] | $10/Ton$CO_2$ |
| Discount rate [8] | 9% |

### *7.10.2 Assumptions and Constraints*

The operating voltages at all buses are limited in the range of 0.95–1.05 p.u. The feeder thermal limits are 5.1 MVA (270 A) [6]. It is assumed that the time-varying voltage dependent industrial load as defined in Eq. (2.1) is considered in this simulation. The loading at each bus follows the industrial load duration curve across a year shown in Fig. 7.1 over a planning horizon of 15 years with a yearly demand growth of 3%. As given by Eq. (7.1), the load factor or average load level over the planning horizon (*LF*) is 0.75. All buses are candidate for DG investment and more than one DG unit can be installed at the same bus. The substation transformers are close to their thermal rating and would need replacing in the near future while the conductors exhibit considerable extra headroom for further demand. For reasons of simplicity, DG units are connected at the start of the planning horizon and operating for the whole time a year (8760 h) at rated capacity throughout the planning horizon. That means the average utilization factor of DG units[1] is 100%. Gas turbine-based DG technology is used. Its size ($S_{DG}$) is pre-specified at 0.8 MVA. The input data given in Table 7.1, are used for benefit and cost analyses.

The total load of the system is 4.07 MVA. Given a pre-defined DG size of 0.8 MVA each and the constraint of DG penetration as defined by Eq. (7.8), the maximum number of DG units is limited to be five with a total size of 4 MVA. To compare the benefits brought to the utility, five following scenarios have been analysed.

- Scenario 1: One biomass DG unit;
- Scenario 2: Two biomass DG units;
- Scenario 3: Three biomass DG units;
- Scenario 4: Four biomass DG units;
- Scenario 5: Five biomass DG units.

[1]The average utilization factor of a DG unit in pencent is defined as the average power generated by the DG unit divided by its rated power, over a given time period.

### 7.10.3 Location, Size and Power Factor

Figure 7.2 presents the 69-bus system with DG units. The optimal locations are identified at buses 62, 35, 25, 4 and 39 where five DG units (i.e., DGs 1, 2, 3, 4 and 5, respectively) are optimally placed. Table 7.2 shows a summary of the results of the location, power factor and size of DG units for the five scenarios as mentioned earlier over the planning horizon of 15 years. As each DG unit is pre-defined at 0.8 MVA, its power factor is adjusted such that the IMO index obtained for each scenario is lowest. The optimal power factor for each location is quite different, in the range of 0.82–0.89 (lagging). The total size is increased from 0.8 to 4 MVA with respect to the number of DG units increased from one to five. It has been found from the simulation that three scenarios (i.e., 3, 4 and 5 DG units) satisfy the technical constraints. When less than three DG units are considered, the violation of the voltage constraint (i.e., the operating voltages are under 0.95 p.u) occurs at several buses in the system.

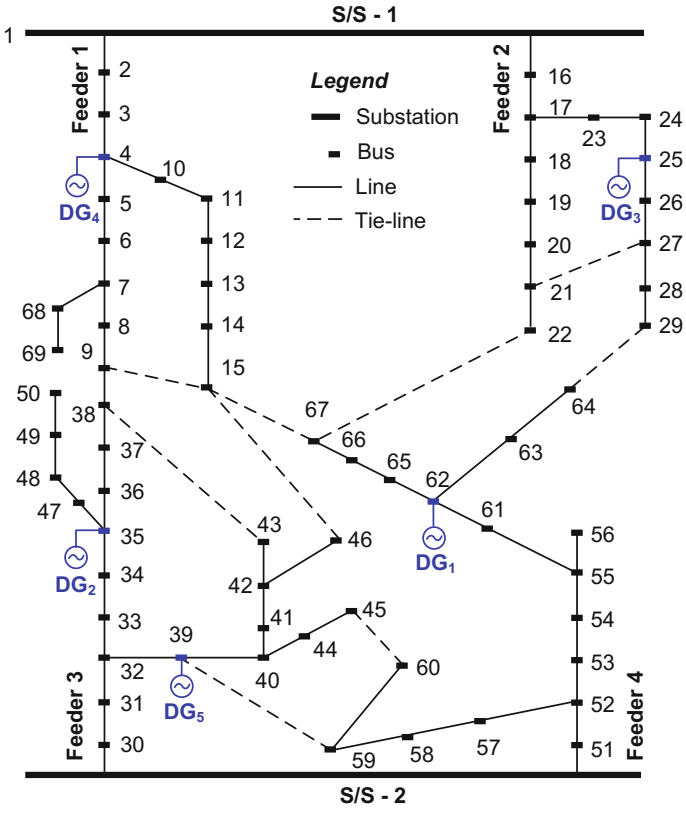


**Fig. 7.2** Single line diagram of the 69-bus test distribution system with DG units

**Table 7.2** Location, size and power factor of DG units

| Scenarios | DG location | DG size (MVA) | DG power factor (lag.) | Total DG size (MVA) | Violation of constraints? |
|---|---|---|---|---|---|
| 1 DG | 62 | 0.8 | 0.87 | 0.8 | Yes |
| 2 DGs | 62<br>35 | 0.8<br>0.8 | 0.87<br>0.89 | 1.6 | Yes |
| 3 DGs | 62<br>35<br>25 | 0.8<br>0.8<br>0.8 | 0.87<br>0.89<br>0.89 | 2.4 | No |
| 4 DGs | 62<br>35<br>25<br>4 | 0.8<br>0.8<br>0.8<br>0.8 | 0.87<br>0.89<br>0.89<br>0.85 | 3.2 | No |
| 5 DGs | 62<br>35<br>25<br>4<br>39 | 0.8<br>0.8<br>0.8<br>0.8<br>0.8 | 0.87<br>0.89<br>0.89<br>0.85<br>0.82 | 4.0 | No |

Figure 7.3 shows a comparison of the ILP, ILQ and IMO indices with different numbers of DG units over the planning horizon, which are related to the active power loss index, reactive power loss index and a multi-objective index. As shown in Fig. 7.3, the indices reduce when the number of DG units is increased from one to five. However, when the number of DG units is further increased, the total penetration of DG units is higher than the total demand as previously mentioned along with an increase in the values of indices. Substantial reductions in the indices are observed in three scenarios (i.e., 3, 4 and 5 DG units) when compared to one and two DG units. For each scenario, the ILP is lower than the ILQ. This indicates that the system with DG units can benefit more from minimising the active power loss than to the reactive power loss.

### *7.10.4 DG Impact*

Figure 7.4 presents the total energy loss of the system for different scenarios without and with DG units over the planning horizon. For each scenario, the total energy loss for each year is estimated as a sum of all the energy losses at the respective load levels of that year. As shown in Fig. 7.4, the system energy loss with no DG units increases over the planning horizon due to the annual demand growth of 3%. A significant reduction in the energy loss over the planning horizon is observed for the scenarios with DG units when compared to the scenario without DG units. The lowest energy loss is achieved for the scenario with five DG units. Higher energy losses can be observed for the scenarios with three or four DG units.

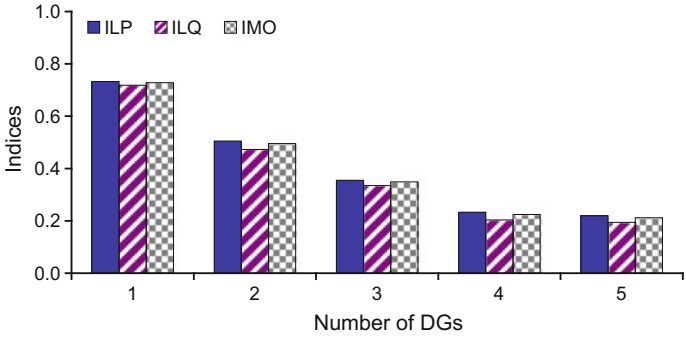


**Fig. 7.3** Indices (*ILP*, *ILQ* and *IMO*) for the system with various numbers of DG units over planning horizon

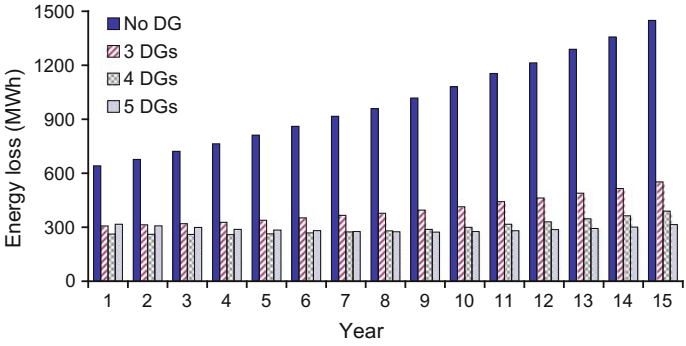


**Fig. 7.4** Losses of the system with and without DG units over planning horizon

Figure 7.5 shows the impact of DG allocation on the voltage stability of the system with and without DG units over the planning horizon of 15 years. For each year, the simulation has been implemented at the maximum demand, where the voltage stability margin (*VSM*) is worst when compared to the other loading levels. In each year, the *VSM* of the system with 3–5 DG units significantly enhances when compared to that of the system without DG units. For example, when three DG units generate an amount of 2.4 MVA at buses 62, 35 and 25 in the first year, as found in Table 7.2, the *VSM* increases to 4.5918 p.u. from the base-case value of 2.8681 p.u. (without DG units). A similar trend has been found for years 2–15 as shown in Fig. 7.5. Furthermore, it can be seen from Fig. 7.5 that a significant increase in the voltage stability margin is found for the scenarios with four or five DG units when compared to three DG units. This is due to the fact that the *ILP*, which is related to the reactive power loss of the system, significantly reduces for the scenario with four or five DG units when compared to three DG units, as shown in Fig. 7.3. In addition, it can be observed from Fig. 7.5 that the *VSM* values with

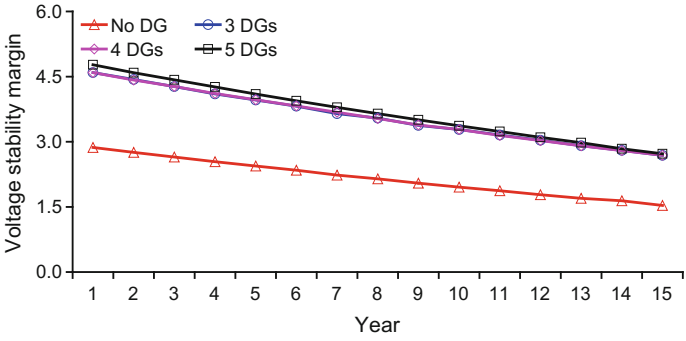


**Fig. 7.5** Voltage stability margin curves for all scenarios over planning horizon

**Table 7.3** Energy loss and voltage stability over planning horizon

| Scenarios | Energy loss | Energy savings | Voltage stability (p.u.) | |
|---|---|---|---|---|
| | (GWh/15 years) | (GWh/15 years) | *AVSM* | Δ*AVSM* |
| Base case | 14.91 | | 2.1667 | |
| 3 DGs | 5.97 | 8.94 | 3.5745 | 1.4078 |
| 4 DGs | 4.46 | 10.45 | 3.5758 | 1.4091 |
| 5 DGs | 4.35 | 10.56 | 3.6855 | 1.5188 |

and without DG units reduce with respect to a yearly demand growth of 3%. Hence, the lowest *VSM* values are found in the year 15.

Table 7.3 shows a summary of the results of energy losses without and with DG units for each scenario over the planning horizon of 15 years. The energy savings due to loss reduction is beneficial. A maximum energy savings is achieved for the scenario with five DG units when compared to three and four DG units. Table 7.3 also presents a summary of the results of voltage stability with and without DG units over the planning horizon. The average voltage stability margin of the system (*AVSM*) is calculated as a sum of the *VSM* values of all years divided by the total planning horizon. An increase in the average voltage stability margin (Δ*AVSM*) is observed after 3–5 DG units are installed in the system. It is observed from Table 7.3 that the *VSM* for each scenario increases with respect to an increase in the number of DG units installed in the system as well as a reduction in the overall energy loss of the system.

### *7.10.5 Benefit and Cost Analysis*

Table 7.4 presents the results of the total benefit and cost for three scenarios (i.e., 3, 4 and 5 DG units) without and with additional benefits over the planning horizon of

**Table 7.4** Analysis of the present value benefit and cost for different scenarios over planning horizon

| Number of DGs | Without additional benefits | | | With additional benefits | | |
|---|---|---|---|---|---|---|
| | 3 DGs | 4 DGs | 5 DGs | 3 DGs | 4 DGs | 5 DGs |
| *R* (k$) | 11,421 | 15,090 | 18,624 | 11,421 | 15,090 | 18,624 |
| *LI* (k$) | – | – | – | 336 | 392 | 387 |
| *EI* (k$) | – | – | – | 244 | 316 | 379 |
| *ND* $\sum P_{DGi}$ (k$) | – | – | – | 860 | 1137 | 1403 |
| *Total benefit*, *B* (*k$*) | 11,421 | 15,090 | 18,624 | 12,862 | 16,934 | 20,793 |
| *R*/*B* (%) | | | | 88.80 | 89.11 | 89.57 |
| (*LI* + *EI* + *ND* $\sum P_{DGi}$)/ *B* (%) | | | | 11.20 | 10.89 | 10.43 |
| *OM* (k$) | 6804 | 8990 | 11,095 | 6804 | 8990 | 11,095 |
| $C_{DG} \sum P_{DGi}$ (k$) | 2065 | 2728 | 3367 | 2065 | 2728 | 3367 |
| *Total cost*, *C* (*k$*) | 8869 | 11,718 | 14,462 | 8869 | 11,718 | 14,462 |

**Table 7.5** Comparison of different scenarios over planning horizon

| Number of DGs | Without additional benefits | | | With additional benefits | | |
|---|---|---|---|---|---|---|
| | 3 DGs | 4 DGs | 5 DGs | 3 DGs | 4 DGs | 5 DGs |
| *BCR* = *B*/*C* | 1.288 | 1.288 | 1.288 | 1.450 | 1.445 | 1.438 |
| *NPV* = *B* − *C* (k$) | 2552 | 3372 | 4162 | 3993 | 5216 | 6331 |
| Payback period (years) | 5.60 | 5.60 | 5.60 | 2.80 | 2.82 | 2.86 |
| Internal rate of return, *IRR* (%) | 16.48 | 16.48 | 16.48 | 32.65 | 32.38 | 31.93 |

15 years. The additional benefit includes the loss incentive (*LI*), emission incentive (*EI*) and network upgrade deferral (*ND*). The total benefit (*B*) is a sum of all the additional benefits and the energy sales (*R*). The total cost (*C*) is a sum of the operation, maintenance and fuel cost (*OM*) and the DG capacity cost ($C_{DG} \sum P_{DGi}$). Table 7.5 shows a comparison of the results for three different scenarios without and with additional benefits over the planning horizon. The results include the benefit-cost ratio (*BCR*), net present value (*NPV* = *B* − *C*), payback period, and internal rate of return (*IRR*).

For exclusion of the additional benefits, it is observed from Table 7.5 that the *BCR* is the same for all the scenarios at 1.288. The best solution is five DG units as the *NPV* is highest at k$4162. This solution generates an *IRR* of 16.48% and a payback period of 5.6 years. For inclusion of the additional benefits, it can be seen from Table 7.4 that the energy sales (*R*) accounts for around 89–90% of the *B*, leaving the total additional benefit (*LI*, *EI* and *ND*) at roughly 10–11%. It is obvious that the *R* has a significant impact on the *BCR* when compared to the total additional benefit. However, the additional benefits, particularly the *LI* play a critical role in decision-making about the total number of DG units or the amount of DG capacity

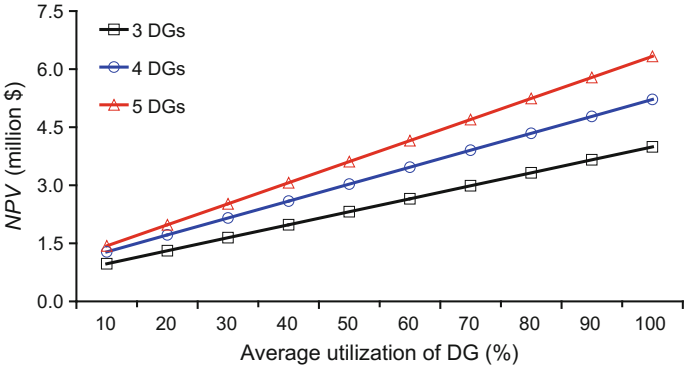


**Fig. 7.6** NPV at various average DG utilization factors for different scenarios over planning horizon

installed. This factor has an impact on the *BCR*. As shown in Table 7.5, the *BCR* slightly drops from 1.450 to 1.438 when the number of DG units is increased from three to five, respectively. The best solution is three DG units with the highest *BCR* of 1.450. This solution generates an *NPV* of k$3993, an *IRR* of 32.65% and a payback period of 2.80 years. In general, in the absence of the additional benefits, the optimal number of DG units is five, while in the presence of the additional benefits, this figure is three. Inclusion of the additional benefits in the study can lead to faster investment recovery with a higher *BCR*, a higher *IRR* and a shorter payback period when compared to exclusion of the additional benefits. In addition, it can be observed from Table 7.5 that the *NPV* value will further increase with increasing DG units installed. However, the system cannot accommodate more than five DG units due to the violation of the maximum DG penetration constraint as defined by Eq. (7.8).

Figure 7.6 shows an increase in the *NPV* with the corresponding average DG utilization factors over the planning horizon of 15 years for three scenarios (i.e., 3, 4 and 5 units) with the additional benefits. It is observed from the figure that given a certain average DG utilization factor in the range of 0–100%, the *NPV* is highest for the scenario with five DG units, whereas this figure is lowest for the scenario with three DG units. In addition, for each scenario, the *NPV* is maximum when the utilization factor is 100% as estimated in Table 7.5. However, in practice, this factor may be less than 100% due to interruption for maintenance and others. Consequently, the respective *NPV* will be reduced as shown in Fig. 7.6.

Figure 7.7 shows the percentage ratio of the total demand plus total loss to the thermal limit (6 MVA) of the transformer over the planning horizon with a demand growth of 3%. For the scenarios with DG units, the curves are plotted at the average DG utilization factor of 100%. Obviously, without DG connection, an investment would be needed to add a new transformer before year 4. However, the selected

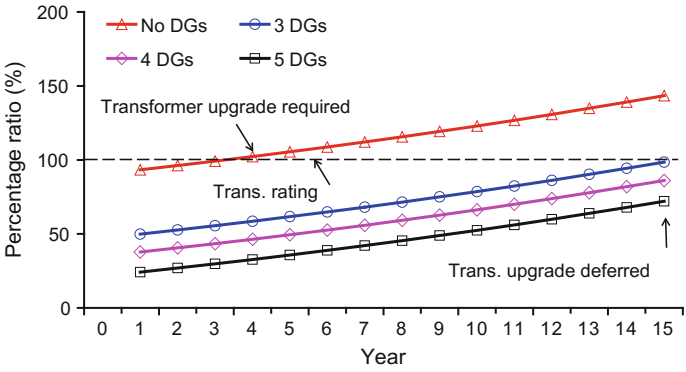


**Fig. 7.7** Percentage ratio of the total demand plus loss to the thermal transformer limit over planning horizon

three-DG scenario can defer in upgrading this current transformer (6 MVA) to 11 years. A higher deferral is achieved for the scenarios with four or five DG units.

## 7.11 Conclusions

This chapter presented an investment-planning framework for integrating multiple DG units in industrial distribution systems where the DG units are assumed to be owned and operated by utilities. In this framework, analytical expressions were reported to efficiently identify the optimal power factor of DG units for minimising energy losses and enhancing voltage stability. The decision for the optimal location, size and number of DG units is achieved through a benefit-cost analysis. The total benefit includes energy sales and three additional benefits including loss reduction, network upgrade deferral and emission reduction. The total cost is a sum of capital, operation and maintenance costs. The results obtained on a 69-bus test distribution system indicated that the additional benefits, particularly the loss incentive have a significant impact on decision-making about the total number of DG units or the amount of DG capacity installed. The additional benefits together accounted for 10–11% of the total benefit when compared to the energy sales of 89–90%. Inclusion of these benefits in the study can lead to faster investment recovery with a high benefit-cost ratio, a high internal rate of return and a short payback period.

When DG units are owned by DG developers, the additional benefits should be shared between the distribution utility and DG developer to encourage DG connection. In this situation, the presented methodology could be used as guidance for the utility on how to plan and operate DG units to obtain the additional benefits.

**Acknowledgments** The work presented in this chapter was taken from the journal paper: D.Q. Hung, N. Mithulananthan, and R.C. Bansal, "An optimal investment planning framework for multiple DG units in industrial distribution systems", Applied Energy, volume 124, pages 67–72, July 2014.

## References

1. Ochoa LF, Padilha-Feltrin A, Harrison GP (2006) Evaluating distributed generation impacts with a multiobjective index. IEEE Trans Power Deliv 21(3):1452–1458. doi:10.1109/TPWRD.2005.860262
2. Ochoa LF, Padilha-Feltrin A, Harrison GP (2008) Evaluating distributed time-varying generation through a multiobjective index. IEEE Trans Power Deliv 23(2):1132–1138. doi:10.1109/TPWRD.2008.915791
3. Singh D, Misra RK (2007) Effect of load models in distributed generation planning. IEEE Trans Power Syst 22(4):2204–2212. doi:10.1109/TPWRS.2007.907582
4. Singh D, Verma KS (2009) Multiobjective optimization for DG planning with load models. IEEE Trans Power Syst 24(1):427–436. doi:10.1109/TPWRS.2008.2009483
5. Canizares CA, Alvarado FL (1993) Point of collapse and continuation methods for large AC/DC systems. IEEE Trans Power Syst 8(1):1–8. doi:10.1109/59.221241
6. Siano P, Ochoa LF, Harrison GP, Piccolo A (2009) Assessing the strategic benefits of distributed generation ownership for DNOs. IET Gen Transm Distrib 3(3):225–236. doi:10.1049/iet-gtd:20080235
7. Piccolo A, Siano P (2009) Evaluating the impact of network investment deferral on distributed generation expansion. IEEE Trans Power Syst 24(3):1559–1567. doi:10.1109/tpwrs.2009.2022973
8. Soroudi A, Ehsan M, Zareipour H (2011) A practical eco-environmental distribution network planning model including fuel cells and non-renewable distributed energy resources. Renew Energy 36(1):179–188. doi:10.1016/j.renene.2010.06.019
9. Das D (2006) A fuzzy multiobjective approach for network reconfiguration of distribution systems. IEEE Trans Power Deliv 21(1):202–209. doi:10.1109/tpwrd.2005.852335

# Appendix A

See Tables A.1, A.2 and A.3.

**Table A.1** System data of 33-bus test distribution system

| Sending bus no. | Receiving bus no. | Resistance (Ω) | Reactance (Ω) | Load at receiving end bus | |
|---|---|---|---|---|---|
| | | | | P (kW) | Q (kVAr) |
| 1 | 2 | 0.0922 | 0.0477 | 100 | 60 |
| 2 | 3 | 0.4930 | 0.2511 | 90 | 40 |
| 3 | 4 | 0.3660 | 0.1864 | 120 | 80 |
| 4 | 5 | 0.3811 | 0.1941 | 60 | 30 |
| 5 | 6 | 0.8190 | 0.7070 | 60 | 20 |
| 6 | 7 | 0.1872 | 0.6188 | 200 | 100 |
| 7 | 8 | 1.7114 | 1.2351 | 200 | 100 |
| 8 | 9 | 1.0300 | 0.7400 | 60 | 20 |
| 9 | 10 | 1.0400 | 0.7400 | 60 | 20 |
| 10 | 11 | 0.1966 | 0.0650 | 45 | 30 |
| 11 | 12 | 0.3744 | 0.1238 | 60 | 35 |
| 12 | 13 | 1.4680 | 1.1550 | 60 | 35 |
| 13 | 14 | 0.5416 | 0.7129 | 120 | 80 |
| 14 | 15 | 0.5910 | 0.5260 | 60 | 10 |
| 15 | 16 | 0.7463 | 0.5450 | 60 | 20 |
| 16 | 17 | 1.2890 | 1.7210 | 60 | 20 |
| 17 | 18 | 0.7320 | 0.5740 | 90 | 40 |
| 2 | 19 | 0.1640 | 0.1565 | 90 | 40 |
| 19 | 20 | 1.5042 | 1.3554 | 90 | 40 |
| 20 | 21 | 0.4095 | 0.4784 | 90 | 40 |
| 21 | 22 | 0.7089 | 0.9373 | 90 | 40 |
| 3 | 23 | 0.4512 | 0.3083 | 90 | 50 |
| 23 | 24 | 0.8980 | 0.7091 | 420 | 200 |

(continued)



N. Mithulananthan et al., *Intelligent Network Integration of Distributed Renewable Generation*, Green Energy and Technology,
DOI 10.1007/978-3-319-49271-1

**Table A.1** (continued)

| Sending bus no. | Receiving bus no. | Resistance (Ω) | Reactance (Ω) | Load at receiving end bus | |
|---|---|---|---|---|---|
| | | | | P (kW) | Q (kVAr) |
| 24 | 25 | 0.8960 | 0.7011 | 420 | 200 |
| 6 | 26 | 0.2030 | 0.1034 | 60 | 25 |
| 26 | 27 | 0.2842 | 0.1447 | 60 | 25 |
| 27 | 28 | 1.0590 | 0.9337 | 60 | 20 |
| 28 | 29 | 0.8042 | 0.7006 | 120 | 70 |
| 29 | 30 | 0.5075 | 0.2585 | 200 | 600 |
| 30 | 31 | 0.9744 | 0.9630 | 150 | 70 |
| 31 | 32 | 0.3105 | 0.3619 | 210 | 100 |
| 32 | 33 | 0.3410 | 0.5302 | 60 | 40 |

Substation voltage = 12.66 kV, MVA base = 10 MVA

**Table A.2** System data of 69-bus *one feeder* test distribution system

| Sending bus no. | Receiving bus no. | Resistance (Ω) | Reactance (Ω) | Load at receiving end bus | |
|---|---|---|---|---|---|
| | | | | P (kW) | Q (kVAr) |
| 1 | 2 | 0.0005 | 0.0012 | 0.00 | 0.00 |
| 2 | 3 | 0.0005 | 0.0012 | 0.00 | 0.00 |
| 3 | 4 | 0.0015 | 0.0036 | 0.00 | 0.00 |
| 4 | 5 | 0.0251 | 0.0294 | 0.00 | 0.00 |
| 5 | 6 | 0.3660 | 0.1864 | 2.60 | 2.20 |
| 6 | 7 | 0.3811 | 0.1941 | 40.40 | 30.00 |
| 7 | 8 | 0.0922 | 0.0470 | 75.00 | 54.00 |
| 8 | 9 | 0.0493 | 0.0251 | 30.00 | 22.00 |
| 9 | 10 | 0.8190 | 0.2707 | 28.00 | 19.00 |
| 10 | 11 | 0.1872 | 0.0691 | 145.00 | 104.00 |
| 11 | 12 | 0.7114 | 0.2351 | 145.00 | 104.00 |
| 12 | 13 | 1.0300 | 0.3400 | 8.00 | 5.50 |
| 13 | 14 | 1.0440 | 0.3450 | 8.00 | 5.50 |
| 14 | 15 | 1.0580 | 0.3496 | 0.00 | 0.00 |
| 15 | 16 | 0.1966 | 0.0650 | 45.50 | 30.00 |
| 16 | 17 | 0.3744 | 0.1238 | 60.00 | 35.00 |
| 17 | 18 | 0.0047 | 0.0016 | 60.00 | 35.00 |
| 18 | 19 | 0.3276 | 0.1083 | 0.00 | 0.00 |
| 19 | 20 | 0.2106 | 0.0690 | 1.00 | 0.60 |
| 20 | 21 | 0.3416 | 0.1129 | 114.00 | 81.00 |
| 21 | 22 | 0.0140 | 0.0046 | 5.30 | 3.50 |

(continued)

**Table A.2** (continued)

| Sending bus no. | Receiving bus no. | Resistance (Ω) | Reactance (Ω) | Load at receiving end bus | |
|---|---|---|---|---|---|
| | | | | P (kW) | Q (kVAr) |
| 22 | 23 | 0.1591 | 0.0526 | 0.00 | 0.00 |
| 23 | 24 | 0.3463 | 0.1145 | 28.00 | 20.00 |
| 24 | 25 | 0.7488 | 0.2745 | 0.00 | 0.00 |
| 25 | 26 | 0.3089 | 0.1021 | 14.00 | 10.00 |
| 26 | 27 | 0.1732 | 0.0572 | 14.00 | 10.00 |
| 3 | 28 | 0.0044 | 0.0108 | 26.00 | 18.60 |
| 28 | 29 | 0.0640 | 0.1565 | 26.00 | 18.60 |
| 29 | 30 | 0.3978 | 0.1315 | 0.00 | 0.00 |
| 30 | 31 | 0.0702 | 0.0232 | 0.00 | 0.00 |
| 31 | 32 | 0.3510 | 0.1160 | 0.00 | 0.00 |
| 32 | 33 | 0.8390 | 0.2816 | 14.00 | 10.00 |
| 33 | 34 | 1.7080 | 0.5646 | 19.50 | 14.00 |
| 34 | 35 | 1.4740 | 0.4673 | 6.00 | 4.00 |
| 3 | 36 | 0.0044 | 0.0108 | 26.00 | 18.55 |
| 36 | 37 | 0.0640 | 0.1565 | 26.00 | 18.55 |
| 37 | 38 | 0.1053 | 0.1230 | 0.00 | 0.00 |
| 38 | 39 | 0.0304 | 0.0355 | 24.00 | 17.00 |
| 39 | 40 | 0.0018 | 0.0021 | 24.00 | 17.00 |
| 40 | 41 | 0.7283 | 0.8509 | 1.20 | 1.00 |
| 41 | 42 | 0.3100 | 0.3623 | 0.00 | 0.00 |
| 42 | 43 | 0.0410 | 0.0478 | 6.00 | 4.30 |
| 43 | 44 | 0.0092 | 0.0116 | 0.00 | 0.00 |
| 44 | 45 | 0.1089 | 0.1373 | 39.22 | 26.30 |
| 45 | 46 | 0.0009 | 0.0012 | 39.22 | 26.30 |
| 4 | 47 | 0.0034 | 0.0084 | 0.00 | 0.00 |
| 47 | 48 | 0.0851 | 0.2083 | 79.00 | 56.40 |
| 48 | 49 | 0.2898 | 0.7091 | 384.70 | 274.50 |
| 49 | 50 | 0.0822 | 0.2011 | 384.00 | 274.50 |
| 8 | 51 | 0.0928 | 0.0473 | 40.50 | 28.30 |
| 51 | 52 | 0.3319 | 0.1114 | 3.60 | 2.70 |
| 9 | 53 | 0.1740 | 0.0886 | 4.35 | 3.50 |
| 53 | 54 | 0.2030 | 0.1034 | 26.40 | 19.00 |
| 54 | 55 | 0.2842 | 0.1447 | 24.00 | 17.20 |
| 55 | 56 | 0.2813 | 0.1433 | 0.00 | 0.00 |
| 56 | 57 | 1.5900 | 0.5337 | 0.00 | 0.00 |
| 57 | 58 | 0.7837 | 0.2630 | 0.00 | 0.00 |
| 58 | 59 | 0.3042 | 0.1006 | 100.00 | 72.00 |
| 59 | 60 | 0.3861 | 0.1172 | 0.00 | 0.00 |

(continued)

**Table A.2** (continued)

| Sending bus no. | Receiving bus no. | Resistance (Ω) | Reactance (Ω) | Load at receiving end bus | |
|---|---|---|---|---|---|
| | | | | P (kW) | Q (kVAr) |
| 60 | 61 | 0.5075 | 0.2585 | 1244.00 | 888.00 |
| 61 | 62 | 0.0974 | 0.0496 | 32.00 | 23.00 |
| 62 | 63 | 0.1450 | 0.0738 | 0.00 | 0.00 |
| 63 | 64 | 0.7105 | 0.3619 | 227.00 | 162.00 |
| 64 | 65 | 1.0410 | 0.5302 | 59.00 | 42.00 |
| 11 | 66 | 0.2012 | 0.0611 | 18.00 | 13.00 |
| 66 | 67 | 0.0047 | 0.0014 | 18.00 | 13.00 |
| 12 | 68 | 0.7394 | 0.2444 | 28.00 | 20.00 |
| 68 | 69 | 0.0047 | 0.0016 | 28.00 | 20.00 |

Substation voltage = 12.66 kV, MVA base = 10 MVA

**Table A.3** System data of 69-bus *four feeder* test distribution system

| Sending bus no. | Receiving bus no. | Resistance (Ω) | Reactance (Ω) | Load at receiving end bus | |
|---|---|---|---|---|---|
| | | | | P (kW) | Q (kVAr) |
| 1 | 2 | 1.097 | 1.074 | 100 | 90 |
| 2 | 3 | 1.463 | 1.432 | 60 | 40 |
| 3 | 4 | 0.731 | 0.716 | 150 | 130 |
| 4 | 5 | 0.366 | 0.358 | 75 | 50 |
| 5 | 6 | 1.828 | 1.790 | 15 | 9 |
| 6 | 7 | 1.097 | 1.074 | 18 | 14 |
| 7 | 8 | 0.731 | 0.716 | 13 | 10 |
| 8 | 9 | 0.731 | 0.716 | 16 | 11 |
| 4 | 10 | 1.080 | 0.734 | 20 | 10 |
| 10 | 11 | 1.620 | 1.101 | 16 | 9 |
| 11 | 12 | 1.080 | 0.734 | 50 | 40 |
| 12 | 13 | 1.350 | 0.917 | 105 | 90 |
| 13 | 14 | 0.810 | 0.550 | 25 | 15 |
| 14 | 15 | 1.944 | 1.321 | 40 | 25 |
| 1 | 16 | 1.080 | 0.734 | 60 | 30 |
| 16 | 17 | 1.620 | 1.101 | 40 | 25 |
| 17 | 18 | 1.097 | 1.074 | 15 | 9 |
| 18 | 19 | 0.366 | 0.358 | 13 | 7 |
| 19 | 20 | 1.463 | 1.432 | 30 | 20 |
| 20 | 21 | 0.914 | 0.895 | 90 | 50 |
| 21 | 22 | 0.804 | 0.787 | 50 | 30 |
| 17 | 23 | 1.133 | 1.110 | 60 | 40 |

(continued)

**Table A.3** (continued)

| Sending bus no. | Receiving bus no. | Resistance (Ω) | Reactance (Ω) | Load at receiving end bus | |
|---|---|---|---|---|---|
| | | | | P (kW) | Q (kVAr) |
| 23 | 24 | 0.475 | 0.465 | 100 | 80 |
| 24 | 25 | 2.214 | 1.505 | 80 | 65 |
| 25 | 26 | 1.620 | 1.110 | 100 | 60 |
| 26 | 27 | 1.080 | 0.734 | 100 | 55 |
| 27 | 28 | 0.540 | 0.367 | 120 | 70 |
| 28 | 29 | 0.540 | 0.367 | 105 | 70 |
| 1 | 30 | 1.080 | 0.734 | 80 | 50 |
| 30 | 31 | 1.080 | 0.734 | 60 | 40 |
| 31 | 32 | 0.366 | 0.358 | 13 | 8 |
| 32 | 33 | 0.731 | 0.716 | 16 | 9 |
| 33 | 34 | 0.731 | 0.716 | 50 | 30 |
| 34 | 35 | 0.804 | 0.787 | 40 | 28 |
| 35 | 36 | 1.170 | 1.145 | 60 | 40 |
| 36 | 37 | 0.768 | 0.752 | 40 | 30 |
| 37 | 38 | 0.731 | 0.716 | 30 | 25 |
| 32 | 39 | 1.097 | 1.074 | 150 | 100 |
| 39 | 40 | 1.463 | 1.432 | 60 | 35 |
| 40 | 41 | 1.080 | 0.734 | 120 | 70 |
| 41 | 42 | 0.540 | 0.367 | 90 | 60 |
| 42 | 43 | 1.080 | 0.734 | 18 | 10 |
| 40 | 44 | 1.836 | 1.248 | 16 | 10 |
| 44 | 45 | 1.296 | 0.881 | 100 | 50 |
| 42 | 46 | 1.188 | 0.807 | 60 | 40 |
| 35 | 47 | 0.540 | 0.367 | 90 | 70 |
| 47 | 48 | 1.080 | 0.734 | 85 | 55 |
| 48 | 49 | 0.540 | 0.367 | 100 | 70 |
| 49 | 50 | 1.080 | 0.734 | 140 | 90 |
| 1 | 51 | 1.080 | 0.734 | 60 | 40 |
| 51 | 52 | 1.080 | 0.734 | 20 | 11 |
| 52 | 53 | 0.366 | 0.358 | 40 | 30 |
| 53 | 54 | 1.463 | 1.432 | 36 | 24 |
| 54 | 55 | 1.463 | 1.432 | 30 | 20 |
| 55 | 56 | 0.914 | 0.895 | 43 | 30 |
| 52 | 57 | 1.097 | 1.074 | 80 | 50 |
| 57 | 58 | 1.097 | 1.074 | 240 | 120 |
| 58 | 59 | 0.270 | 0.183 | 125 | 110 |
| 59 | 60 | 0.270 | 0.183 | 25 | 10 |
| 55 | 61 | 0.810 | 0.550 | 10 | 5 |

(continued)

**Table A.3** (continued)

| Sending bus no. | Receiving bus no. | Resistance (Ω) | Reactance (Ω) | Load at receiving end bus | |
|---|---|---|---|---|---|
| | | | | P (kW) | Q (kVAr) |
| 61 | 62 | 1.296 | 0.881 | 150 | 130 |
| 62 | 63 | 1.188 | 0.807 | 50 | 30 |
| 63 | 64 | 1.188 | 0.807 | 30 | 20 |
| 62 | 65 | 0.810 | 0.550 | 130 | 120 |
| 65 | 66 | 1.620 | 1.101 | 150 | 130 |
| 66 | 67 | 1.080 | 0.734 | 25 | 15 |
| 7 | 68 | 0.540 | 0.367 | 100 | 60 |
| 68 | 69 | 1.080 | 0.734 | 40 | 30 |

Substation voltage = 11 kV, MVA base = 10 MVA

# Appendix B

See Tables B.1 and B.2.

**Table B.1** Mean and standard deviation of solar irradiance

| Hour | μ (kW/m$^2$) | σ (kW/m$^2$) | Hour | μ (kW/m$^2$) | σ (kW/m$^2$) |
|---|---|---|---|---|---|
| 6 | 0.019 | 0.035 | 13 | 0.648 | 0.282 |
| 7 | 0.096 | 0.110 | 14 | 0.590 | 0.265 |
| 8 | 0.222 | 0.182 | 15 | 0.477 | 0.237 |
| 9 | 0.381 | 0.217 | 16 | 0.338 | 0.204 |
| 10 | 0.511 | 0.253 | 17 | 0.190 | 0.163 |
| 11 | 0.610 | 0.273 | 18 | 0.080 | 0.098 |
| 12 | 0.657 | 0.284 | 19 | 0.017 | 0.032 |

**Table B.2** Characteristics of the PV module

| PV module characteristics | Value |
|---|---|
| Nominal cell operating temperature, $N_{OT}$ (°C) | 43 |
| Current at maximum power point, $I_{MPP}$ (A) | 7.76 |
| Voltage at maximum power point, $V_{MPP}$ (V) | 28.36 |
| Short circuit current, $I_{sc}$ (A) | 8.38 |
| Open circuit voltage, $V_{oc}$ (V) | 36.96 |
| Current temperature coefficients, $K_i$ (A/°C) | 0.00545 |
| Voltage temperature coefficients, $K_v$ (V/°C) | 0.1278 |



N. Mithulananthan et al., *Intelligent Network Integration of Distributed Renewable Generation*, Green Energy and Technology,
DOI 10.1007/978-3-319-49271-1